THE FLORIDA STATE UNIVERSITY

COLLEGE OF ARTS AND SCIENCES

STUDYING CHEMICAL AND SEQUENCE LENGTH HETEROGENEITIES IN COPOLYMERS

By

IMAD HAIDAR AHMAD

A Dissertation submitted to the
Department of Chemistry and Biochemistry
in partial fulfillment of the
requirements for the degree of
Doctor of Philosophy

Degree Awarded:
Spring Semester, 2011

The members of the committee approve the dissertation of Imad Haidar Ahmad defended on February 15, 2011

_____
André M. Striegel
Professor Directing Dissertation

_____
Rufina G. Alamo
University Representative

_____
Oliver Steinbock
Committee Member

_____
Joseph B. Schlenoff
Committee Member

Approved:

_____
Joseph B. Schlenoff, Chair, Department of Chemistry and Biochemistry

The Graduate School has verified and approved the above-named committee members.

ACKNOWLEDGEMENTS

First and foremost, I am ever thankful to God, the Creator and the Guardian.

"My God,
The uninterrupted flow of Thy graciousness hast distracted me from thanking Thee!
The flood of Thy bounty has rendered me incapable of counting Thy praises!
The succession of Thy kind acts has diverted me from mentioning Thee in laudation!
Thy boons are abundant, my tongue is too weak to count them!
Thy favors are many, my understanding falls short of grasping them, not to speak of exhausting them!
So how can I achieve thanksgiving?" - The Whispered Prayer of the Thankful by Imam Zein Al-Abideen

I would like to express my deep appreciation and gratitude to my advisor, Professor André M. Striegel. It is difficult to overstate my gratitude to him. I am deeply indebted to him for all guidance, encouragement, motivation, good teaching, and advice during these five years.

Besides my advisor, I would like to thank the rest of my thesis committee: Professor Joseph Schlenoff, Professor Oliver Steinbock, and Professor Rufina Alamo for their encouragement, insightful comments, and hard questions. I appreciate the time they took to evaluate this thesis.

This dissertation is the end of my journey in obtaining my PhD. I must thank Professor Ali Safa who encouraged me and helped me to start this journey. I appreciate all his help when I was applying to the graduate program at FSU. I have learned from you a lot about not only Chemistry, but life as well.

I would like to thank past and present members of the Striegel group (Seth Ostlund, Dr. Marcus Boon, Dustin Richard, Michelle Smith, Shen Dong, Dr. Amandaa Brewer, Samantha Isenberg, Taylor Buley, Steven Rowland, Kelsey Mcneel, and Mallory Harlow) for all of the help, time, and suggestions that they have given me.

It is a pleasure to thank those who made this thesis possible: Dr. Deborah Striegel, Dr. Andreas Reisch, Dr. Abdulkader Baroudi, Lara Al-Hariri, Kassem Hallal, Ali Younis, and Sami Tlais.

My deepest gratitude goes to my family for the support they provided me through my life. This work would have been impossible without them. I am indebted to my father (Amin) and my mother (Jamilie), for their care and love. They are exceptional figures by all means. I have no suitable word that can fully describe my family. They worked industriously to support our lovely family and spared no effort to provide the best possible environment for me to grow up and attend school. On the same level, I would

like to acknowledge my loving and caring brothers (Tarek and Rageb) and my sister (Lozan). They have been models for me to follow unconsciously.

I cannot ask for more from my wife, Shereen Fakih, as she is simply perfect. She is the person who stood beside me and encouraged me constantly. This accomplishment is as much hers as it is mine. Without her patience and sacrifice, this journey would have looked so much more intimidating. I would like also to thank all my father-in-law (Ali), my mother-in-law (Zainab), and my brothers-in-law (Ismael, Mohammad, and Basel) for their help and support.

I am grateful to all who stood next to me and helped me during this journey. I would like to thank my uncles (Colonel Mohammad Haidar Ahmad, Professor Ali Haidar Ahmad, Hasan Haidar Ahmad, Housein Haidar Ahmad) my Aunt (Alia) as well as their families. Unfortunately some people who had great influence on me are already passed away before the completion of this thesis. My grandfather (Rageb), my uncles (Aref and Adel), and my aunt (Adla), your memory will never be erased and I know that you will be very proud of me.

TABLE OF CONTENTS

LIST OF TABLES

LIST OF FIGURES

LIST OF ABBREVIATIONS OR SYMBOLS

M ..... molar mass

MMD..... molar mass distribution

SLH ..... sequence length heterogeneity

[η] ..... intrinsic viscosity

A_2 ..... second Virial Coefficient

R_G ..... radius of gyration

R_η ..... viscometric radius

R_T ..... thermodynamic radius

a..... Mark-Houwink slope; indicates conformation

SLS..... static light scattering

THF ..... Tetrahydrofuran

PS ..... polystyrene

PMMA ..... polymethyl methacrylate

t-BMA ..... *tert*- butyl methacrylate

SEC ..... size-exclusion chromatography

MALS ..... multi-angle light scattering

UV ..... ultraviolet detector

VISC ..... viscometric, viscometer

DLS ..... dynamic Light Scattering

DRI..... differential Refractometer

∂n/∂c..... refractive index increment

Ψ* ..... coil interpenetration function

ABSTRACT

The work described in this thesis includes research done on two major projects, chemical heterogeneity and sequence length heterogeneities in copolymers. In the chemical heterogeneity project, we present a method by which to obtain the absolute, chemical-heterogeneity-corrected molar mass averages and distributions of copolymers and apply the method to two gradient random copolymers of styrene and methyl methacrylate and styrene and *t*-butyl methacrylate. In the first copolymer, the styrene percentage decreases from approximately 30% to approximately 19% as a function of increasing molar mass while in the second it varies between 60% and 70% as as a function of molar mass. The method consists of separation by SEC with detection using multi-angle static light scattering (MALS), differential viscometry (VISC), differential refractometry (DRI), and ultraviolet absorption spectroscopy (UV), and relies on the preferential absorption of styrene over methyl methacrylate and *tert*-butyl methacrylate at 260 nm. Using this quadruple-detector SEC/MALS/UV/VISC/DRI approach, the percentage of styrene (*%St*) in each elution slice is determined. This *%St* is then used to determine the specific refractive index increment, corrected for chemical composition, at each elution slice, which is then used to obtain the molar mass at each slice, corrected for chemical composition. From this corrected molar mass and from the chemical-composition-corrected refractometer response, the absolute, chemical-heterogeneity-corrected molar mass averages and distribution of the copolymer are calculated. The corrected molar mass and intrinsic viscosity at each SEC elution slice are used to construct a chemical-heterogeneity-corrected Mark-Houwink plot. The slice-wise corrected *M* data are used, in conjunction with the MALS-determined $R_{G,z}$ of each slice, to construct a conformation plot corrected for chemical heterogeneity. The corrected molar mass distribution (MMD) of the gradient copolymers extends over an approximately 30,000 g/mol wider range than the uncorrected MMD in the styrene-methyl methacrylate random copolymer and 60,000 g/mol in the case of styrene-*tert*-butyl methacrylate random copolymer. Additionally, correction of the Mark-Houwink and conformation plots for the effects of chemical heterogeneity shows that the copolymer adopts a more compact conformation in solution than originally concluded.

The sequence length heterogeneity (SLH) project shows a novel method for detecting SLH based on a change in the conformation of the copolymer in solution. Sequence length heterogeneity is defined as the change, as a function of copolymer molar mass (*M*), in the average number of continuous monomers of a given repeat unit. SLH can influence polymeric properties such as thermal stability, mechanical behavior, transparency, and the ability of copolymers to reduce interfacial surface tension. Here, we demonstrate the relation between SLH and the change as a function of *M* of a dimensionless size parameter, the ratio of the viscometric radius and the radius of gyration, irrespective of chemical heterogeneity or *M* polydispersity. Multi-detector size-exclusion chromatography (SEC) provides for a convenient method by which to experimentally establish this relation and, consequently, a method by which to determine whether SLH is present in a copolymer, whether the degree of randomness of a copolymer changes across the molar mass distribution (MMD), or whether two

copolymers differ from each other in degree of randomness at a given *M* and/or across their MMDs. Results from our SEC and FT-IR measurements of block, random, alternating, and gradient copolymers of styrene (S) and methyl methacrylate (MMA) and their respective homopolymers agree with results from a probability theory based model of SLH in linear random copolymers. The multi-detector SEC method employs instrumentation available in most polymer separations laboratories and the relations developed should be applicable to copolymers other than the S-MMAs studied here.

CHAPTER ONE

INTRODUCTION

The purpose of the current study is to contribute to the knowledge of heterogeneities in copolymers, specifically the chemical heterogeneity and sequence length heterogeneity. In the chemical heterogeneity project, we present a method by which to obtain the absolute, chemical-heterogeneity-corrected molar mass averages and distributions of copolymers. In the sequence length heterogeneity project, we shows a novel method for detecting SLH based on a change in the conformation of the copolymer in solution.

1.1 Copolymers: Definition and types

Copolymers are defined as macromolecules that comprise two different monomeric functionalities within one chain. The arrangement of the different functionalities within the polymeric chain corresponds to the different types of copolymers: Block when both two functionalities are assembled in the form of two blocks connected at one junction point, sequentially alternating in an alternating copolymer, and randomly distributed in the random copolymer. Gradient random copolymers are a special type of random copolymers where the percentage composition gradually changes as the chain grows. These different types of copolymers are shown in Figure 1, where the two different colors correspond to the different functionalities.

Figure 1. Types of copolymers used in this study. (a) Block copolymer, (b) alternating copolymer, (c) random copolymer, and (d) gradient random copolymer. Different colors indicate different monomeric types.

The four different types of copolymers possess different properties that affect not only their behavior in solution but also their end-use applications. These properties depend on the chemistry of the monomers in the chain, on the percentage composition, as well as on the arrangement of the monomers (i.e., on type of copolymer). Some specific applications related to the different types of copolymers are: 1) Block copolymers have exhibited potential in the area of drug delivery,[1] due to the ability of a block copolymer to form micelles in solvents that are good for only one of the two monomers, which allows for drug encapsulation within the micelle formed by block copolymers. 2) Alternating copolymers are capable of delivering holes and electrons in light emitting diodes, due to the electrochemical stability of the alternating copolymer, which is related to the highly

regulated arrangement of the monomers within the sequence.[2, 3] 3) Random copolymers can locate themselves at the interface of two immiscible phases, thereby reducing the surface tension between the fluids.[4]

1.2 Copolymer applications

Copolymers have a wide range of applications that depend on the type of copolymer (alternating, block, or random) and the ability to control chemical and physical properties of the copolymer by changing the relative ratio of the different monomers. Examples of such applications are:

Intraocular lens implants. Copolymers containing reversible disulfide bonds have the ability to be liquefied when reduced or to be gelled when oxidized. The ability of these copolymers to switch between two different states under different conditions offers the potential for use in ophthalmologic applications, such as in intraocular lens implantation.[5] A natural ocular lens changes its physiological chemical content due to aging or stressing, thus resulting in irreversible changes in mechanical and optical properties of the lens. A good implant candidate should be a substance possessing properties comparable to those of natural eye, such as transparency, elasticity, and biocompatibility.[6] Poly(acrylamide-*co*-*N*-*N*-bis(acryloyl)-cystamine), a thiol-containing copolymer, forms a gel under physiological conditions and meets the prerequisites necessary for an implanted lens. The rate of gelling of this copolymer can be manipulated by controlling the percentage of SH groups, the concentration of copolymer, and the molar mass of the copolymer.[5]

Biomedical hydrogels. Hydrogels are water rich polymeric substances, usually used for biomedical purposes such as contact lens fabrication due to their clarity, flexibility, hydrophilicity, and high water content. Silicone hydrogels are used for this purpose due to the ability of oxygen to pass easily through the lens, thus nourishing the cornea and extending the maximum time contacts can be worn.[7-10] Copolymers are important for contact lenses fabrication because of the following: 1) Copolymers can be used hydrogels such as poly[2-hydroxyl methacrylate-*co*-methacrylic acid]. 2) are used as surfactants due to the increased surface wettability of the contact lens provided by copolymers such as block copolymers of polyethylene oxide and polypropylene oxide.[10]

Protein mimics. Random copolymers with hydrophilic and hydrophobic functionalities distributed throughout the chain are similar to proteins in the way that the polymer comprises groups with polarities similar to the hydrophilic carbonyl group and hydrophobic alkyl group in proteins. The possibility of protein-like copolymers was first predicted by computer simulation, followed by actual synthesis.[11, 12] Poly[(*N*-vinylcaprolactam)-*co*-(*N*-vinylimidazole)], a catalyst used in studying the hydrolysis of ester substrates,[13] was the first successfully synthesized protein-like copolymer.[14] These types of copolymers are also used as models to study the localization, delocalization, or adsorption of proteins next to a lipid bilayer membrane. When adsorbed to a membrane surface, protein-like copolymers are used to study the relationships between the adsorption energy and the hydrophobicity of proteins.[15]

Viscosity index improvers. The viscosity of a copolymer solution is an adjustable property that depends on parameters such as molar mass and concentration, the thermodynamic state of solution, the percentage composition of the polymer, monomer chain length, and solvent additives.[16, 17] For example, the viscosity of acrylonitrile and acrylamide copolymers dissolved in dimethyl sulfoxide changes with adding DMF and/or H_2O, or by adding KCl.[16] The potential of a copolymer solution to change its viscosity with changes in experimental conditions imparts copolymers such as butyl acrylate α-olefins the ability to be used as viscosity index improvers.[17]

Optical waveguides An optical waveguide is a structure that directs a light wave to travel along a desired path. Candidates for waveguides should possess special physical, chemical, and mechanical properties, such as adjustable refractive index, excellent transmission of light, thermal stability, and rigidity.[18-20] Copolymeric materials excel for optical waveguide fabrication because they can tune these different properties and because they can be stretched as films. Examples of copolymeric optical waveguides are thin copolymeric films of octaflouropentyl methacrylate / hydroxyethyl methacrylate, styrene methyl methacrylate (S-MMA)[21] or of styrene acrylonitrile.[18, 19]

1.3 Dilute solution properties of copolymers

Dilute solution conditions will be followed in this study, where solvated polymers are present at very low concentrations, with the distance separating the polymeric chains from each other much larger than the size of the polymer in solution. With this condition fulfilled, interchain interaction between polymeric chains can be assumed to be negligible. Due to the relative ease of performing polymeric studies in dilute solution (as compared to *e.g.*, studies in the melt state), these studies are used for deriving absolute properties of the polymers under more complicated conditions, as in the melt or in concentrated solutions, where the structure of a polymer is affected by interchain interactions. The polymeric properties obtained from these dilute solution studies, i.e., the chemical heterogeneity and the distribution of monomers in a copolymeric chain, are absolute molecular properties related to the nature of the copolymer. Consequently, detecting chemical heterogeneity and monomer distribution in a copolymeric chain in the form of sequence length heterogeneity (explained thoroughly later in this chapter) in random copolymers under dilute solution conditions is essential for understanding the effect of these both heterogeneities on copolymeric properties as well as on the behavior of such copolymers under more complicated conditions, such as intrachain interaction between monomers in a copolymer chain.[22-26]

1.4 Background: Heterogeneities in copolymers

1.4.1 Chemical Heterogeneity

Chemical heterogeneity is defined as the change in the relative percentages of monomers in a copolymer across its molar mass distribution, as shown in Figure 2. A major source of this heterogeneity is due to synthesis of copolymers via free radical polymerization, where different monomers with different reactivities are incorporated in the copolymeric chain. Thus, during the copolymerization process the amount of generic monomers *S* and *M* integrated into a copolymeric chain is controlled by the reactivity ratios r_S and r_M of these monomers. These reactivity ratios are defined according to the following equations:[27-30]

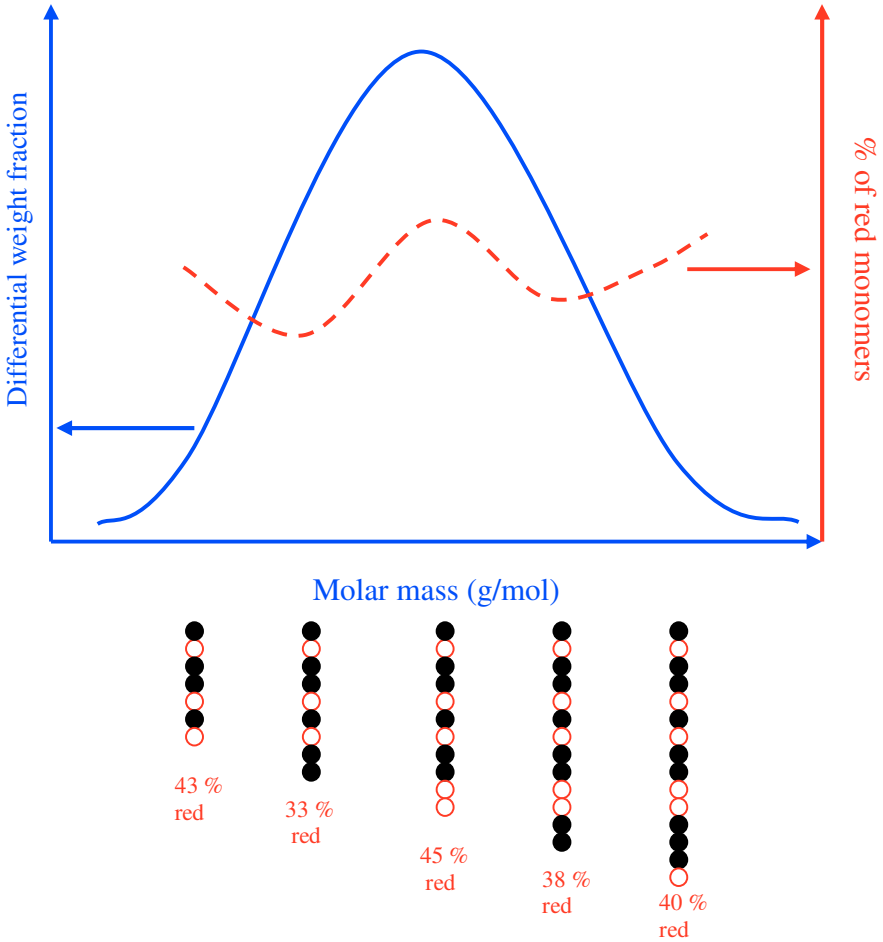

Figure 2. Chemical heterogeneity in a generic random copolymer.

$$S^* + S \xrightarrow{K_{SS}} SS^* \quad (1)$$

$$S^* + M \xrightarrow{K_{SM}} SM^* \quad (2)$$

$$M^{*} + S \xrightarrow{K_{MS}} MS^{*} \quad (3)$$

$$M^{*} + M \xrightarrow{K_{MM}} MM^{*} \quad (4)$$

$$r_S = \frac{K_{SS}}{K_{SM}} \qquad and \qquad r_M = \frac{K_{MM}}{K_{MS}} \quad (5)$$

where S^{*}, M^{*} represents the active monomers, i.e., free radicals of S and M respectively; K_{SS}, K_{SM}, K_{MM}, and K_{MS} represent the rate constants corresponding to the four reaction, r_S represent the reactivity ratio of monomer S; and r_M represents the reactivity ratio of monomer M.

In the case where $r_S = r_M$, both monomers are added with equal probabilities; otherwise, when $r_S \neq r_M$, the monomer with the higher reactivity ratio will be dominant (i.e. in a greater amount) in the copolymeric chain. Unequal monomer reactivities results in a different rate of incorporation of each type of monomer into the copolymeric chain: The more reactive monomer will be incorporated preferentially over its less reactive counterpart, resulting in the depletion of the more reactive monomer from the stock solution as the copolymerization process proceeds. This depletion results in a decrease in the percentage composition of the more reactive compared to the less reactive monomer during the copolymerization process (i.e. as the molar mass of the copolymer increases),[29] as shown in Figure 3. One way to decrease this drift in composition is by allowing the copolymerization reaction to proceed only for short times.

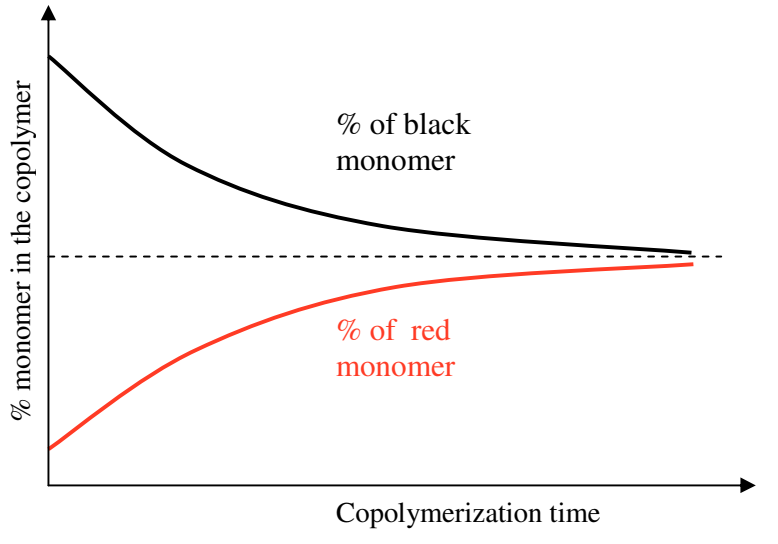

Figure 3. Schematic change in percentage composition of a copolymer during polymerization.

1.4.2 Sequence Length Heterogeneity

Sequence length heterogeneity (SLH) is the change in the average number of continuous and similar (i.e., same chemical repeat unit) monomers in a copolymer ($n_{average}$) as the chain grows. Figure 4 provides a visual aid to understanding SLH. Three different possible cases are shown in this figure: 1) Absence of SLH (shown in the change from 4a to 4b), 2) presence of SLH, resulting in an increase in the dispersity of the monomers into each other as the molar mass increases (shown in the change from 4a to 4c), and 3) SLH resulting in a copolymer becoming more blocky as the chain grows (shown in the change from of 4a to 4d). Sequence length heterogeneity may exist in the case of a random copolymer, i.e., a polymer comprising two different types of monomers randomly distributed within the chain. The random arrangement of monomers in the chain results in a distribution of the number of continuous and similar monomers. The change in this distribution as a function of molar mass is given the term "sequence length heterogeneity" and abbreviated as SLH.

Sequence length heterogeneity originates from the different probabilities with which monomers arrange in a copolymeric chain and from chemical heterogeneity (i.e., from the change in the relative percentage of a particular monomer among copolymeric chains of different molar mass).[31] Determining whether SLH exists in a random copolymer and whether the copolymer is of blocky, statistical, or alternating nature is essential for understanding the effect of the distribution of the monomers in a copolymeric chain on the properties of said copolymer.

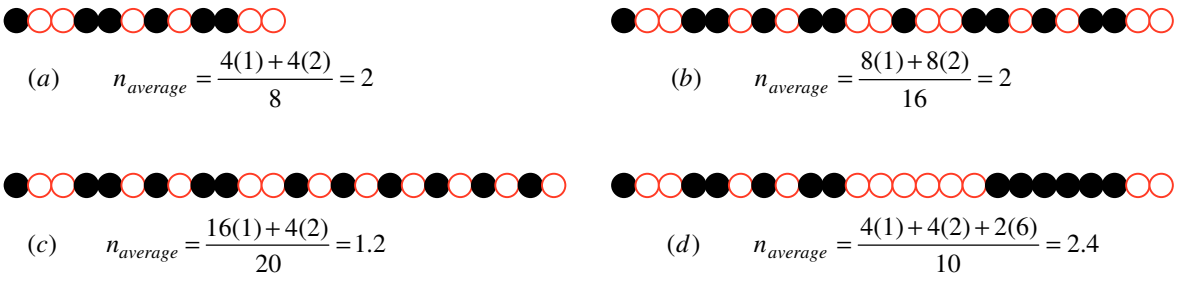

Figure 4. Sequence length heterogeneity (SLH) in random copolymers. (a) Random copolymer of molar mass *M*; (b), (c), and (d) random copolymers of molar mass 2*M*. There is absence of SLH in the change from (a) to (b), where the average number of continuous and similar monomers ($n_{average}$) is constant, whereas SLH occurs in the change from (a) to (c) and from (a) to (d). In the change from (a) to (c), the copolymer becomes more alternating ($n_{average}$ decreases), whereas the copolymer becomes more blocky when changing from (a) to (d) ($n_{average}$ increases).

1.5 Projects

1.5.1 Chemical heterogeneity: Determination and consequences in copolymer characterization

In this first project, we present a method by which to obtain the absolute, chemical-heterogeneity-corrected molar mass averages and distributions of copolymers and apply the method to a gradient random copolymer of styrene and methyl methacrylate as well as to a gradient random copolymer of styrene and *tert*-butyl methacrylate. The method consists of separation by size-exclusion chromatography (SEC) with detection using multi-angle static light scattering (MALS), differential viscometry (VISC), differential refractometry (DRI), and ultraviolet-visible absorption (UV-vis) spectroscopy, and relies on the preferential absorption of styrene over methyl methacrylate at 260 nm. Using this quadruple-detector SEC/MALS/UV/VISC/DRI approach, the percentage of styrene (*%St*) in each elution slice is determined. This *%St* is then used to determine the specific refractive index increment, corrected for chemical composition, at each elution slice, which is then used to obtain the molar mass at each slice, also corrected for chemical composition. From this corrected molar mass and from the chemical-composition-corrected refractometer response, the absolute, chemical-heterogeneity-corrected molar mass averages and distribution of the copolymer are calculated. The corrected molar mass and intrinsic viscosity at each SEC elution slice are used to construct a chemical-heterogeneity-corrected Mark-Houwink plot (plot of intrinsic viscosity $[\eta]$ versus molar mass M). The slice-wise corrected M data are used, in conjunction with the MALS-determined z-average radius of gyration ($R_{G,z}$) of each slice, to construct a conformation plot (plot of R_G versus molar mass) corrected for chemical heterogeneity.

1.5.2 Sequence length heterogeneity: Detection and influence on the dilute solution properties of copolymers

In this second project we provide a novel, semi-quantitative method for detecting the change in the distribution of the monomers in a random copolymer as the copolymeric chain grows. The change in the monomer distribution is detected in the form of sequence length heterogeneity (SLH). Detecting SLH is based on relating the dispersion of the monomers in the copolymeric chain to the number of junction points between different monomers. At the junction points, the intrachain repulsion between the two different monomers is expected to be higher than the repulsion between two monomers of the same chemical heterogeneity. The increased intrachain repulsion resultant from the former case slightly expands the structure of the copolymer. This expansion is evidenced in changes in the dimensionless ratio of the viscometric radius to the radius of gyration (R_η/R_G) of the copolymer which is indicative of the conformation of the copolymer, in solution.

The rate of occurrence of junction points in a random copolymers is affected by chemical heterogeneity, SLH, or both. We were able to show using SEC/MALS/VISC/DRI/UV whether R_η/R_G, and thus SLH, in styrene-methyl methacrylate random

copolymers was changing due to chemical heterogeneity or due to the change arrangement of the two monomers in the copolymeric chain. The existence of SLH in the random copolymers was confirmed by quantitating the area under the peak at ~ 1074 cm^{-1} in the IR spectrum, which is proportional to the amount of styrene-methyl methacrylate junctions in the copolymer at this IR absorption and thus to the dispersion of the monomers in a copolymeric chain.

CHAPTER TWO

BACKGROUND

2.1 Determining Chemical Heterogeneity

The aim of this chapter is to discuss the research methods we chose for studying chemical and sequence length heterogeneities in copolymers and the reasons for choosing them. Relevant methods from the literature are discussed and compared to our method of choice.

2.1.1 Previous approaches: Accomplishments and limitations

Chemical heterogeneity i.e., the change in chemical composition across the molar mass distribution of a copolymer, can be detected by coupling a separation technique (*e.g.*, SEC or thermal field flow fractionation (ThFFF)) to detectors that are capable of generating different signals for the two different functionalities in the copolymer. Examples of such detectors are nuclear magnetic resonance (NMR) detector, fourier transform infra-red (FTIR) spectroscopy detector, the combination of ultraviolet (UV) and differential refractometer (DRI) detectors, and mass spectrometry (MS).

Size-exclusion chromatography coupled on-line to NMR (SEC-NMR)

Size-exclusion chromatography and nuclear magnetic resonance (NMR) spectroscopy can be coupled online for the purpose of determining the percentage composition for a copolymer. The main advantage of using NMR as a quantitative concentration detector for SEC is the possibility of detecting both monomers in a copolymer simultaneously without the need for calibration, thus permitting quantitation of chemical heterogeneity. SEC-NMR can also be used for characterizing other copolymeric properties such as molar mass, sequence length distribution, tacticity, etc. For example, off-line ^{1}H NMR and on-line SEC-^{1}H NMR are used to study the chemical heterogeneity and to determine triad percentages in copolymers of styrene and ethyl acrylate [30] A sophisticated on-line probe is needed for coupling NMR to SEC, however. Limitations of off-line SEC-NMR are that the technique is time consuming, labor intensive, and the information obtained is dependent on the number of analyzed fractions

The main drawbacks of SEC-NMR are 1) Low sensitivity. 2) Inability to quantitate the NMR data when the peaks of the two functionalities overlap, or when the spectra are overcrowded. 3) The need for highly pure deuterated solvents,[30, 32-35] and 4) The expensive cost of the instrumental setup, including the online probe.[36-38]

Thermal field flow fractionation (ThFFF) and SEC-ThFFF

Thermal field flow fractionation (ThFFF) is a separation technique that fractionates polymers on the basis of their ratio of thermal diffusion (D_T) and transitional diffusion (D) coefficeints.[39,40] Because D_T varies with copolymer composition, ThFFF is capable of separating copolymers of different percentage compositions. When coupled to SEC, a separation method based on size, this two-dimensional separation technique can be used for determining the chemical heterogeneity in a copolymer. In ThFFF, a gradient thermal field is created between a hot top wall and a cold bottom wall in the flow channel. The analytes are driven by the temperature gradient toward one of the walls, based on their chemical composition. Therefore, the analytes are separated due to their different velocities in the channel. The retention time of the analytes is a function of their Soret coefficient S, which is defined as the ratio of the thermal diffusion coefficient D_T to the transitional diffusion coefficient D ($S = D_T/D$).[39-41] Determination of D_T/D is shown below.

$$R = \frac{V^o}{V_r} \tag{6}$$

$$R = 6\,\lambda\left[\coth\left(\frac{1}{2\lambda}\right) - 2\,\lambda\right] \tag{7}$$

$$\lambda = \frac{D}{D_T\,\Delta T} \tag{8}$$

where R is the retention ratio, V^o the void volume, V_r the retention volume, λ is a parameter dependent on the applied field, ΔT is the temperature gradient across the tube.

The retention ratio (R) is determined from the retention volume V_r and the void volume V^o using equation (6), then R is used to determine the parameter λ using equation (7). The Soret coefficient, which is proportional to the reciprocal of λ, will be experimentally determined using equation (8).

The ability of ThFFF to detect the presence of chemical heterogeneity is due to the fact that D_T is independent of molar mass, size, and branching, but dependent on the composition of the copolymer and solvent.[42, 43] D_T is calculated from the retention ratio using equation (8), where λ is determined based on equation (6) and (7) while the diffusion coefficient (D) is obtained from another technique such as dynamic light scattering.

The advantage of the ThFFF-SEC technique is its ability to separate copolymers according to size, chemical nature, and chemical composition.[39] Some pitfalls of this technique are: 1) It requires expensive instrumentation. 2) Inability to fully characterize a copolymer unless the two functionalities in the chain have different D_T values. 3) The effect of the distribution of monomers in a copolymeric chain on the diffusion coefficient of the polymer results in a inconsistency in the Soret coefficient.

Coupling SEC to ThFFF is an ideal combination because of the separation in the two methods is orthogonal. Fractions in the first dimension are separated based on size in solution (and thus can be related to molar mass) while in the second dimension the sample is fractionated according to chemical composition. Therefore, coupling SEC to FFF, where SEC is the first dimension and FFF is the second dimension is capable of determining chemical heterogeneity and chemical composition distribution. The detectors used for SEC-ThFFF may be the detection methods used for liquid chromatography techniques. Ultraviolet (UV) detectors are usually used for such setup because of their availability, simplicity, and relatively low cost. Other detection methods such as MALS, DLS, and DRI can be also used.

Multi-detector SEC

Size-exclusion chromatography coupled to both a universal concentration-sensitive detector (*e.g.*, DRI) and a selective concentration-sensitive detector (*e.g.*, UV-vis) can be used to determine chemical heterogeneity in copolymers where one monomer absorbs preferentially in the UV-vis region over the other monomer. The principle of this technique is based on comparing the signal from the DRI detector, which is sensitive to the concentration of both monomers in the copolymer, to the signal of the UV detector at a certain wavelength, which is proportional to the concentration of one of the two functionalities in the copolymer. The signals from the UV and DRI detectors for an *AB* copolymer, defined through equations (9) and (10), and the ratio of the two signals will be proportional to the relative concentration of monomer *A* in the *AB* copolymer, as shown in equation (11).[44, 45] The detailed derivation of the percentage composition in a styrene-methyl methacrylate copolymer is shown in Section 2.1.2.

$$S_{DRI,i} = k_{DRI} \times C_{AB,i} \times \left(\frac{\partial n}{\partial c}\right)_i \tag{9}$$

$$S_{UV,i} = K_{UV} \times C_{A,i} \tag{10}$$

$$\Rightarrow \left(\frac{C_A}{C_{AB}}\right)_i \propto \frac{S^{UV}}{S^{RI}} \tag{11}$$

where i is defined as the slice eluting from the SEC columns at time t, $S_{DRI,i}$ is the signal from the DRI detector at time i, k_{DRI} is the DRI instrument constant, $C_{AB,i}$ is the concentration of AB copolymer at slice i, $\left(\frac{\partial n}{\partial c}\right)_i$ is the specific refractive index of the copolymer at slice i, $S_{UV,i}$ is the signal from UV detector at time i, K_{UV} is the UV instrument constant, and $C_{A,i}$ is the concentration of A in an AB copolymer at a slice i.

For the purpose of determining the molar mass and percentage composition simultaneously, a multi-angle static light scattering (MALS) detector can be added to this

setup or a calibration curve can be used. In both cases, the molar mass obtained is biased and a correction is needed, details of which will be discussed later.

Conditions needed for determining chemical heterogeneity via multi-detector SEC are as follows: 1) One monomer should absorb preferentially over the other in the UV region. 2) The signals from the UV detector and the DRI detector should be linearly dependent on concentration, independently of monomer arrangement with the chain. 3) The specific refractive index ($\partial n/\partial c$) and the molar absorptivity (ε) of the constituent homopolymers should be constant across the molar mass distribution of the analyzed copolymer, i.e., the oligomeric region of the copolymer should be insignificant.

SEC-FTIR

Infrared spectroscopy is another analytical technique capable of differentiating among functional groups in a copolymer. The coupling of size-exclusion chromatography with Fourier-transform infrared (FTIR) spectroscopy allows the determination of the comonomer content in a copolymer if the FTIR generates two different signals for the two monomers in the copolymer. There are two ways of coupling FTIR to SEC: Either using a flow-through cell or by using a solvent elimination interface. In the latter, the copolymer is deposited on an IR-transparent substrate, usually a rotating germanium disc. As the mobile phase is deposited it evaporates, resulting in zero background absorption and elimination of any interference from the mobile phase.[35, 46, 47] Styrene-methyl methacrylate copolymers are examples of copolymers analyzed by SEC-FTIR for the purpose of detecting chemical heterogeneity. [48, 49]

Highly pure, IR-transparent solvents are needed for on-line SEC-FTIR analysis while, in the solvent-elimination approach, several factors need to be monitored to improve analysis efficiency. Examples of such factors are the spreading out, thickness homogeneity, and deposition homogeneity of the deposited spots. Additionally, spectral analysis of the IR data should not be complicated by extensive presence of overlapping bands for the two functionalities in the copolymer. Advantages of the on-line over the solvent-elimination approach to SEC-FTIR include better reproducibility and simplicity of analysis.[50]

SEC-MS

Mass spectrometry (MS) coupled to SEC is a fast-growing technique for analyzing synthetic polymers.[35, 51-56] Soft ionization methods such as electrospray ionization and matrix-assisted laser desorption/ionization are used for copolymer analysis to minimize mass degradation. SEC-MS can be used for determining chemical heterogeneity in copolymers, but this analysis can be complicated because of several copolymeric properties affecting ionization and spectral analysis, such as chemical heterogeneity, molar mass distribution, local polydispersity, sequence length heterogeneity, functionality type distribution due to different initiation and termination processes, and

chemical composition distribution.[51, 52] Often, supporting information from other analytical techniques (*e.g.*, SEC-NMR) is needed to help interpret the results from SEC-MS. [54, 55, 57]

Besides an expensive and sophisticated instrumental setup, analysis of copolymers by mass spectrometry coupled to SEC can be complicated by the degradation of high molar mass (>10^6 g/mol) polymers which results in an inaccurate determination of molar mass distributions.[54]

2.1.2 Our method: Quantitating Chemical Heterogeneity in Copolymers using Dual Detector Size-Exclusion Chromatography

Determination of the percentage composition of styrene in a styrene-methyl methacrylate copolymer by SEC/UV/DRI relies on the preferential absorption of styrene over methyl methacrylate at 260 nm. The signals from the DRI detector (S_{DRI}) and the UV detector (S_{UV}) at each elution slice *i* from the SEC columns are given as follows,

$$S_{DRI,\,i} = k_{DRI} \times C_{copolymer,\,i} \times \left(\frac{\partial n}{\partial c}\right)_{copolymer,\,i} \tag{12}$$

At λ = 260 nm:
$$S_{UV,\,i} = K_{UV} \times C_{styrene,\,i} \tag{13}$$

where K_{UV} and k_{DRI} are the calibration constants of the UV and DRI detectors, respectively, $C_{copolymer}$ is the concentration of the copolymer in solution, $C_{styrene}$ is the concentration of styrene in the dissolved copolymer, and ($\partial n/\partial c$) is the specific refractive index increment of the copolymer.

$C_{copolymer}$ and $C_{styrene}$ can be calculated by rearranging equations (12) and (13) as:

$$C_{copolymer,\,i} = \frac{S_{DRI,\,i}}{k_{DRI} \times (\partial n / \partial c)_{copolymer,\,i}} \tag{14}$$

$$C_{styrene,\,i} = \frac{S_{UV,\,i}}{K_{UV}} \tag{15}$$

The weight of styrene in the copolymer (w_{St}) can then be calculated based on equations (14) and (15):

$$w_{St} = \frac{C_{styrene,i}}{C_{copolymer,i}} = \frac{\frac{S_{UV,i}}{K_{UV}}}{\frac{S_{DRI,i}}{k_{DRI} \times (\partial n / \partial c)_{copolymer,i}}} = \frac{k_{DRI} \times (\partial n / \partial c)_{copolymer,i} \times S_{UV,i}}{K_{UV} \times S_{DRI,i}} \quad (16)$$

Let $\frac{S_{UV,i}}{S_{DRI,i}} = Z_i$, and substitute Z_i into equation (16):

$$w_{St} = \frac{C_{styrene}}{C_{copolymer}} = \frac{k_{DRI} \times (\partial n / \partial c)_{copolymer,i} \times Z_i}{K_{UV}} \quad (17)$$

To calculate the value of $\frac{k_{DRI}}{K_{UV}}$, a narrow polydispersity polystyrene is analyzed by SEC/UV/DRI. The signals of the UV and DRI detectors are as follows:

$$(S_{DRI})_{styrene} = k_{DRI} \times C_{styrene} \times \left(\frac{\partial n}{\partial c}\right)_{styrene} \quad (18)$$

$$(S_{UV})_{styrene} = K_{UV} \times C_{styrene} \quad (19)$$

$\frac{k_{DRI}}{K_{UV}}$ can be calculated by dividing equation (19) by equation (18):

$$\left(\frac{S_{UV}}{S_{DRI}}\right)_{styrene} = \frac{K_{UV}}{K_{DRI}} \times \frac{1}{(\partial n / \partial c)_{styrene}} \Rightarrow \frac{K_{UV}}{K_{DRI}} = \left(\frac{S_{UV}}{S_{RI}}\right)_{styrene} \times (\partial n / \partial c)_{styrene} \quad (20)$$

Let $F = \left(\frac{S_{UV}}{S_{DRI}}\right)_{styrene}$, then

$$\frac{K_{UV}}{K_{DRI}} = F \times \left(\frac{\partial n}{\partial c}\right)_{styrene} \quad (21)$$

w_{st} can be calculated by substituting equation (21) into equation (17),

$$w_{St,i} = \frac{(\partial n / \partial c)_{copolymer,i} \times Z_i}{F \times (\partial n / \partial c)_{St}} \quad (22)$$

However because, $(\partial n / \partial c)_{copolymer,i} = \left[(\partial n / \partial c)_{styrene} \times w_{styrene,i} + (\partial n / \partial c)_{MMA} \times w_{MMA,i}\right]$

then $(\partial n/\partial c)_{copolymer,i} = \left[(\partial n/\partial c)_{styrene} \times w_{styrene,i} + (\partial n/\partial c)_{methyl\ methacrylate} \times (1 - w_{styrene,i})\right]$ (23)

By substituting equation (23) into equation (22), the following equation is obtained:

$$w_{St,i} = \frac{\left[(\partial n/\partial c)_{St} \times W_{St,i} + (\partial n/\partial c)_{MMA} \times (1 - W_{St,i})\right] \times Z_i}{F \times (\partial n/\partial c)_{St}} \tag{24}$$

Rearrangement of equation 24 to calculate $w_{St,i}$ proceeds as follows,

$$w_{St,i}\left[F \times (\partial n/\partial c)_{St} - (\partial n/\partial c)_{St} \times Z_i + (\partial n/\partial c)_{\mathrm{MMA}} \times Z_i\right] = (\partial n/\partial c)_{\mathrm{MMA}} \times Z_i \tag{25}$$

Therefore, the chemical heterogeneity at each elution slice *i*, $w_{St,i}$, can be calculated according to following equation:

$$w_{St,i} = \frac{Z_i \times (\partial n/\partial c)_{MMA}}{F \times (\partial n/\partial c)_{St} - Z_i\left[(\partial n/\partial c)_{St} - (\partial n/\partial c)_{MMA}\right]} \tag{26}$$

The percentage of styrene at each elution slice *i* $(\%St)_i$, can be calculated by multiplying the $w_{St,i}$ calculated in equation (26) by 100%, as follows:

$$(\%St)_i = \frac{Z_i\left(\frac{\partial n}{\partial c}\right)_{PMMA}}{F\left(\frac{\partial n}{\partial c}\right)_{PS} - Z_i\left[\left(\frac{\partial n}{\partial c}\right)_{PS} - \left(\frac{\partial n}{\partial c}\right)_{PMMA}\right]} \times 100\% \tag{27}$$

2.1.3 Our method: Novelty, importance, and gaps filled

Chemical heterogeneity affects the separation process of copolymers by size-based as well as by so-called "interactive" liquid chromatographic techniques.[58-61] Also affected are the determination of copolymer molar mass averages and distributions by size-exclusion chromatography (SEC), not only when calibration curves are applied for determining the various *M* averages and distributions, but also when molar-mass-sensitive detectors such as the static light scattering (SLS) photometer are used for this purpose.

The molar mass averages and molar mass distribution (MMD) of random copolymers are usually obtained from SEC by applying calibration curves based on narrow polydispersity standards of homopolymers, or by using on-line SLS detection in conjunction with concentration-sensitive detection. When chemical heterogeneity is present in copolymers, both the calibration curve and light scattering approaches yield a biased, chemical-heterogeneity-dependent molar mass. The error associated with the molar mass obtained from applying a calibration curve is a result of the different

chemical repeat units and/or architecture of the standards used in constructing the curve, as compared to the repeat units and conformation of the copolymer being examined. The source of bias when using an SLS detector is somewhat different.

In our approach, we show how to obtain the chemical-heterogeneity-corrected absolute molar mass through the use of SEC coupled to multi-angle static light scattering (MALS), differential refractive index (DRI), and ultraviolet (UV) detectors. We correct for the bias in molar mass by calculating the chemical-composition-corrected $\partial n/\partial c$, for a gradient random copolymer, at each slice eluting from the SEC columns. The chemical-heterogeneity corrected $\partial n/\partial c$ is then used to correct the signal from the static light scattering detector to obtain the chemical-heterogeneity-corrected absolute molar mass which, once obtained, is used to determine the chemical-heterogeneity-corrected concentration, molar mass averages, and molar mass distributions.

2.2 Sequence Length Heterogeneity (SLH)

2.2.1 Previous approaches: Accomplishments and limitations

Previous work has focused on using either the sequence length distribution, which is conceptually different than SLH (similar to the difference between chemical composition distribution and chemical heterogeneity), or the instantaneous monomer sequence length to study how copolymeric randomness changes as a function of molar mass.

Sequence length distribution

In a random copolymer, the different arrangements of monomers in the copolymeric chain result in a distribution of the sequence length of different monomers. This variability in the lengths of the sequences of the monomers in a copolymeric chain is defined as sequence length distribution (SLD), as shown in the generic plot in Figure 5. In this plot, the relative abundances of chains of different sequence lengths are shown.

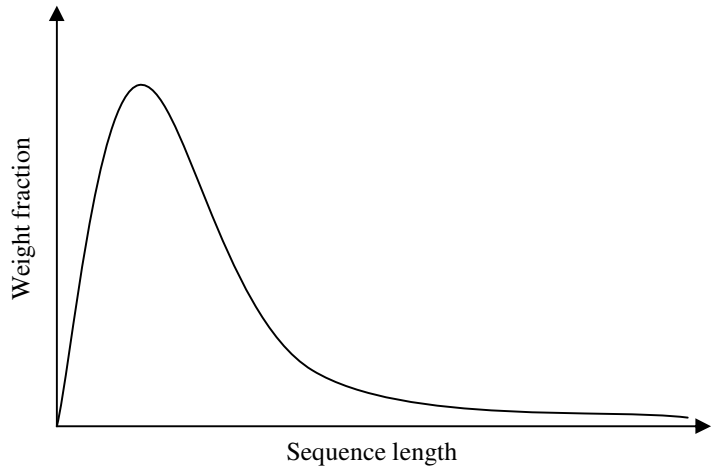

Figure 5. Sequence length distribution in a copolymer

The sequence length distribution is conceptually different from the sequence length heterogeneity. Figure 6 is a visual aid to understanding the SLH. The distribution in the sequence length at a specific molar mass, i.e., at A, B, C, or D, represents the SLD at that specific molar mass (*M*), with the apex of the SLD plot representing the average sequence length for that *M*. The change in the average sequence length across the molar mass distribution of the copolymer (i.e., from A to B to C to D, and so on) is termed "sequence length heterogeneity".

Several approaches, computational, theoretical, and experimental has been employed to detect and quantitate the sequence length distribution in copolymers.[62, 63] The experimental work included using detection methods such as FT-IR[64, 65], NMR[66-73], static light scattering, and differential scanning calorimetry. FTIR was used to detect SLD by studying the effect of the neighboring groups of a monomer on the absorption of one of the functional groups in that same monomer. An example is the effect of a styrene groups on the carbonyl absorption of a methyl methacrylate monomer in a copolymer of styrene and methyl methacrylate.[64, 65] Light scattering in conjunction with differential scanning calorimetry was used to detect the presence of SLD by studying the coil-to-globule chain transition at critical conditions.[74] NMR is used to detect SLD based on the effect of nearest monomeric units and next-nearest monomeric units on the resonance of various carbons and hydrogens.[66-73, 75, 76] knowledge of SLD as a function of each slice is not determined when detecting SLH, a two dimensional chromatography technique is needed for determining both SLH and SLD.

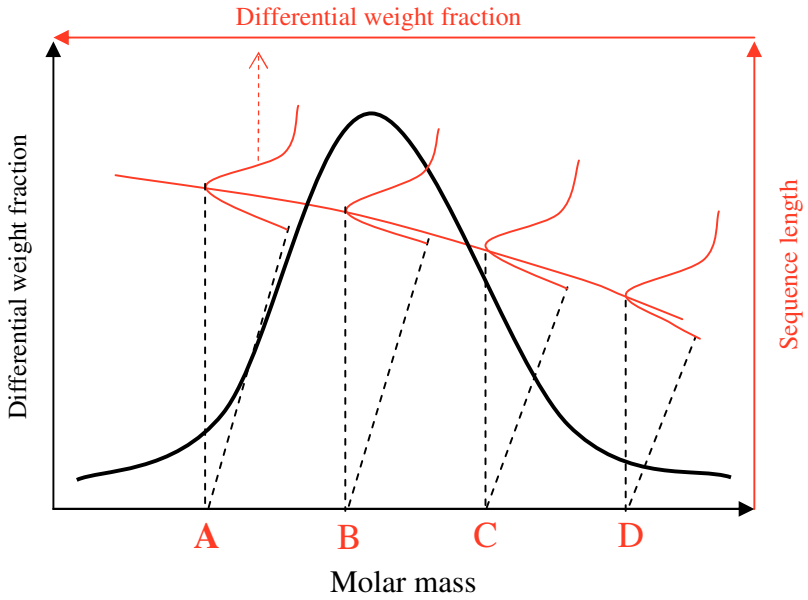

Figure 6. Sequence length distribution and sequence length heterogeneity *versus* molar mass distribution.

Instantaneous number-average sequence length

The instantaneous number-average (x_n) and weight-average (x_w) sequence length are calculated based on equations (28) and (29). (Detailed derivation of both equations is given in the next section of this chapter):

$$x_n = \frac{f_S(r_S - 1) + 1}{f_S + 1} \tag{28}$$

$$x_w = \frac{f_S(2r_S - 1) + 1}{f_S + 1} \tag{29}$$

where f_S is the mole ratio of monomer *S* in the copolymer and r_S is the reactivity ratio of monomer *S*.

An automatic, continuous, online monitoring of polymerization reactions (ACOMP) setup coupled to a train of detectors (light scattering, viscometer, differential refractometer, and UV-Visible) is needed to determine both instantaneous averages x_n and x_w.[77, 78] The ACOMP-quadruple detector setup is used to monitor reactions in real-time during polymerization by automatically and gradually diluting a flowing stream of polymer solution out of the reactor toward a train of detectors.[79]

Determining the Number-Average (x_n) and Weight-Average (x_w) Instantaneous Sequence Length

In a copolymer, the probabilities of two monomers (*S* and *M*) to are shown in the following reactions, along with their corresponding reaction rates:

$$S* + S \xrightarrow{K_{SS}} SS* \quad \Rightarrow \quad R_{SS} = K_{SS} \times [S*] \times [S] \tag{30}$$

$$S* + M \xrightarrow{K_{SM}} SM* \quad \Rightarrow \quad R_{SM} = K_{SM} \times [S*] \times [M] \tag{31}$$

$$M* + S \xrightarrow{K_{MS}} MS* \quad \Rightarrow \quad R_{SM} = K_{MS} \times [M*] \times [S] \tag{32}$$

$$M* + M \xrightarrow{K_{MM}} MM* \quad \Rightarrow \quad R_{MS} = K_{MM} \times [M*] \times [M] \tag{33}$$

where $S*$ and $M*$ represents the active monomers, i.e., free radicals of *S* and *M,* respectively; and K_{SS}, K_{SM}, K_{MM}, and K_{MS} represent the rate constant corresponding to the equations (30) – (33), respectively.

The reactivity ratios for the *S* and *M* monomers are

$$r_S = \frac{K_{SS}}{K_{SM}} \quad \text{and} \quad r_M = \frac{K_{MM}}{K_{MS}} \tag{34}$$

The probability of forming a dimer of two S monomers (P_{SS}) can be calculated from:

$$P_{SS} = \frac{R_{SS}}{R_{SS} + R_{SM}} \tag{35}$$

The rates of reactions (30) and (31) can be substituted into equation (35) to obtain:

$$P_{SS} = \frac{R_{SS}}{R_{SS} + R_{SM}} = \frac{K_{SS} \times [S^*] \times [S]}{K_{SS} \times [S^*] \times [S] + K_{SM} \times [S^*] \times [M]} \tag{36}$$

The numerator and the denominator in equation (36) are then divided by $K_{SM} \times [S^*]$ to obtain the final form of P_{SS}:

$$P_{SS} = \frac{\frac{K_{SS}}{K_{SM}} \times [S]}{\left(\frac{K_{SS}}{K_{SM}} \times [S]\right) + [M]} = \frac{r_S [S]}{r_S [S] + [M]} \tag{37}$$

Similarly, P_{SM} can be calculated from:

$$P_{SM} = \frac{R_{SM}}{R_{SS} + R_{SM}} = \frac{[M]}{r_S [S] + [M]} \tag{38}$$

For a chain ending with an S^* monomer, there are two possible monomers (S and M) to be added to this chain. Therefore, the probability of adding S to S^* and M to S^* is equal to unity.

$$P_{SS} + P_{SM} = 1 \tag{39}$$

Similarly, P_{MM}, P_{MS} and ($P_{MM} + P_{MS}$) are determined as:

$$P_{MM} = \frac{R_{MM}}{R_{MM} + R_{MS}} = \frac{r_M [M]}{r_M [M] + [S]} \tag{40}$$

$$P_{MS} = \frac{R_{MS}}{R_{MM} + R_{MS}} = \frac{[S]}{r_M [M] + [S]} \tag{41}$$

$$P_{MM} + P_{MS} = 1 \tag{42}$$

Based on equations (37) – (39), the probability of forming a chain of S monomers of a polymerization degree of x is:

$$P_{(S)_x} = (P_{SS})^{x-1} \times P_{SM} = (P_{SS})^{x-1} \times (1 - P_{SS}) \tag{43}$$

The number-average sequence length of *S* monomers (x_n) and the weight-average sequence length of *S* monomers (x_w) can be determined according to the following equations:

$$x_n = \frac{\sum_{x=1}^{\infty} x(P_{(S)x})}{\sum_{x=1}^{\infty} (P_{(S)x})} = \frac{\sum_{x=1}^{\infty} x(P_{SS})^{x-1}(1-P_{SS})}{\sum_{x=1}^{\infty} (P_{SS})^{x-1}(1-P_{SS})} = \frac{\sum_{x=1}^{\infty} x(P_{SS})^{x-1}}{\sum_{x=1}^{\infty} (P_{SS})^{x-1}} \tag{44}$$

$$x_w = \frac{\sum_{x=1}^{\infty} x^2(P_{(S)_x})}{\sum_{x=1}^{\infty} x(P_{(S)_x})} = \frac{\sum_{x=1}^{\infty} x^2(P_{SS})^{x-1}(1-P_{SS})}{\sum_{x=1}^{\infty} x(P_{SS})^{x-1}(1-P_{SS})} = \frac{\sum_{x=1}^{\infty} x^2(P_{SS})^{x-1}}{\sum_{x=1}^{\infty} x(P_{SS})^{x-1}} \tag{45}$$

To determine (x_n) and (x_w), $\sum_{x=1}^{\infty} x^2(P_{SS})^{x-1}$, $\sum_{x=1}^{\infty} x(P_{SS})^{x-1}$, and $\sum_{x=1}^{\infty} (P_{SS})^{x-1}$ are determined based on the subsequent calculations and explanations.

Based on equation (43), the following probabilities can be calculated for a linear chain:

1. Probability for (S) monomer next to (*M*) monomer:
$$P_{(S)_1} = (P_{SS})^0 \times (1-P_{SS}) = (1-P_{SS}) \tag{46}$$

2. Probability for two (S) monomers next to (*M*) monomer:
$$P_{(S)_2} = (P_{SS})^1 \times (1-P_{SS}) \tag{47}$$

3. Probability for three (S) monomers next to (*M*) monomer
$$P_{(S)_3} = (P_{SS})^2 \times (1-P_{SS}) \tag{48}$$

4. Probability for four (S) monomers next to (*M*) monomer
$$P_{(S)_4} = (P_{SS})^3 \times (1-P_{SS}) \tag{49}$$

As seen in equations (46) – (49), the probability propagates according to the geometric sequence expressed in equation (50) and shown in Figure 7:

$$\begin{array}{cccc} (1-P_{SS})\times(P_{SS})^0, & (1-P_{SS})\times(P_{SS})^1, & (1-P_{SS})\times(P_{SS})^2 & \cdots \\ a\times r^0 \quad , & a\times r^1 \quad , & a\times r^2 & \cdots \end{array} \tag{50}$$

Therefore, the common ratio (*r*) and the scale ratio (*a*) are as follows:

$$Common\ \ ratio(r) = P_{SS} \tag{51}$$

$$Scale\ ratio\ (a) = 1 - P_{SS} \tag{52}$$

Based on equations (50) – (52), the probability of obtaining a chain of a degree of polymerization (n) of (S) monomers is:

$$P_{(S)_n} = (P_{SS})^{n-1} \times (1 - P_{SS}) \tag{53}$$

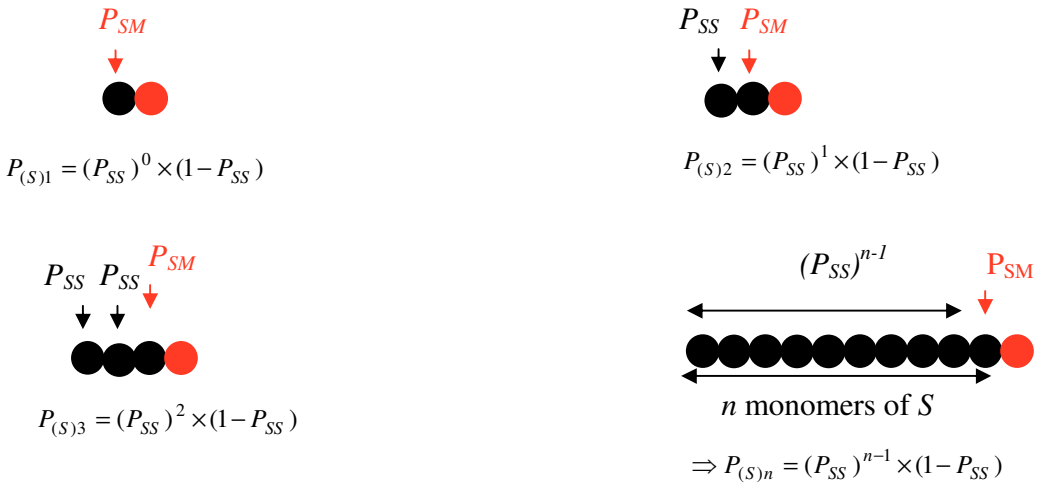

Figure 7. Determining the probability of forming a chain of n repeating units of S monomers

Determining $\sum x(p_{SS})^{x-1}$

In a geometric progression, $\sum_{n=1}^{n} xr^{x-1}$ can be calculated based on the following equation:

$$\sum_{n=1}^{n} xr^{x-1} = \frac{1 - r^{n+1}}{(1-r)^2} - \frac{(n+1)r^n}{1-r} = \frac{(1 - r^{n+1}) - ((1-r)(n+1)r^n)}{(1-r)^2} \tag{54}$$

Equation (54) can be simplified into equation (55), as follows:

$$\sum_{n=1}^{n} xr^{x-1} = \frac{1 - nr^n - r^n + nr^{n+1}}{(1-r)^2} = \frac{1 - r^n(n+1-nr)}{(1-r)^2} \tag{55}$$

But the common ratio (r) in equation (55) is smaller than one, because $P_{SS} + P_{SM} = 1$

$$r = P_{SS} < 1 \quad \Rightarrow \quad r < 1 \tag{56}$$

For n $\rightarrow \infty$, equation (55) can be simplified into equation (57):

$$\sum_{n=1}^{\infty} x r^{x-1} = \frac{1}{(1-r)^2} \tag{57}$$

Equation (51) can then be substituted into equation (57) to obtain

$$\sum_{n=1}^{\infty} x (P_{SS})^{x-1} = \frac{1}{(P_{SS})^2} \tag{58}$$

Determining $\sum (p_{SS})^{x-1}$

In a geometric progression, $\sum_{1}^{n} r^{x-1}$ is calculated from the following equation:

$$\sum_{n=1}^{\infty} r^{x-1} = \frac{(r^{n+1}-1)}{r-1} \tag{59}$$

But because $r < 1$, as shown in equation (56), then:

$$\sum_{n=1}^{\infty} r^{x-1} = \frac{1}{(1-r)} \tag{60}$$

Equation (51) can be substituted into equation (57) to obtain:

$$\sum_{n=1}^{\infty} (p_{SS})^{x-1} = \frac{1}{(1-p_{SS})} \tag{61}$$

The number-average sequence length of S monomers (x_n) can be calculated by substituting equations (61) and (58) into equation (44), to give:

$$x_n = \frac{\sum_{x=1}^{\infty} x (P_{SS})^{x-1}}{\sum_{x=1}^{\infty} (P_{SS})^{x-1}} = \frac{\frac{1}{(1-p_{SS})^2}}{\frac{1}{(1-p_{SS})}} = \frac{1}{(1-p_{SS})} \tag{62}$$

Determining $\sum x^2 (p_{SS})^{x-1}$

In a geometric progression, $\sum_{1}^{n} x^2 r^{x-1}$ can be calculated from the following equation:

$$\sum_{x=1}^{\infty} x^2 r^x = \frac{r(1+r)}{(1-r)^3} \tag{63}$$

But because $r^x = r^{x-1} \times r$, then:

$$\sum_{x=1}^{\infty} (x^2 r^{x-1}) r = \frac{r(1+r)}{(1-r)^3} \tag{64}$$

Equation (64), can be simplified by dividing both sides by *r*:

$$\sum_{x=1}^{\infty} x^2 r^{x-1} = \frac{(1+r)}{(1-r)^3} \tag{65}$$

Equation (51) can be substituted into equation (65) to obtain

$$\sum_{x=1}^{\infty} x^2 p_{SS}{}^{x-1} = \frac{(1+P_{SS})}{(1-P_{SS})^3} \tag{66}$$

The weight-average sequence length of *S* monomers (x_w) can be calculated by substituting equations (58) and (66) into (45), as follows

$$x_w = \frac{\sum_{x=1}^{\infty} x^2 (P_{SS})^{x-1})}{\sum_{x=1}^{\infty} x (P_{SS})^{x-1}} = \frac{\frac{1+P_{SS}}{(1-P_{SS})^3}}{\frac{1}{(1-p_{SS})^2}} = \frac{1+P_{SS}}{1-P_{SS}} \tag{67}$$

<u>Determining x_n and x_w in terms of mole fraction:</u>

$$f_S = \frac{[S]}{[M]+[S]} \tag{68}$$

$$f_M = \frac{[M]}{[M]+[S]} \tag{69}$$

where f_S and f_M are the mole ratios of *S* and *M* monomers, respectively.

Dividing the numerator and denominator in equation (37) by ([*S*] + [*M*]) one obtains:

$$p_{SS} = \frac{\left(\frac{r_S[S]}{[S]+[M]}\right)}{\left(\frac{r_S[S]+[M]}{[S]+[M]}\right)} \tag{70}$$

Equations (68) and (69) can be substituted into equation (70) to calculate P_{SS} via the following:

$$P_{SS} = \frac{r_S f_S}{r_S f_S + f_M} \tag{71}$$

Equation (71) can then be simplified using the substitution $f_M = 1 - f_S$ to:

$$P_{SS} = \frac{r_S f_S}{r_S f_S + (1 - f_S)} = \frac{f_S(r_S - 1) + 1}{r_S f_S} \tag{72}$$

Therefore, the number-average sequence length of *S* monomers (x_n) and the weight-average sequence length of *S* monomers (x_w) can be calculated in terms of f_S as follows:

$$x_n = \frac{1}{1 - P_{SS}} = \frac{1}{1 - \frac{r_S f_S}{f_S(r_S - 1) + 1}} = \frac{f_S(r_S - 1) + 1}{f_S(r_S - 1) + 1 - f_S r_S} = = \frac{f_S(r_S - 1) + 1}{f_S + 1} \tag{73}$$

$$x_w = \frac{1 + P_{SS}}{1 - P_{SS}} = \frac{1 + \frac{r_S f_S}{f_S(r_S - 1) + 1}}{1 - \frac{r_S f_S}{f_S(r_S - 1) + 1}} = \frac{f_S(r_S - 1) + 1 + r_S f_S}{f_S(r_S - 1) + 1 - r_S f_S} = \frac{2 f_S r_S - f_S + 1}{f_S + 1} \tag{74}$$

And the sequence length polydispersity x_w/x_n is defined as:

$$\frac{x_w}{x_n} = \frac{2 f_S r_S - f_S + 1}{f_S(r_S - 1) + 1} \tag{75}$$

2.2.2 Our method: Novelty, importance, and gaps filled

In our approach, we detect sequence length heterogeneity (SLH) in the form of a change in conformation of the copolymer in solution detected, in turn, using the ratio of the viscometric radius to the radius of gyration (R_η/R_G). This relation between SLH and R_η/R_G is based on relating SLH to the intrachain repulsion between monomers which manifests itself in the form of entropic change affecting the conformation of the copolymer in solution. This intrachain repulsion occurs at the junction points between dissimilar monomers.[80-82] Consequently, the change in the dispersion of the monomers in a copolymeric chain, i.e., the SLH, results in a change in intrachain repulsion along the copolymeric chain due to the variation in the percentage of the number of junction points as a function of the degree of polymerization. These intrachain enthalpic interactions force the chain to adopt a conformation that minimizes intrachain repulsion. Therefore, the change in enthalpy is balanced by a change in entropy in the form of conformational change.[81] Here, we use the ratio of the viscometric radius to the radius of gyration, R_η/R_G, to determine the conformation of the copolymer in solution and to detect the SLH by detecting the change in conformation.

Sequence length heterogeneity can be detected using online IR or NMR (i.e., SEC-NMR or SEC-FTIR experiments described in Section 2.1.1), but may be

complicated by one or more of the following reasons: Low solvent purity (<99.9%); presence of overlapped or broad IR or NMR Absorbances or resonances, making quantitation of peak area difficult, if not impossible; low signal to noise ratio spectra; highly expensive and specialized equipment.

A distinct advantage of the present method is that it relies solely on physical properties (angular dissymmetry and intrinsic viscosity) of the copolymer solution; i.e., success is not contingent upon chemical properties such as the preferential UV absorption of one monomer over another in a copolymer. An additional advantage of the method is that it does not rely on specialized equipment. Rather, it utilizes a type of separation-detector combination that is nowadays commonplace in most polymer characterization laboratories.

CHAPTER THREE

DESCRIPTION OF EXPERIMENTS AND INSTRUMENTATION

3.1 Description of experiments:

3.1.1 Off-line experiments

In off-line mode, the detector is decoupled from the separation system and a series of dissolutions is injected directly into the detector. As a result of the absence of a separation technique, only average (bulk) properties of the entire polymer (or polymer solution) are obtained from this mode of analysis. Two types of off-line experiments were performed: The $\partial n/\partial c$ experiment using the differential refractometer (DRI), and the Zimm plot experiment using the multi-angle static light scattering (MALS) detector.

Determination of the specific refractive index is essential for calculating the percentage composition of the copolymer, by relating the $(\partial n/\partial c)$s of the copolymers and the $(\partial n/\partial c)$s of their constituent homopolymers, as previously shown in equation (23). Besides using $\partial n/\partial c$ to calculate the percentage composition of a copolymer, $\partial n/\partial c$ values are used for calculating concentration and molar mass of a polymer, as will be explained in chapter five.

Zimm plots are used for determining the second virial coefficient (A_2) which determines the ability of a solvent to dissolve and solvate a polymer. In addition to the A_2 values obtained from the Zimm plot, average values of molar mass and radius of gyration are also determined.

3.1.2 On-line experiments (SEC/MALS/VISC/DRI) or (SEC/MALS/UV/DRI)

In online mode, the separation technique enables fractionating the sample according to molecular size. An advantage of online over off-line experiments is the ability to obtain the distribution of properties on-line, instead of property averages obtained by the offline experiments. Examples of properties acquired from online SEC/MALS/VISC/DRI are 1) Distribution of molar mass, 2) Distribution of intrinsic viscosities, 3) Distribution of the radius of gyration. These distributions are important to obtain plots such as the Mark-Houwink plots of the intrinsic viscosity versus molar mass and the conformation plots of the radius of gyration versus the molar mass. From these plots, we can determine the structure of a polymer or copolymer in solution, among others.

3.2 Instrument description

3.2.1 Size-exclusion chromatography

SEC is an "inverse sieving" separation technique based on the fractionation of molecules according to their size in solution, where small molecules can access more pore volume inside the column packing material than can larger molecules, resulting in the earlier elution of larger molecules in a sample versus that of the smaller molecules. A good visual aid to understand the mechanism of separation in SEC is shown in Figure 8. The size separation range of macromolecules in SEC can be related to the molar mass of the macromolecules by using standards of known molar mass, chemistry, and architecture; thus, the SEC separation profile can be translated into a molar mass distribution (MMD) via a retention time versus molar mass calibration curve.

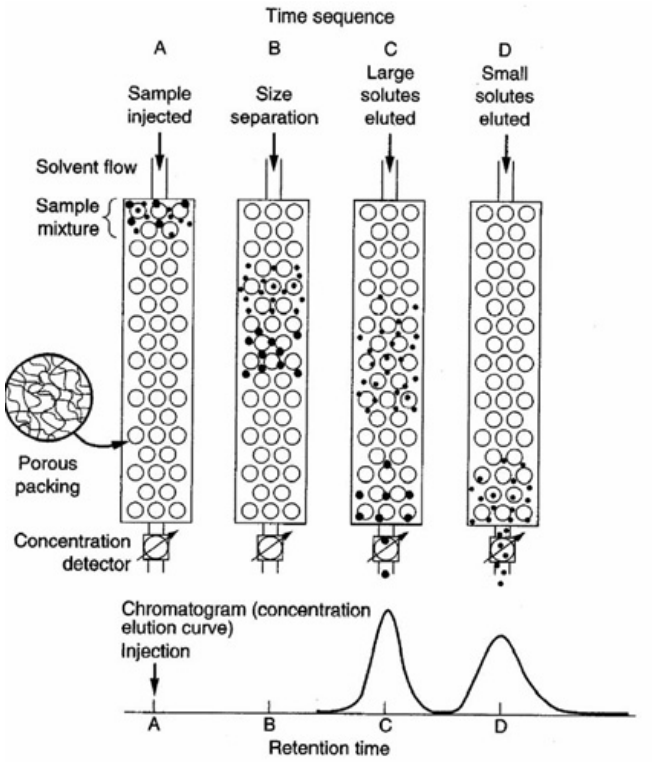

Figure 8. Mechanism of size-exclusion chromatography (SEC)[83]

The relation mentioned above, relating the molar mass to molecular size, is only valid for polymers of the same chemistry and structures as the standards. To overcome the problem that standards of the same chemistry and structure do not exist for all polymers as the analytes, MALS is used as a detection method for SEC because it is capable of determining the absolute (i.e., calibration-curve-independent) molar mass.

3.2.2 Multi-angle static light scattering (MALS) detector

Multi-angle static light scattering (MALS) is a powerful detection method capable of determining the absolute molar mass and size distribution of macromolecules as well as the thermodynamic state of the polymer solution. One advantage of using a MALS photometer as an SEC detector, for the purposes of determining molar mass, is that *M* averages and distributions from SEC/MALS are absolute, i.e., calibration-curve-independent. This contrasts with the calibrant-relative results obtained by SEC analysis using a single concentration-sensitive detector and calibration curves.[84-86]

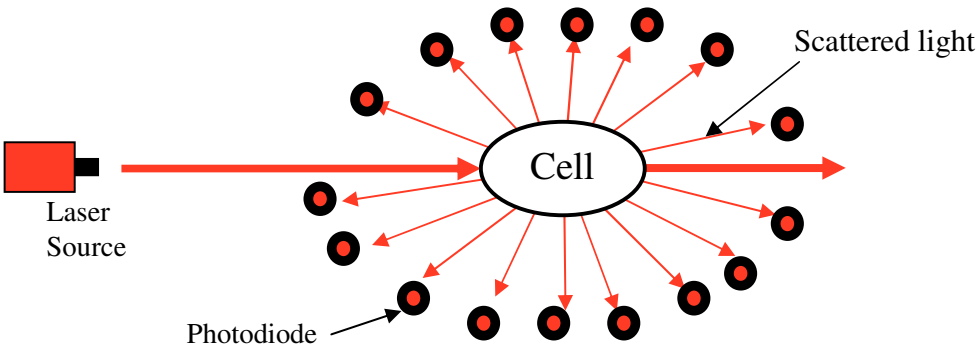

Figure 9. Multi-angle static light scattering (MALS) detection - Top view

As shown in Figure 9, the MALS photodiodes placed at different angles measure, at each angle, the excess Rayleigh ratio $R(\theta)$, defined as the amount of light scattered by the analyte in solution in excess of that scattered by the solvent. This measured scattered light is used to obtain the weight-average molar mass, M_w, of the analyte using the relations[84-86]

$$\frac{K^* c}{R(\theta)} = \frac{1}{P(\theta)}\left(\frac{1}{M_w} + 2A_2 c + 3A_3 c^2 + \ldots \right) \tag{76}$$

$$K^* = \frac{4\pi^2 n_0^2 \left(\frac{\partial n}{\partial c}\right)^2}{N_A \lambda_0^4} \tag{77}$$

$$\frac{1}{P(\theta)} = 1 + \frac{16\pi^2}{3\lambda^2} R_{G,z}^2 \sin^2\left(\frac{\theta}{2}\right) + \ldots \tag{78}$$

where c is the concentration of the polymer solution, $R(\theta)$ is the excess Rayleigh scattering ratio, A_2 is the second virial coefficient, A_3 is the third virial coefficient, θ is the scattering angle at which the observation is being made, n_0 is the refractive index of the

neat solvent, $\partial n/\partial c$ is the specific refractive index increment of the polymer solution, N_A is Avogadro's number, λ_0 is the vacuum wavelength of the incident light, λ is the wavelength of light in the medium (defined as $\lambda \equiv \lambda_0/n_0$) , $P(\theta)$ is the particle form factor, and $R_{G,z}$ is the z-average radius of gyration.

There are two modes of operation in the MALS detector: Online mode, when MALS is coupled to SEC (or other separation techniques) and the batch mode, when the MALS detector is used (i.e., decoupled from the separation method). In the offline mode, the scattered light for different concentrations are measured at sixteen different angles, and thus $R_{G,z}$, A_2, and M_w are obtained from equations (76)-(78). In online mode, MALS is capable of determining the molar mass distribution and the size distribution of a polymer, but not A_2.

3.2.3 Differential Viscometry (VISC)

The method of operation of the viscometer is based on Poiseuille's law, which relates the pressure drop ΔP of an incompressible solvent flowing through a tube of known length and radius r to the viscosity of the solution as shown in the equation below.[86]

$$\Delta P = \frac{8 L \eta Q}{\pi r^4} \tag{79}$$

where Q is the volumetric flow rate, and η is the fluid viscosity.

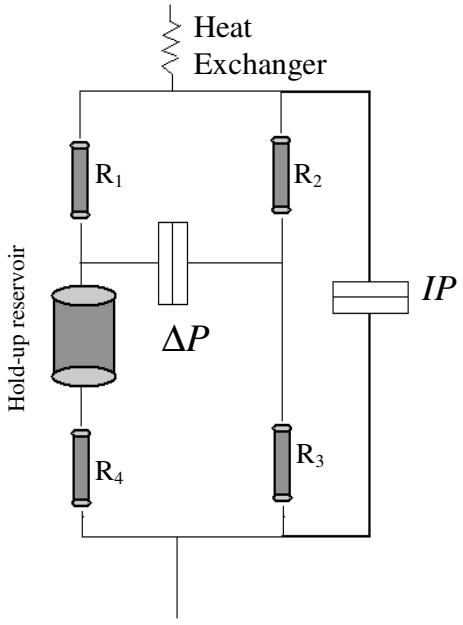

Figure 10. Wheatstone bridge viscometer design

The viscometer, as shown in Figure 10, is made up of a Wheatstone bridge type design consisting of four stainless steel capillary tubes (R_1, R_2, R_3 and R_4), two pressure transducers (ΔP and IP), a volume delay tube, and a heat exchanger to maintain constant temperature. The solution enters the Wheatstone bridge through the heat exchanger to stabilize the temperature (because viscosity is dependent on temperature), and then the solution splits into the two tubes R_1 and R_2. The solution flowing from R_1 toward R_4 is delayed inside hold-up reservoir while the solution from R_2 continues uninterrupted toward R_3. The inlet pressure P_i is measured by the inlet pressure transducer IP. The drop in pressure is related to the presence of the analyte in the solution when the sample passes through R_3 and the neat solvent passes through R_4. The measured pressure drop is related to the specific viscosity η_{sp} (the increase in the viscosity of the solution is due to the presence of the sample in solvent) according to the following equation:[86]

$$\eta_{sp} = \frac{4\Delta P}{P_i - 2\Delta P} \tag{80}$$

Besides determination of η_{sp}, online viscometers are capable of determining other parameters such as the intrinsic viscosity, $[\eta]$, when coupled to a concentration-sensitive detector, and the viscometric radius, R_η, (the radius of a hard sphere that affects the solvent viscosity as much as the analyte does), when coupled to MALS. The intrinsic viscosity and the viscometric radius are defined according to the equations[22]

$$[\eta] \equiv \lim_{c \to 0} \frac{\eta_{sp}}{c} \tag{81}$$

$$R_\eta = \left(\frac{3[\eta]M}{10\pi N_A} \right)^{1/3} \tag{82}$$

3.2.4 Differential Refractometry (DRI)

The differential refractometer is the detector of choice for concentration measurements in SEC, due to the fact that it is a reliable, nondestructive detector, independent of flow rate, and (essentially) universal. In a refractometer there are two compartments, one for the sample to flow through and the other for the reference solvent (Figure 11). The process of measuring the concentration of the analyte is done in two steps. First, both reference and sample compartment are filled with the neat solvent, and the position of the diffracted beam is denoted as position zero. Second, the sample cell is filled with the sample solution while the neat solvent is still trapped inside the reference cell. As the sample solution travels through the sample cell, the angle of refraction shifts from the zero position to a new angle. This change in angle of refraction is used to obtain the refractive index of the solution and, from this datum, the concentration of the analyte is calculated according to the following equation:[87]

$$c = \frac{n - n_0}{n_p - n_0} \tag{83}$$

where n is the refractive index of the solution, n_0 the refractive index of the neat solvent, and n_p is the refractive index of the analyte.

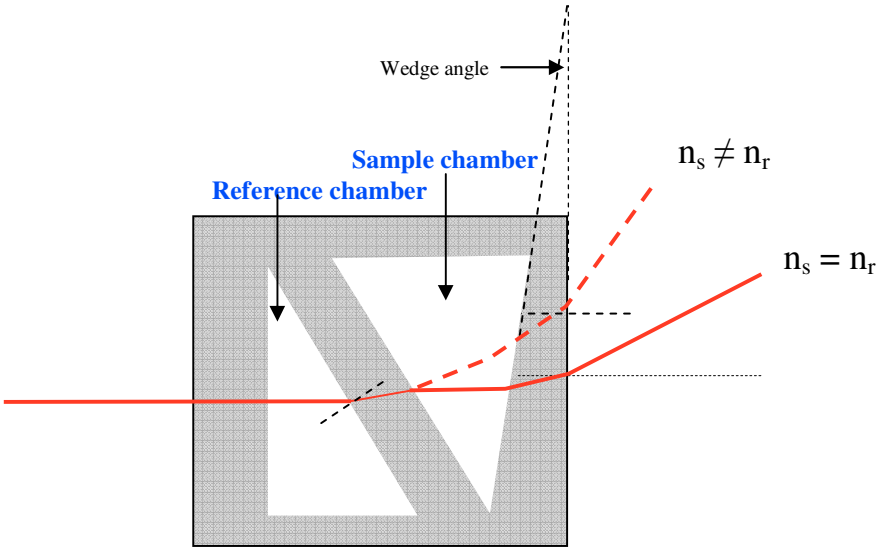

Figure 11. Differential refractometer.

The increased sensitivity of modern refractometers compared to older models is due to the use of photodiode arrays to determine the angle of diffraction. This enhances the refractometer sensitivity by more than a factor of 200. Additionally, due to the special design of the new refractometer cell, i.e., incorporation of a wedge angle as shown in Figure 11, new DRIs are capable of measuring the absolute refractive index of the solvent or solution in the reference chamber.

3.2.5 Ultraviolet-visible detector (UV-Vis)

The UV-Vis detector is a concentration-sensitive detector that can be used to selectively determine the concentration of a specific analyte in solution by monitoring the wavelength. The determination of the concentration of an analyte in solution is based on the Beer-Lambert law, which relates the absorbance of light at a specific wavelength to the concentration of the analyte in solution as per;

$$A = \varepsilon \times b \times C \tag{84}$$

where A is the measured absorbance of analyte in excess of the solvent, ε is the molar absorbtivity of the analyte in solution, b is the path length through the sample, and C is the concentration of analyte in solution.

Here, we use an on-line UV-Vis detector coupled to SEC, in conjunction with the DRI detector, to determine the composition of a copolymer at each elution slice by selectively determining the concentration of one of the monomers in a copolymer.

CHAPTER FOUR:

A COUPLED MALS-DRI METHOD FOR SIMULTANEOUS ZIMM AND ∂N/∂C PLOT CONSTRUCTION[88]

4.1 Introduction

Two of the most laborious and time-consuming experiments in dilute-solution polymer science are the construction of a Zimm or related (e.g., Berry, Debye, Guinier) plot and the construction of a $\partial n/\partial c$ plot. In this chapter, we propose performing both experiments simultaneously, by coupling the detectors to each other, still off-line from any separation media. This new approach saves time and labor and reduces material consumption and waste generation.

To construct a Zimm plot, a series of polymer solutions of varying, but known, concentrations are injected directly into a variable- or multi-angle light scattering (MALS) photometer. For each sample solution, the scattering is measured at a multiplicity of angles. The slope of the line constructed from the angular data extrapolated to zero concentration is proportional to $R_{G,z}$, the z-average radius of gyration. To construct a Zimm plot, a series of polymer solutions of varying, but known, concentrations are injected directly into a variable- or multi-angle light scattering (MALS) photometer. For each sample solution, the scattering is measured at a multiplicity of angles. The slope of the line constructed from the angular data extrapolated to zero concentration is proportional to $R_{G,z}$, the z-average radius of gyration. When the concentration data are extrapolated to zero angle, the slope of this extrapolated line is proportional to A_2, the second virial coefficient. The common y-intercept of the two extrapolated lines equals $1/M_w$.[84, 86, 89, 90] From these data, other dilute solution parameters can be derived, such as the thermodynamic radius R_T and the coil interpenetration function Ψ^*.[22, 89, 91, 92]

The $\partial n/\partial c$ plot is used to determine the specific refractive index increment (the $\partial n/\partial c$) of a polymer solution. Like a Zimm plot, a $\partial n/\partial c$ plot is constructed by injecting several solutions of varying, but known, concentration directly into a differential refractive index (DRI) detector. By "directly" it is meant that the refractometer, like the static light scattering photometer, is used in so-called off-line, batch mode, i.e., not connected to chromatographic columns or to some other separation method. The specific refractive index increment of a polymer solution is needed in order to determine M_w via static light scattering methods, according to Rayleigh-Gans-Debye theory.[84] (Reed, W. F., in ref.[86], pp. 13-51.) For a copolymer (random, block, or alternating), the bulk percentage of each homopolymer present in the copolymer can be calculated, if the $\partial n/\partial c$ values of the copolymer and the individual homopolymers are known.[93]

The above explanations of how to construct Zimm and $\partial n/\partial c$ plots do not do justice to the experimental difficulties encountered in each case: Samples need to be weighed out and solvent for dissolution needs to be measured, both with high accuracy; glassware and solvent need to be ultra-clean, free of any particulate matter; solutions need to be carefully filtered and, quite often, the first few milliliters of filtrate needs to be discarded, due to particulate matter leaching from the syringe filters; and the photodiodes of the MALS detector need to be normalized. In addition to careful sample preparation, the experiments themselves are quite lengthy, as five or more sample solutions are usually injected into the MALS or DRI detectors, at flow rates as low as 0.1-0.2 mL/min. It is not unusual for it to take 60-90 minutes, subsequent to sample preparation, to obtain one acceptable Zimm plot, and an addition 60-90 minutes to generate one acceptable $\partial n/\partial c$ plot.

In our MALS-DRI coupled approach, sample injected into the first detector (MALS) continues into the second detector (DRI). As we demonstrate, this set-up permits construction of both a Zimm plot and a $\partial n/\partial c$ plot from a single set of solutions and through a single set of injections. Coupling these two procedures presents several advantageous: The time involved in the determinations is virtually halved, as the experiments for the Zimm and $\partial n/\partial c$ plots can now be done together. This same is true for sample preparation, sample and solvent consumption, consumption of disposables (*e.g.*, syringes, syringe filters, etc.), waste generation, and the accompanying financial costs.

4.2 Experimental

Materials

Narrow polydispersity ($M_w/M_n \leq 1.05$) linear polystyrene (PS) and poly(methyl methacrylate) (PMMA) standards were obtained from Varian/Polymer Laboratories; tetrahydrofuran (THF) was from EMD.

Decoupled multi-angle light scattering (MALS): Zimm plot construction

In "decoupled" experiments, the MALS and DRI detectors were not connected to each other, while in "coupled" experiments the detectors were connected to one another. In the latter case, the MALS detector came first and the DRI detector second. For both types of MALS experiment, the angular scattering range examined extended from 38° to 147°.

For decoupled MALS experiments, a series of at least five sample dissolutions of PS and PMMA in THF at 25 ^{o}C, ranging from 1.0-6.0 mg/mL, were injected directly into the light scattering photometer, a Wyatt Dawn EOS, using a Razel model A-99EJ syringe pump. Flow rate was 0.21 mL/min. Sample solutions were filtered through 0.45 μm Teflon syringe filters, neat solvent for baseline determination through a 0.02 μm Teflon syringe filter. Normalization of the photodiodes of the MALS unit was performed using an 8.45×10^3 g mol^{-1} narrow polydispersity linear PS standard ($M_w/M_n \leq 1.03$). Data

acquisition and processing were done with Wyatt's ASTRA V software (V. 5.3.2.13). From these experiments, the Zimm (Berry) plots shown in Figures 12B and 13B were constructed.

Decoupled differential refractometry (DRI): $\partial n/\partial c$ plot construction

Decoupled differential refractometry experiments followed a procedure identical to that described in the previous section, but using a Wyatt Optilab rEX differential refractometer instead of the MALS detector. From these experiments, the $\partial n/\partial c$ plots in Figures 14B and 15B were constructed.

It should be noted that solutions from the same sample dissolutions were injected into each detector, and these dissolutions were also used for the coupled MALS-DRI experiments described in the next section. In other words, data from the same sample dissolutions are being compared throughout all the experiments. Also, the wavelength of the lamp in the DRI detector is filtered to match the wavelength of the laser in the MALS detector (λ_0 = 685 nm).

Coupled MALS-DRI: Simultaneous Zimm and $\partial n/\partial c$ plot construction

In this set-up, the MALS and DRI detectors were coupled to each other, MALS first and DRI second due to back-pressure considerations with the DRI cell. Again, the procedure was the same as that described in the *Decoupled MALS* section, save for the fact that solutions injected into the MALS photometer then proceeded into the DRI detector. While this may seem straightforward, we note that nobody appears to have reported this type of coupled experiment, and all the literature and extensive personal communications indicate that Zimm and $\partial n/\partial c$ plots are being obtained through separate (decoupled) MALS and DRI experiment.

Zimm (Berry) plots from coupled MALS-DRI experiments are shown in Figures 12A and 13A. $\partial n/\partial c$ plots from coupled MALS-DRI experiments are shown in Figure 14A and 15A.

4.3 Results and Discussion

Results from both the coupled and decoupled Zimm plot and $\partial n/\partial c$ plot experiments, for both the PS and PMMA samples, are given in Table 1 and Figures 12 - 15. The data were collected in two modes, as outlined in the *Experimental* section: First, with the individual MALS and DRI detectors, decoupled from each other. Second, with the detectors coupled to each other ("Coupled MALS-DRI"). Values given in Table 1 include the second virial coefficient (A_2), the z-average radius of gyration ($R_{G,z}$), and the weight-average molar mass (M_w), derived from the Berry plots shown in Figures 12 and 13, as well as the specific refractive index increment ($\partial n/\partial c$) values, obtained from the $\partial n/\partial c$ plots shown in Figures 14 and 15. The y-axis in Figure 12 and 13 is defined in equation 76 and the x-axis is sin2(θ/2)+kc where θ is the scattering angle θ, c is the concentration, and k is a

constant chosen to spread out the plot. We have chosen to plot the MALS data using Berry plots rather than Zimm plots as we found that, in all cases, the former provided a better fit to the data than the latter. This is likely due to the thermodynamically good solvent/temperature conditions of the experiments, that are evidenced by the large and positive A_2 values measured for all solutions.

From the comparisons established in Table 1 and in Figures 12 - 15, we see that the data and values obtained from the coupled- and decoupled-detector experiments are comparable to each other. M_w values from decoupled MALS experiments were calculated using $\partial n/\partial c$ values obtained from decoupled DRI experiments; M_w values from coupled MALS-DRI experiments were calculated using $\partial n/\partial c$ values obtained from coupled MALS-DRI experiments. In comparing results from coupled and decoupled experiments to each other, for PS the percent difference between $\partial n/\partial c$ values was 3%, between M_w values 6%, between A_2 values 6%, and between $R_{G,z}$ values 0%. For the type of batch-mode MALS experiments performed here, the percentage difference between M_w values is predicted by theory to be twice the percentage difference between $\partial n/\partial c$ values.[94] When both the MALS and DRI detectors are connected on-line to *e.g.*, a size-exclusion chromatography system, a given percentage error in the $\partial n/\partial c$ value will result in the same percentage error in the calculated value of M_w, assuming there are no other sources of experimental error.

Table 1 – Comparison of results obtained from coupled MALS-DRI method and when detectors are used individually

	Polystyrene		**Poly(methyl methacrylate)**	
	Coupled Detectors	**Decoupled Detectors**	**Coupled Detectors**	**Decoupled Detectors**
$\partial n/\partial c$ (mL g^{-1})	0.194 ± 0.002	0.188 ± 0.002	0.0856 ± 0.0017	0.0858 ± 0.0017
$M_w \times 10^5$ (g mol^{-1})	4.492 ± 0.039	4.802 ± 0.049	7.892 ± 0.047	7.899 ± 0.060
$R_{G,z}$ (nm)	22 ± 2	22 ± 2	28 ± 1	28 ± 1
$A_2 \times 10^{-4}$ (mol mL g^{-2})	3.707 ± 0.029	3.485 ± 0.032	1.889 ± 0.012	1.868 ± 0.015
R_T (nm)	20 ± 1	20 ± 1	23 ± 1	23 ± 1
Ψ*	0.52 ± 0.14	0.56 ± 0.15	0.40 ± 0.04	0.40 ± 0.04

For PMMA, percentage differences between values of any parameter never exceeded 1%. Also, if $\partial n/\partial c$ values obtained by the coupled and decoupled approaches for PS are averaged, and this average value (0.191 mL g^{-1}) is used for coupled and

decoupled MALS experiments, the differences between the values for M_w and A_2, as determined by the coupled and decoupled MALS methods, vanish.

The results obtained from the Zimm and the $\partial n/\partial c$ plots can be used to calculate other dilute-solution parameters, such as the thermodynamic radius R_T and the coil interpenetration function Ψ^*. The thermodynamic radius represents the radius of a solid sphere with the same excluded volume as the polymer, at the given solvent and temperature conditions of the solution. This radius is defined according to:[22, 91]

$$R_T = \left(\frac{3A_2 M_w^2}{16\pi N_A} \right)^{1/3} \tag{85}$$

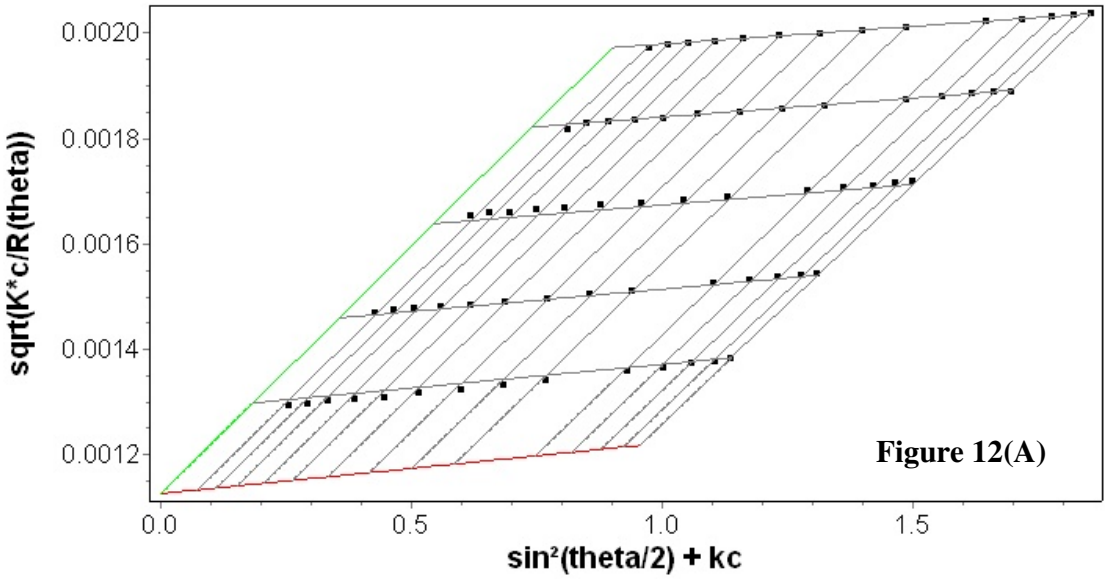

Figure 12(A)

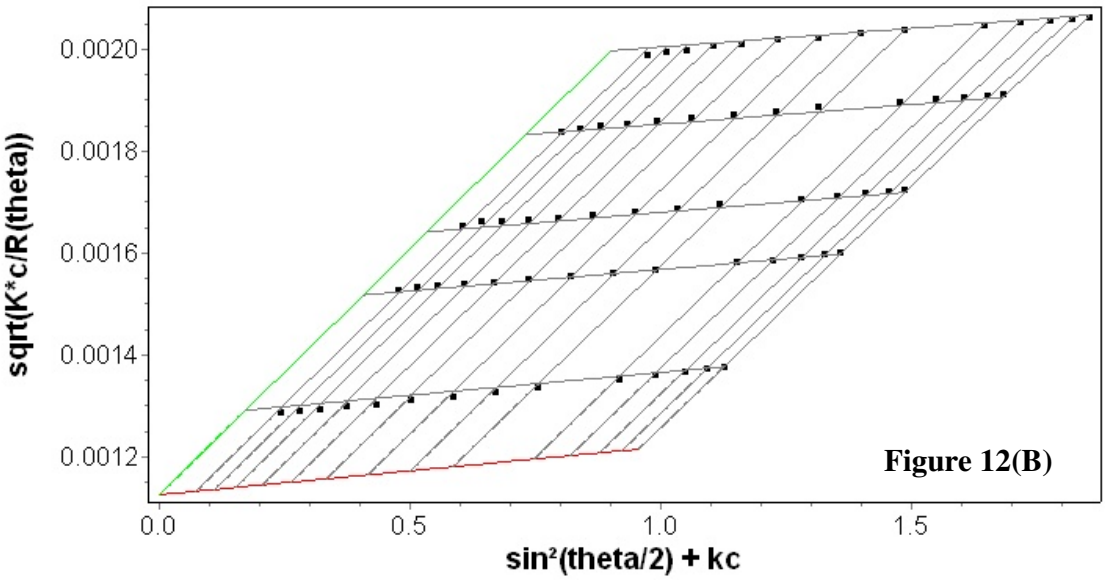

Figure 12. Berry plots for poly(methyl methacrylate) sample, obtained by (A) Coupled MALS-DRI method, (B) With MALS detector decoupled from DRI detector.

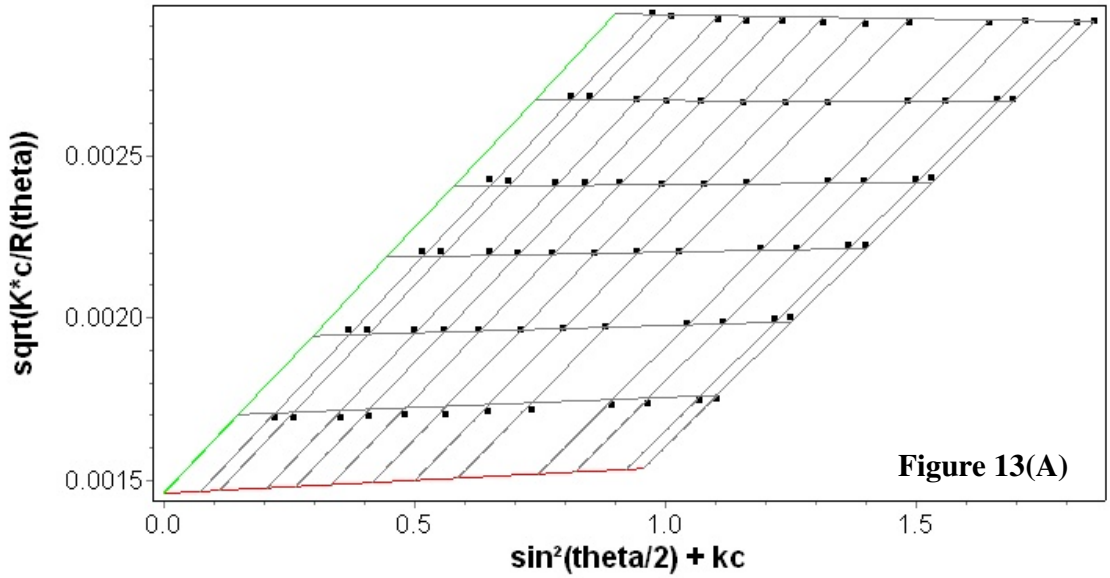

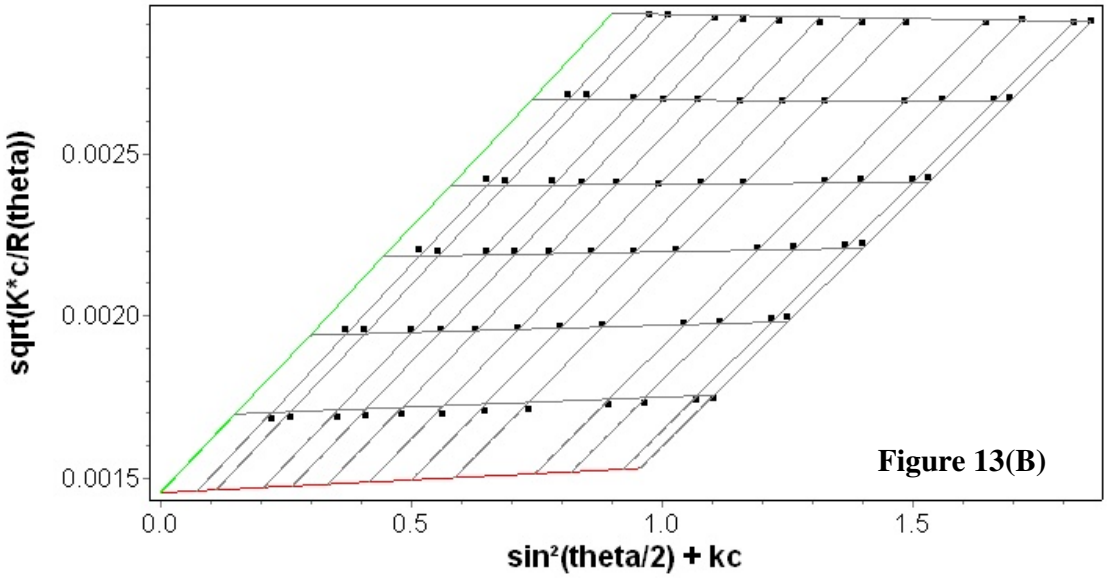

Figure 13: Berry plots for polystyrene sample, obtained by (A) Coupled MALS-DRI method, (B) With MALS detector decoupled from DRI detector.

The coil interpenetration function Ψ* is a dimensionless quantity, indicative of the degree of dilute solution interpenetration of the hydrodynamic volumes occupied by two consecutively-connected polymer chain segments. As is the case with R_T, the coil interpenetration function is defined in terms of parameters obtained from a Zimm plot, once the $\partial n/\partial c$ value is known:[22].

$$\Psi^* = \frac{A_2 M_w^2}{4\pi^{3/2} N_A R_G{}^3} \tag{86}$$

Alternatively, Ψ* is defined in terms of R_G and R_T as:

$$\Psi^* = \frac{4}{3\sqrt{\pi}} \frac{R_T^3}{R_G^3} \tag{87}$$

The thermodynamic radius and the coil interpenetration function have been used to gain a deeper understanding of dilute solution thermodynamics of polymer solutions, of the concept of size in polymer science, and, when used in conjunction with other parameters such as the polymer draining function, to relate dimensionless radii ratios to long-chain branching in macromolecules.[22, 91, 92] As seen in Table 1, values of R_T and Ψ* obtained with the coupled MALS-DRI method are comparable to values obtained when the detectors are decoupled from each other.

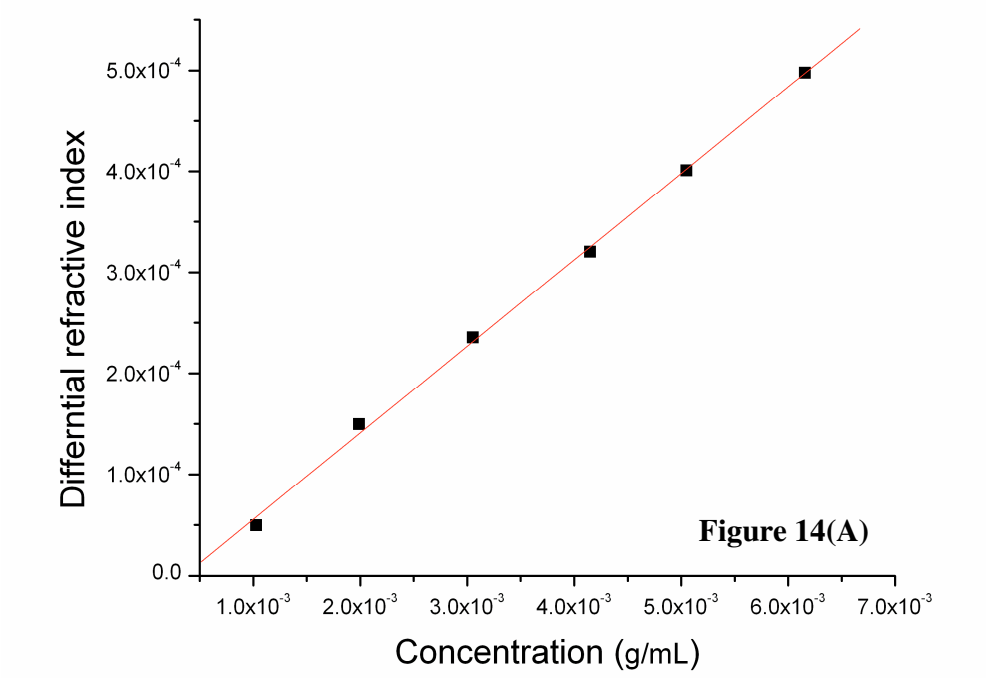

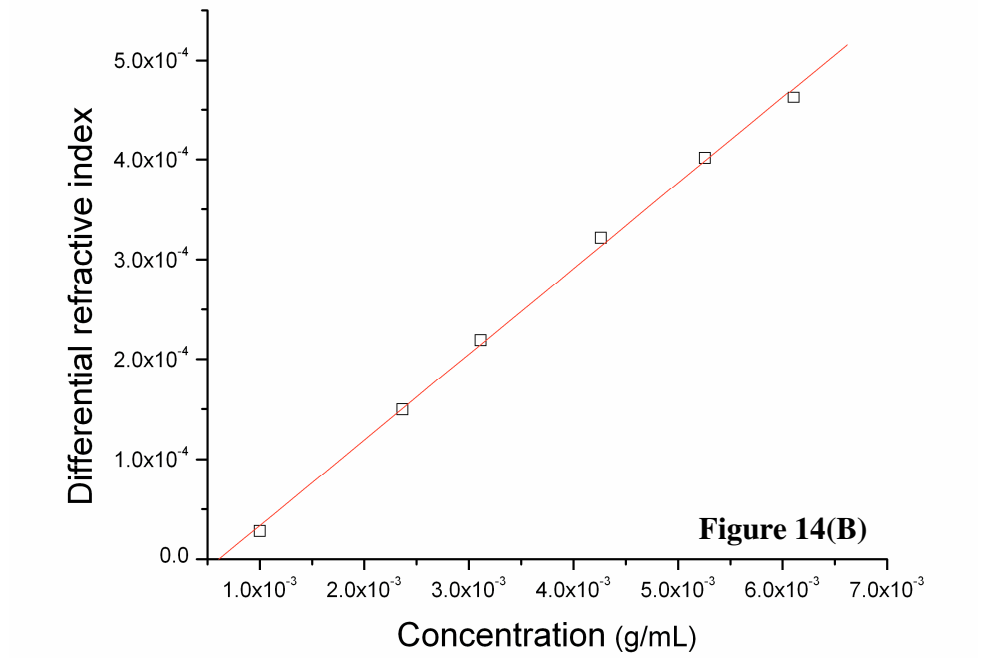

Figure 14. $\partial n/\partial c$ plots for poly(methyl methacrylate) sample, obtained by (A) Coupled MALS-DRI method, (B) With DRI detector decoupled from MALS detector. For all calculations error bars are smaller than point markers and, therefore, not shown.

To summarize, we have shown that the coupled MALS-DRI method of constructing Zimm and $\partial n/\partial c$ plots yields values of $\partial n/\partial c$, M_w, $R_{G,z}$, and A_2 comparable to

the values obtained when the MALS and DRI detectors are used individually. Parameters derived from these values, such as the thermodynamic radius and the coil interpenetration function, were likewise comparable when calculated from data obtained by either the coupled or decoupled methods. The precision in the results obtained by the coupled and decoupled approaches are also comparable. Use of the coupled MALS-DRI method results in a substantial savings of time and financial resources, through reduced solvent and disposables usage and reduced waste generation. Equally and, oftentimes, more importantly, the coupled MALS-DRI method should see favor in experiments where sample availability is limited.

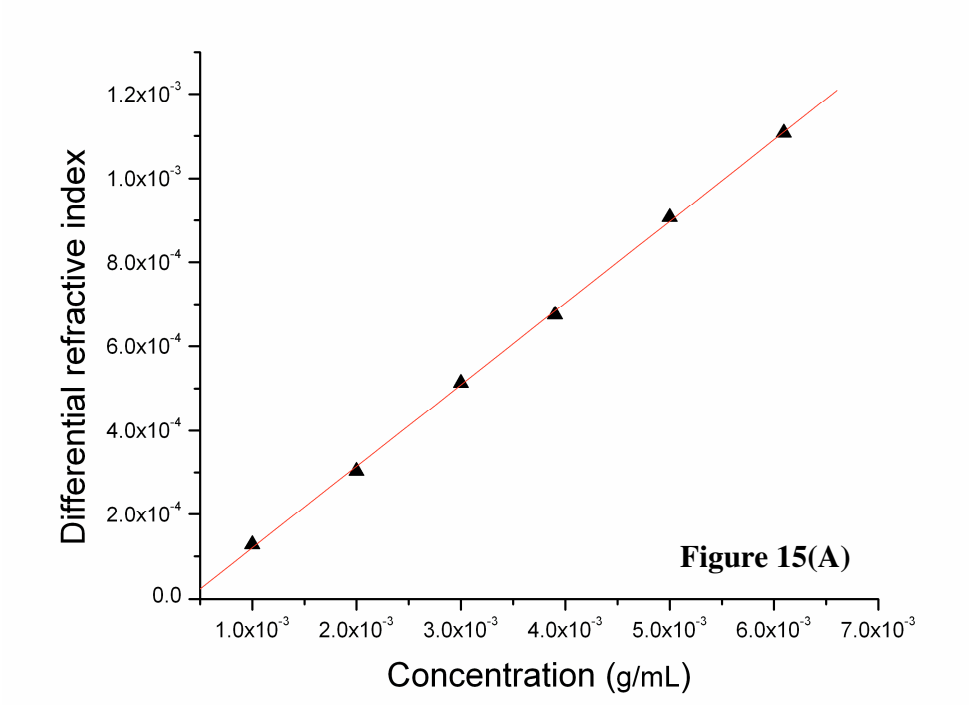

Figure 15(A)

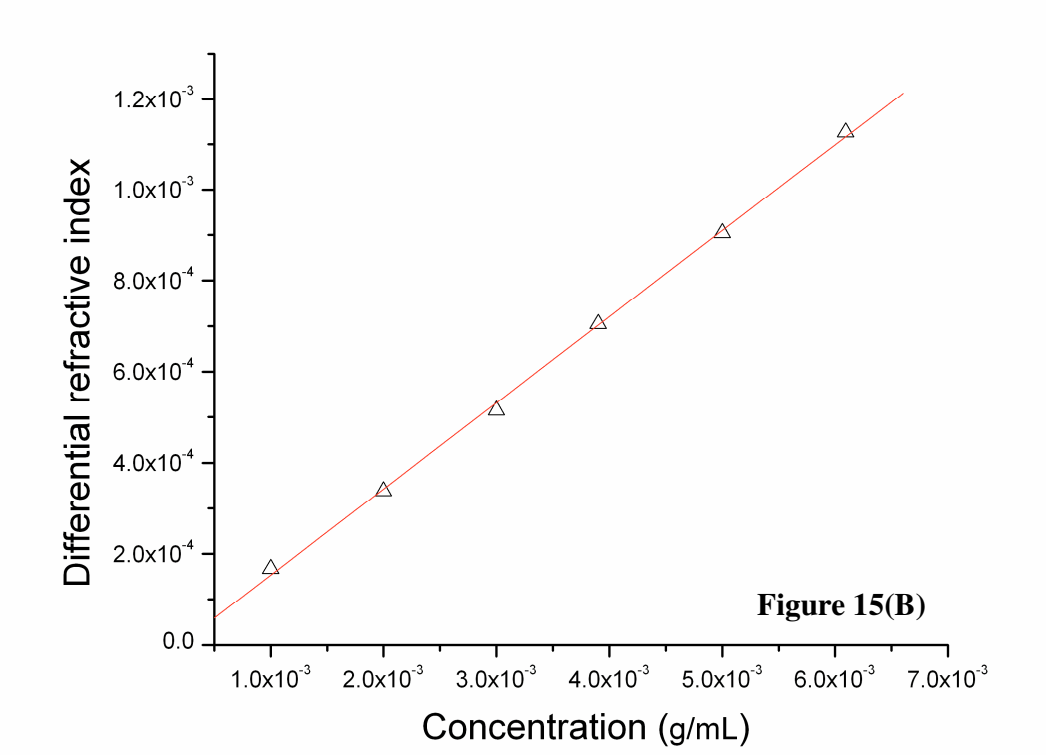

Figure 15. $\partial n/\partial c$ plots for polystyrene sample, obtained by (A) Coupled MALS-DRI method, (B) With DRI detector decoupled from MALS detector. For all calculations error bars are smaller than point markers and, therefore, not shown.

CHAPTER FIVE

DETERMINING THE ABSOLUTE, CHEMICAL-HETEROGENEITY-CORRECTED MOLAR MASS AVERAGES, DISTRIBUTION, AND SOLUTION CONFORMATION OF RANDOM COPOLYMERS

5.1 Objective

In gradient random copolymers, the relative ratios of the various functionalities change gradually and unidirectionally with respect to one another as the molar mass of the copolymer increases. This change in the percentage composition, generally termed "chemical heterogeneity," results in a change of the specific refractive index increment ($\partial n/\partial c$) of the copolymer as a function of its molar mass. This $\partial n/\partial c$ value is used for obtaining the absolute, i.e., calibrant-independent molar mass (M) using static light scattering techniques. In a polydisperse gradient random copolymer, using an average value for $\partial n/\partial c$ (such as that obtained from standard off-line, batch-mode differential refractometry (DRI) experiments explained in section 3.1) to obtain M results in biased molar mass averages and distributions. This bias in M results in erroneous values of the slope of the conformation plot (plot of the radius of gyration versus M) and the Mark-Houwink plot (plot of the intrinsic viscosity versus M). Both slopes are indicative of the conformation of the polymer in solution and/or of polymer architecture. Therefore, chemical heterogeneity results in an incorrect information about the structure of the copolymer in solution. In this project, we use size-exclusion chromatography coupled to multi-angle static light scattering, DRI, differential viscometry, and UV-Vis detectors to obtain the chemical-heterogeneity-corrected molar mass averages and distributions, as well as chemical-heterogeneity-corrected conformation, of a gradient random copolymer of polystyrene and poly(methyl methacrylate).

5.2 Chemical heterogeneity: importance and effects on copolymeric properties

Chemical heterogeneity affects both copolymeric properties and performance. Physical properties such as melting point and gas permeation[95], conductivity[96], fractionation in binary solvents[97], and refractive index and specific refractive index increment ($\partial n/\partial c$), are all affected by chemical heterogeneity[44], as well as properties such as the dynamic shear modulus and mechanical damping[98], the fracture energy at the interface between two immiscible polymers[99], and the separation process of copolymers by size-based as well as so-called "interactive" liquid chromatographic techniques[58-60, 100]. Also affected are the determination of copolymer molar mass averages and distributions by size-exclusion chromatography (SEC), not only when calibration curves are applied for determining the various M averages and distributions, but also when molar-mass-sensitive detectors such

as the static light scattering (SLS) photometer are used for this purpose. Lastly, our conclusions about the conformation the copolymer adopts in solution, arrived at via Mark-Houwink and conformation plots, are also affected by chemical heterogeneity, as will be shown here.

The molar mass averages and molar mass distribution (MMD) of random copolymers are usually obtained from SEC by applying calibration curves based on narrow polydispersity standards of homopolymers, or by using on-line SLS detection in conjunction with concentration-sensitive detection[86, 89, 90, 101]. When chemical heterogeneity is present in copolymers, both the calibration curve and light scattering approaches yield a biased, chemical-heterogeneity-dependent molar mass. The error associated with the molar mass obtained from applying a calibration curve is a result of the different chemical repeat units and/or architecture of the standards used in constructing the curve, as compared to the repeat units and conformation of the copolymer being examined. The source of bias when using an SLS detector is somewhat different.

In static light scattering the molar mass obtained is considered an absolute, calibrant-independent quantity that depends, crucially for our present discussion, on the specific refractive index increment ($\partial n/\partial c$) of the copolymer solution. The relation is given by the well-known Equation (76), oftentimes referred to as the Rayleigh-Gans-Debye approximation[90].

In a copolymer, the specific refractive index increment depends on the relative percentages of the monomers in a copolymer.[93, 102] For a copolymer possessing chemical heterogeneity, the molar mass obtained from static light scattering is biased when using, as is usually done, the average $\partial n/\partial c$ value of the bulk copolymer, obtained from unfractionated solutions and using a standard off-line, batch-mode differential refractometry (DRI) approach (such as that described in the section 3.1)

5.3 Chemical Heterogeneity: Our approach to detect chemical heterogeneity

Here, we demonstrate how to obtain the chemical-heterogeneity-corrected absolute molar mass and solution conformation of a copolymer through the use of SEC coupled to multi-angle static light scattering (MALS), differential refractive index (DRI), differential viscometry (VISC), and ultraviolet (UV) detectors. We correct for the bias in molar mass by calculating the chemical-composition-corrected $\partial n/\partial c$ value, for a gradient random copolymer of styrene and methyl methacrylate, at each slice eluting from the SEC columns. In this type of random copolymer the relative ratio of the two chemical functionalities, styrene and methyl methacrylate in the present case, changes gradually and unidirectionally as the molar mass of the copolymer increases. These corrected $\partial n/\partial c$ values are then incorporated into the static light scattering equation (equation (76)), as applied to each slice eluting from the SEC columns. Once the chemical-composition-corrected M_w and concentration of each slice are obtained, the chemical-heterogeneity-corrected molar mass averages and distribution can be calculated.

As part of this study, we also obtain the chemical-heterogeneity-corrected solution conformation of the gradient copolymer. This involves correction of the conformation plot for bias in molar mass M and correction of the Mark-Houwink plot for bias in both M and in intrinsic viscosity [η].

5.4 Chemical Heterogeneity: importance of our Approach

Obtaining the chemical-heterogeneity-corrected molar mass is essential for characterizing copolymeric properties that depend on M, such as the width of the rubbery plateau[103], stress and strain[104], crystallization kinetics[105, 106], melting point[105, 107], and phase structure[105, 107], and properties that depend on the conformation in solution such as photophysical behavior[108] and the conformation the copolymer adopts in films[109]. Previously, chemical heterogeneity has been reported as a function of either calibrant-relative molar mass or of an SLS-determined molar mass not corrected for compositional bias.[30, 32, 39, 42-45, 109-120] In studies where molar mass was corrected for chemical-heterogeneity-bias, either a paucity of fractions were collected for off-line NMR and MALDI-MS analysis[121] or the use of low-angle static light scattering detection (and/or the absence of a viscometric detector)[122, 123] precluded obtaining information regarding the solution structure of the copolymers.

Here, our use of MALS and viscometry detection in conjunction with DRI and UV detection allows us to correct not only the molar mass averages and distribution for chemical heterogeneity, but also the Mark-Houwink and conformation plots and the structural and conformational information derived therefrom.

5.5 Experimental approach to detect chemical heterogeneity and correct bias in copolymeric properties

5.5.1 Materials

Narrow polydispersity ($M_w/M_n \leq 1.05$) linear polystyrene (PS) and poly(methyl methacrylate) (PMMA) standards were obtained from Varian/Polymer Laboratories (Amherst, MA USA), the gradient random copolymers P(St-*co*-MMA) and the random copolymer P(St-*co*-*t*BMA) were obtained from Polymer Source. Unstabilized tetrahydrofuran (THF) was from EMD (Gibbstown, NJ, USA). All materials were used as received, without further purification.

5.5.2 Multi-Detector Size-Exclusion Chromatography (SEC/MALS/UV/VISC/DRI)

For the multi-detector SEC experiments, a concentration of 1 mg/mL of the copolymer in THF was prepared and left on a laboratory wrist-action shaker overnight to ensure

dissolution. For increased precision, two different 1 mg/mL solutions of the sample were prepared and, from each dissolution, two injections were performed for a total of four injections. The SEC system consisted of a Waters 2695 Separations Module (Waters, Milford, MA, USA), three PLgel 10 μm particle size Mixed-B SEC columns, (Varian/Polymer Laboratories), and four detectors connected in series: A DAWN EOS multi-angle static light scattering photometer (Wyatt Technology Corp., Santa Barbara, CA, USA), followed by a Model 166 UV detector (Beckman-Coulter, Fullerton, CA, USA), followed by an Viscostar differential viscometer (Wyatt), followed by an Optilab rEX differential refractometer (Wyatt). The wavelength of the lamp in the UV detector is set to 260 nm, where styrene (St) absorbs preferentially over methyl methacrylate (MMA). A 31,400 g/mol narrow polydispersity (M_w/M_n = 1.02) PS linear standard was used for normalization of the MALS unit photodiodes, as well as for calculating interdetector delays and for interdetector band broadening correction.[124] Data acquisition was performed using Wyatt's ASTRA software (V.5.3.2.13), plotting and calculations were performed with OriginPro 7.5 (V.7.5885, Origin Lab Corp., Northampton, MA, USA).

5.5.3 Specific Refractive Index Increment ($\partial n/\partial c$) Determination

The specific refractive index increments ($\partial n/\partial c$) of the polymers in THF at 25 °C were: 0.191 ± 0.002 mL/g for PS, 0.087 ± 0.001 mL/g for PMMA, and 0.114 ± 0.002mL/g for the gradient random copolymer P(St-*co*-MMA). The samples were dissolved in THF and left overnight on a wrist-action shaker to ensure full dissolution and solvation. For offline $\partial n/\partial c$ determination, six dilutions of each sample, ranging from 1.0-6.0 mg/mL, were injected directly into the Optilab rEX differential refractometer (Wyatt) using a Razel model A-99EJ syringe pump. Flow rate was 0.08 mL/min. Sample solutions were filtered through 0.45 μm Teflon syringe filters, neat THF for baseline determination through a 0.02 μm Teflon syringe filter. The wavelength of the lamp in the DRI detector is filtered to match the vacuum wavelength of the laser in the MALS detector (λ_0 = 685 nm). Data acquisition and processing were done with Wyatt's ASTRA V software (V. 5.3.2.13).

5.6 Results and Discussion

5.6.1 Calculating the chemical composition at each SEC elution slice

The UV and DRI detectors of the SEC/MALS/UV/VISC/DRI system were employed to determine the percentage composition (given as weight percent styrene, *%St*) of each slice *i* of the gradient copolymer P(St-*co*-MMA) eluting from the SEC columns. This *%St* was determined according to equation (88).

$$(\%St)_i = \frac{Z_i\left(\frac{\partial n}{\partial c}\right)_{PMMA}}{F\left(\frac{\partial n}{\partial c}\right)_{PS} - Z_i\left[\left(\frac{\partial n}{\partial c}\right)_{PS} - \left(\frac{\partial n}{\partial c}\right)_{PMMA}\right]} \times 100\% \qquad (88)$$

$$where \quad F = \frac{S_{UV,PS}}{S_{DRI,PS}} = constant \qquad and \qquad Z_i = \frac{S_{UV,i}}{S_{DRI,i}}$$

where F is the ratio of the signal of the UV detector to that of the DRI detector for a polystyrene homopolymer, and Z_i is the ratio of the UV signal to the DRI signal for the gradient copolymer at each slice i.

5.6.2 Correcting molar mass averages and distribution for chemical heterogeneity

The signals from the differential refractive index (S_{DRI}) and static light scattering (S_{SLS}) detectors are both directly dependent on the specific refractive index increment $\partial n/\partial c$, as shown in equations (89) and (90), respectively. In turn, the ratio of the signals from the static light scattering and differential refractive index detectors is proportional to the product of molar mass and specific refractive index increment, as shown in equation (91):

$$S_{DRI} \propto c \times \left(\frac{\partial n}{\partial c}\right) \qquad (89)$$

$$S_{SLS} \propto M \times \left(\frac{\partial n}{\partial c}\right)^2 \times c \qquad (90)$$

$$\frac{S_{SLS}}{S_{DRI}} \propto \frac{M \times \left(\frac{\partial n}{\partial c}\right)^2 \times c}{\left(\frac{\partial n}{\partial c}\right) \times c} = M \times \left(\frac{\partial n}{\partial c}\right) \qquad (91)$$

When analyzing a copolymer by SEC, at each elution slice i the specific refractive index increment $(\partial n/\partial c)_i$ is directly dependent on the percentage composition of the copolymer fraction eluting in said slice. Thus, if chemical heterogeneity is present in a random copolymer, so also will the copolymer have a heterogeneity in specific refractive index increment: The $\partial n/\partial c$ of the copolymer will change as a function of M, as a result of the change in chemical composition as a function of M. It is this $\partial n/\partial c$-heterogeneity that causes the bias in molar mass averages and distributions when these parameters are determined by SEC with SLS and a single concentration-sensitive detector (be it DRI, UV, etc.), and it is this bias that we here seek to correct. The chemical-heterogeneity-corrected molar mass of each slice, $M_{corrected,i}$, is obtained from equation (92) (it should be realized that this is the corrected weight-average molar mass of each slice; each slice is

assumed to be narrow enough to be considered virtually monodisperse with respect to M):

$$M_{corrected,i} = M_{uncorrected,i} \times \frac{\left(\frac{\partial n}{\partial c}\right)_{uncorrected}}{\left(\frac{\partial n}{\partial c}\right)_{corrected,i}} \tag{92}$$

where $(\partial n/\partial c)_{uncorrected}$ is the specific refractive index increment of the bulk copolymer solution, obtained via the traditional off-line, batch-mode DRI approach described in the Experimental; $M_{uncorrected,i}$ is the molar mass of each slice, uncorrected for chemical heterogeneity and obtained from the traditional SEC/SLS/DRI approach; and $(\partial n/\partial c)_{corrected,i}$ is the specific refractive index increment of each slice, corrected for chemical heterogeneity as explained next. We note that equations (88), (92), and (93) are valid because PMMA has, as stated in the experimental, zero absorbance at 260 nm, whereas PS absorbs strongly at this wavelength.

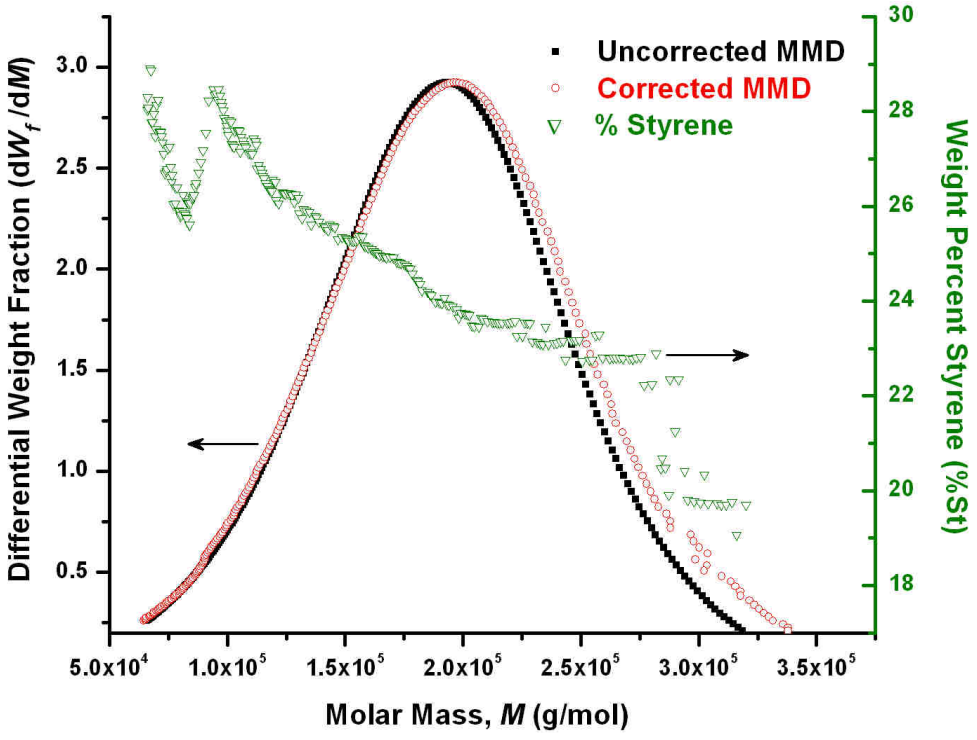

Figure 16. Chemical heterogeneity, and correction of molar mass distribution due to chemical heterogeneity, in a gradient copolymer of styrene and methyl methacrylate. (■) Represents uncorrected MMD. (o) Represents corrected MMD. (▽) Represents chemical heterogeneity (given as weight percent styrene, *%St*).

It should be realized that $M_{corrected,i}$ is the corrected weight-average molar mass of each slice; each slice is assumed to be narrow enough to be considered virtually

monodisperse with respect to M. While local polydispersity (i.e., the heterogeneity of structures and/or chemical species of different molar mass, but which occupy the same hydrodynamic volume, present in a single SEC elution slice[90, 125, 126] may still be an issue, the lack of branching and the similarity in the hydrodynamic volumes occupied by PS and PMMA under the present conditions both contribute to minimizing this effect.

The *%St* of the gradient random copolymer used in this study changes gradually, from ~30% at the low molar mass end of the molar mass distribution to ~19% at the high molar mass end, as shown in Figure 16. The $\partial n/\partial c$ value for each slice *i*, corrected for chemical heterogeneity, can be calculated according to

$$\left(\frac{\partial n}{\partial c}\right)_{corrected,i} = \left(\frac{\partial n}{\partial c}\right)_{PS} (\%St)_i + \left(\frac{\partial n}{\partial c}\right)_{PMMA} (\%MMA)_i \qquad (93)$$

where $(\%St)_i$, the weight percentage of styrene in SEC elution slice *i*, is determined using equation (88); $(\%MMA)_i$ corresponds to the weight percentage of methyl methacrylate in the same elution slice of the copolymer, obtained from the relation $(\%MMA)_i = [100\% - (\%St)_i]$; and $(\partial n/\partial c)_{PS}$ and $(\partial n/\partial c)_{PMMA}$ are the specific refractive index increments of the individual homopolymers at the same experimental conditions used to analyze the gradient random copolymer. The $\partial n/\partial c$ values of the PS and PMMA homopolymers are 0.191 mL/g and 0.087 mL/g, respectively (see Experimental). Accordingly, the $\partial n/\partial c$ of the gradient random copolymer used in this study is expected to decrease as molar mass increases (i.e., as elution volume decreases), a direct result of the generally decreasing styrene percentage in the copolymer as a function of increasing molar mass (see Figure 16).

For comparison purposes, we first calculated the molar mass averages and distribution of the gradient copolymer using the "traditional" SEC/MALS/DRI approach, which relies on the average $\partial n/\partial c$ value of the bulk copolymer ($(\partial n/\partial c)_{uncorrected} = 0.114$ mL/g; see Experimental). Results from these calculations are given in the second column ("Uncorrected") of Table 2 and as filled squares in Figure 16. Because of chemical heterogeneity, the *M* averages and distribution are biased and a correction is needed to ensure their accuracy. According to equation (92), the molar mass at the low end of the uncorrected molar mass distribution is overestimated because the average $\partial n/\partial c$ of the bulk copolymer, obtained from the offline-DRI experiment, is larger than the corrected $\partial n/\partial c$ obtained for a low-*M* slice using equation (93). (As can be seen in Figure 16, for the gradient copolymer studied this underestimation is negligible and the corrected and uncorrected molar mass distributions overlap in the low-*M* region). Conversely, the molar mass at the high end of the uncorrected distribution is underestimated, because the average $\partial n/\partial c$ value is lower than the corrected $\partial n/\partial c$ value for a slice at this end of the MMD. As a result, the corrected MMD covers an approximately 30,000 g/mol wider range than does the uncorrected distribution, as seen in Figure 16.

The average $\partial n/\partial c$ value of 0.114 mL/g for the bulk copolymer solution, used for obtaining the uncorrected molar mass averages and distribution, corresponds to an average percentage composition of ~25 *%St*. Because the *%St* in the gradient copolymer ranges from ~30–19 *%St*, the absolute value of the error in the percentage composition at both the high and low ends of the molar mass distribution is ~5%. Even though the percentage error in the specific refractive index increment is comparable at both ends of the distribution, the magnitude of the error in molar mass at each end is different (as expected for the case of determinate, proportional error): The magnitude of the error in *M* at the high end of the distribution is larger than that at the low end of the distribution. As seen in Figure 16 (and as mentioned parenthetically above), the corrected and uncorrected MMDs virtually overlay one another in the low molar mass region, clearly not the case at high molar masses. This difference between the magnitude of the error at the high and low ends of the MMD is due to the dependence of the corrected molar mass on the magnitude of the uncorrected molar mass, i.e., of $M_{corrected}$ on $M_{uncorrected}$, as shown in equation (92). Therefore, the absolute value of the error in molar mass of a copolymer, due to the error in percentage composition, increases as the molar mass of the copolymer increases, as per:

$$\left|M_{error,i}\right| = \left|M_{corrected,i} - M_{uncorrected,i}\right| = M_{uncorrected,i} \times \left| \frac{\left(\frac{\partial n}{\partial c}\right)_{uncorrected}}{\left(\frac{\partial n}{\partial c}\right)_{corrected,i}} - 1 \right| \qquad (94)$$

As expected, the values of the various statistical moments (averages) of *M* are also affected by chemical heterogeneity. As can be seen when comparing the second ("Uncorrected") and third ("Corrected") columns of Table 2, because of chemical heterogeneity the uncorrected moments underestimate the true *M*, and the error in *M* associated with each moment increases with increasing statistical moment, such that $\left|M_{n,error}\right| < \left|M_{w,error}\right| < \left|M_{z,error}\right|$. This increase in error with increasing statistical moment is due to the molar mass fractions added during correction of the MMD for chemical heterogeneity, with an incrementally greater percentage of molar mass being added at higher molar masses than at lower ones, as seen in Table 2 and Figure 16.

Finally, because the individual *M* averages are obtained from equation (95)[90],

$$M_{\beta} = \frac{\sum c_i M_i^{x}}{\sum c_i M_i^{x-1}} \qquad \text{(when } x = 0, \beta = n\text{; when } x = 1, \beta = w\text{; when } x = 2, \beta = z\text{)} \qquad (95)$$

the refractometer response must be corrected at each elution slice to ensure that accurate concentrations c_i are used in determining M_n, M_w, M_z, etc., as well as the MMD of the copolymer. This is done by incorporating the $(\partial n/\partial c)_{corrected,i}$, obtained using equation (93), into the following rearranged form of equation (89):

$$c_{i,corrected} \propto \frac{S_{DRI,i}}{\left(\frac{\partial n}{\partial c}\right)_{i,corrected}} \tag{96}$$

where $S_{DRI,i}$ is the signal from the refractometer for slice i. The proportionality sign is converted into an equality sign by using the calibration constant for the individual refractometer employed.

Table 2: Correction of SEC/MALS-determined molar mass averages and polydispersity for error due to chemical heterogeneity.

	Uncorrected	Corrected
M_n (g/mol)	170,000 ± 11,900	175,000 ± 11,900
M_w (g/mol)	200,000 ± 800	209,000 ± 800
M_z (g/mol)	234,000 ± 2,100	250,000 ± 2,100
M_w/M_n	1.18 ± 0.08	1.19 ± 0.07

5.6.3 Chemical-heterogeneity-corrected Mark-Houwink and conformation plots

Another copolymeric property affected by chemical heterogeneity is the intrinsic viscosity $[\eta]$, defined in equation (97)[86, 89, 90, 101]:

$$[\eta]_i \equiv \lim_{c\to 0} \frac{\eta_{sp,i}}{c_i} \tag{97}$$

The intrinsic viscosity at elution slice i is the ratio of the specific viscosity of that slice $\eta_{sp,i}$ obtained from the differential viscometer (VISC), to the concentration c_i of the slice obtained from the differential refractometer (DRI), for a near-infinitely-dilute solution. As a result of this dependence of the intrinsic viscosity on concentration for a gradient copolymer, the intrinsic viscosity is biased due to chemical heterogeneity and a correction is needed, as shown in equation (98):

$$[\eta]_{corrected,i} = [\eta]_{uncorrected,i} \times \frac{\left(\frac{\partial n}{\partial c}\right)_{corrected,i}}{\left(\frac{\partial n}{\partial c}\right)_{uncorrected}} = \lim_{c\to 0}\left(\frac{\eta_{sp,i}}{c_{corrected,i}}\right) \propto \lim_{c\to 0}\frac{\eta_{sp,i}}{S_{DRI,i}} \times \left(\frac{\partial n}{\partial c}\right)_{corrected,i} \tag{98}$$

The conformation a polymer adopts in dilute solution is usually determined by one of two common methods, the Mark-Houwink plot (the plot of the intrinsic viscosity $[\eta]$ as a function of molar mass M, with both axes plotted on a logarithmic scale) and the conformation plot (the plot of the radius of gyration R_G as a function of M, with both axes plotted on a logarithmic scale). For a copolymer with chemical heterogeneity both these plots will be biased, the conformation plot due to chemical-heterogeneity-bias in M, the

Mark-Houwink plot due to bias in both $[\eta]$ and M. It is of interest to note that while the various R_G averages ($R_{G,n}$, $R_{G,w}$, $R_{G,z}$, and so on) and the R_G distribution are biased due to chemical heterogeneity, the $R_{G,z}$ values measured *at each slice* using MALS are not. This is because accurate calculation of the R_G distribution and of $R_{G,n}$, $R_{G,w}$, $R_{G,z}$, etc. of the bulk copolymer depends on accurate knowledge of the concentration of copolymer in each slice (as per equation (101) in Section 5.8). Conversely, the $R_{G,z}$ of each slice is determined by angular dissymmetry (i.e., by the difference in the amount of light scattered by the polymer solution at one angle versus another), independent of concentration. The equation for correcting the $R_{G,z}$ of the bulk sample (i.e., not the $R_{G,z}$ of individual slices which, again, is not necessary) is derived in Section 5.8.

In the present case, the correction of the $R_{G,z}$ of the bulk sample for the effects of chemical heterogeneity results in a change in radius which is exceeded by the uncertainty of the measurement, i.e., the change in $R_{G,z}$ is less than ±1 nm. The difference between the corrected and uncorrected $R_{G,z}$ values of the bulk copolymer will become more noticeable either for larger copolymers, when chemical heterogeneity is greater, or both. We next examine the correction for chemical heterogeneity of the Mark-Houwink and conformation plots.

The Mark-Houwink plot is obtained when the eponymous equation $[\eta] = KM^a$ is written as:

$$\log[\eta] = a \log M + \log K \tag{99}$$

and the intrinsic viscosity is plotted versus molar mass, with both axes on a logarithmic scale. The slope of this equation, a, is indicative of the structure of the polymer in solution and its value ranges from 0 for a hard sphere to 2 for a rigid rod, with a value in the range of 0.5–0.8 for a linear random coil at good solvent/temperature conditions[89, 90, 101]. For a gradient copolymer, a bias in the Mark-Houwink plot results from the chemical heterogeneity bias in both $[\eta]$ and M. To obtain a chemical-heterogeneity-corrected plot, equation (98) is used to correct the bias in $[\eta]$ and equation (92) is used to correct the bias in M.

The corrected and uncorrected Mark-Houwink plots are is shown in Figure 17. A significant change is observed in the slope, a (as well as in the y-intercept, log K). Before correction, the slope $a = 0.71 \pm 0.01$; after correction, $a = 0.60 \pm 0.01$. The particular change in slope subsequent to correction for chemical heterogeneity indicates that the gradient copolymer is less extended in solution than was originally concluded from the uncorrected Mark-Houwink plot.

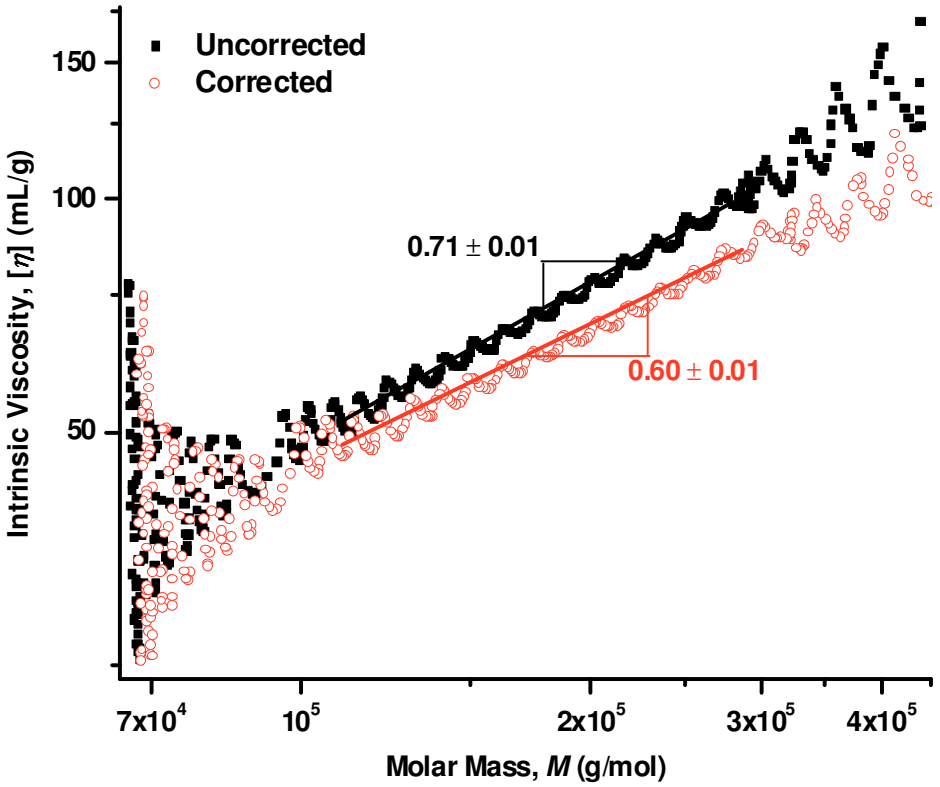

Figure 17. Correction of Mark-Houwink plot for effects of chemical heterogeneity in a gradient copolymer of styrene and methyl methacrylate. Solid lines correspond to first-order linear fit of data between 110,000 and 300,000 g/mol.

The conformation plot is based on the relation $R_G = kM^{\alpha}$ when written as the equation for a straight line:

$$\log R_G = \alpha \log M + \log k \tag{100}$$

As with a, the slope of the Mark-Houwink plot, α, the slope of the conformation plot is also indicative of the conformation of the polymer in solution. The value of this slope varies between 0.33 for a hard sphere of uniform density to a value of 1 in the case of a rigid rod, with a value of ~0.5–0.6 for a linear random coil structure at good solvent/temperature conditions[28, 86, 89, 90, 101].

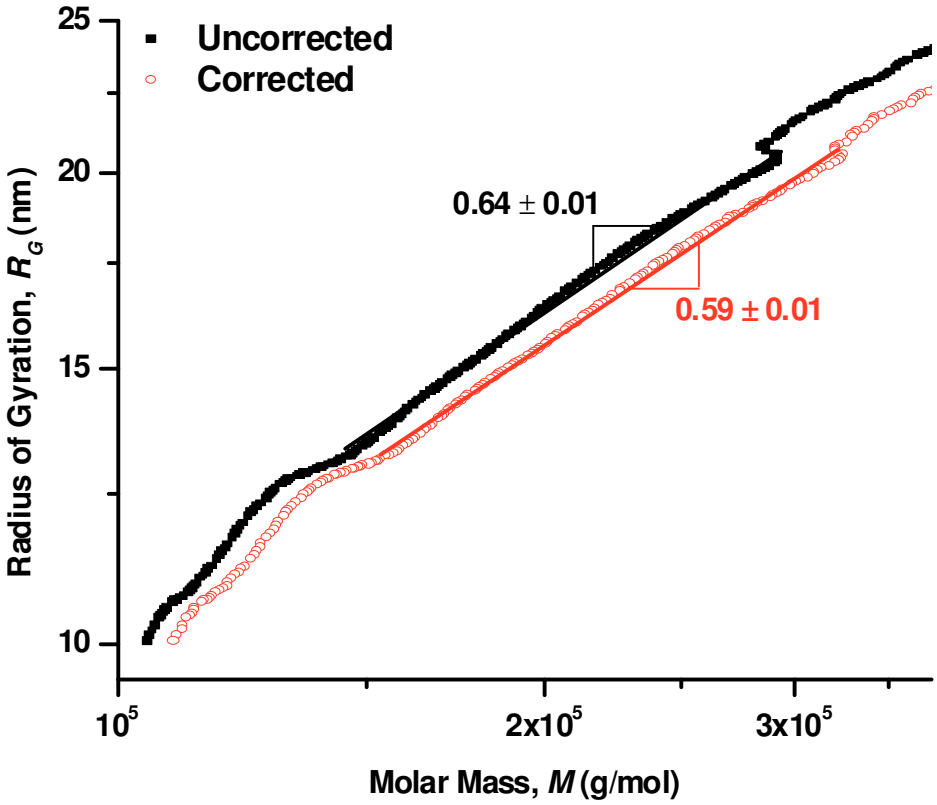

Figure 18. Correction of conformation plot for chemical heterogeneity in a gradient copolymer of styrene and methyl methacrylate. Solid lines correspond to first-order linear fit of data between 13 and 20 nm

Correction of the conformation plot for chemical heterogeneity effects is performed using equation (92) to correct for the bias in M. As mentioned above, no correction is needed for the R_G values at each slice, which constitute the y-axis of the plot. Figure 18 shows the corrected and the uncorrected conformation plot of the gradient copolymer of polystyrene and polymethyl methacrylate. The corrected value of the slope α is 0.59 ± 0.01, the uncorrected value is 0.64 ± 0.01. As was the case with the Mark-Houwink plot, the corrected conformation plot shows that the gradient copolymer adopts a less extended conformation in solution than originally believed. To our knowledge, this is the first report on correcting Mark-Houwink and conformation plots for the effects of chemical heterogeneity.

5.6.4 Determining the absolute, chemical-heterogeneity-corrected molar mass averages and distribution of styrene-co-t-butyl methacrylate.

Using the same approach followed in Section 5.6.2, the chemical-heterogeneity-corrected molar mass averages and distribution of a styrene-*co*-*t*-butyl methacrylate random copolymer is calculated, as shown in Figure 19 and Table 3. In this styrene-*co*-*t*-butyl

methacrylate random copolymer, the *%St* varies between values of ~ 50% to ~ 60%. Eventhough the refractive index increments of methyl methacrylate and *t*-butyl methacrylate are very close to each other, the error in molar mass distribution and molar mass averages in the case of S-BMA random copolymer is different than that of the S-MMA random copolymer. The bias in the molar mass due to chemical heterogeneity in the S-*t*BMA copolymer is more pronounced that of the S-MMA copolymer because the molar mass of the former is less than that of the latter, which results in larger bias in molar mass, as proved in equation (94).

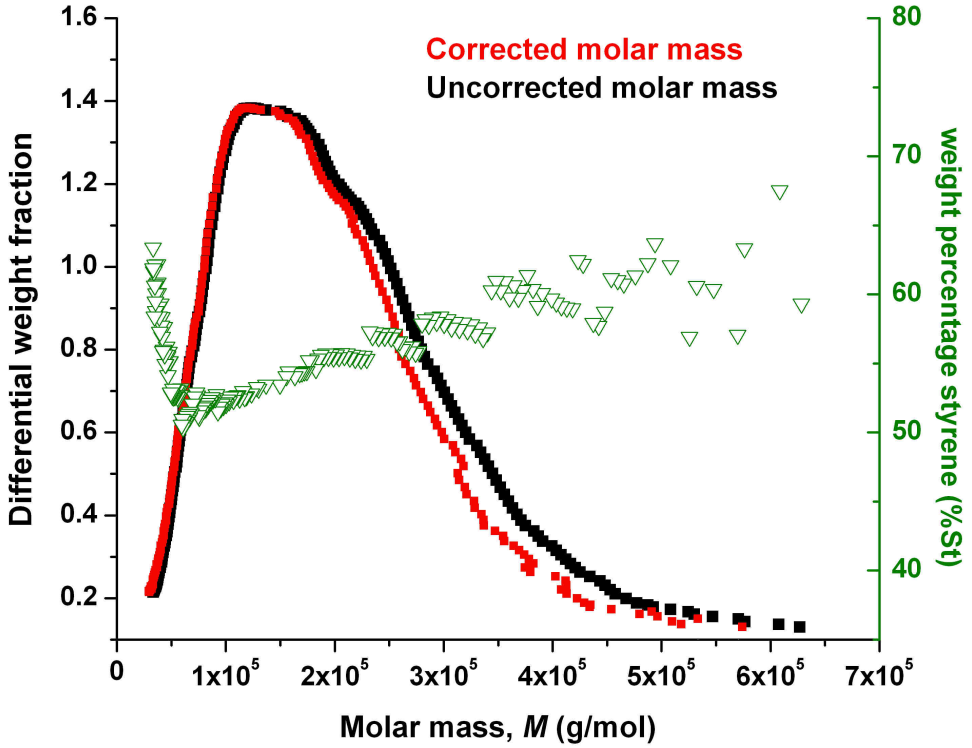

Figure 19. Chemical heterogeneity, and correction of molar mass distribution due to chemical heterogeneity, in a gradient copolymer of styrene and *t*-butyl methacrylate. (■) Represents uncorrected MMD. (■) Represents corrected MMD. (▽) Represents chemical heterogeneity (given as weight percent styrene, *%St*).

Table 3: Correction of SEC/MALS-determined molar mass averages and polydispersity for error due to chemical heterogeneity.

	Uncorrected	Corrected
M_n (g/mol)	160,000 ± 1,000	150,000 ± 1,000
M_w (g/mol)	224,000 ± 1,000	205,000 ± 1,000
M_z (g/mol)	281,000 ± 1,000	254,000 ± 2,000
M_w/M_n	1.39 ± 0.01	1.36 ± 0.01

5.7 Conclusions

The molar mass averages and distributions of broadly polydisperse homo- and copolymers are obtained most commonly and conveniently using size-exclusion chromatography and, in general, most accurately using a combination of a static light scattering (SLS) photometer and a single concentration-sensitive detector. For copolymers possessing chemical heterogeneity, however, the concomitant heterogeneity in specific refractive index increment across the chromatographic elution profile yields a bias in the molar mass averages and distributions obtained by the SEC/SLS method. Failure to correct this bias can adversely affect properties that depend on the different *M* averages, especially on higher moments such as M_w and M_z (as chemical-heterogeneity-bias increases with increasing statistical moment of *M*), such as flex life and stiffness [127], resistance to degradation[128], and miscibility of polymer-polymer blends[129, 130]. Chemical heterogeneity also affects our conclusions about the conformation of the copolymer in solution, as derived from the Mark-Houwink and conformation plots. Other Conclusions for this project are explained in Section 7.3.

5.8 Correcting the $R_{G,z}$ of a Bulk Copolymer for Chemical Heterogeneity

In an SEC/MALS/DRI experiment, the *z*-average radius of gyration $R_{G,z}$ of a bulk *homopolymer* polymer (i.e., not the $R_{G,z}$ of each SEC elution slice, to which we shall refer here for simplicity as r_i) which, by definition, does not necessitate correction for chemical heterogeneity, is calculated according to:

$$R_{G,z} = \frac{\sum_i c_i M_i r_i^2}{\sum_i c_i M_i} \tag{101}$$

We want to find the corrected $R_{G,z}$ value of a copolymer which possesses chemical heterogeneity, given the corrected concentration *c* and molar mass *M* values. We have

$$R_{G,z\ uncorrected} = \frac{\sum_i (c_i + \delta_{c_i})(M_i + \delta_{M_i}) r_i^2}{\sum_i (c_i + \delta_{c_i})(M_i + \delta_{M_i})} \tag{102}$$

where c_i is the corrected *c* value at slice *i*, M_i is the corrected *M* value at slice *i*, δ_{c_i} is the amount of correction of *c* at slice *i*, and δ_{M_i} is the amount of correction for *M* at slice *i* (with the realization that the various δ terms may be either positive or negative).

By expansion

$$\sum_i (c_i + \delta_{c_i})(M_i + \delta_{M_i}) = \sum_i c_i M_i + \delta_{c_i} M_i + \delta_{M_i} c_i + \delta_{c_i} \delta_{M_i} \quad (103)$$

Because $\sum_i c_i M_i$ is needed in the corrected $R_{G,z}$ equation, let the right hand side of equation (103) be written as

$$\sum_i c_i M_i + \varepsilon_i \quad (104)$$

where $\varepsilon_i = \delta_{c_i} M_i + \delta_{M_i} c_i + \delta_{c_i} \delta_{M_i}$.

Substituting equation (104) into equation (102) results in

$$R_{G,z\ uncorrected} = \frac{\sum_i c_i M_i r_i + \varepsilon_i r_i^2}{\sum_i c_i M_i + \varepsilon_i r_i} \quad (105)$$

Manipulation of equation (105) results in

$$(\sum_i c_i M_i + \varepsilon_i) R_{G,z\ uncorrected} - \sum_i \varepsilon_i r_i^2 = \sum_i c_i M_i r_i^2 \quad (106)$$

Dividing both sides by $\sum_i c_i m_i$ yields

$$\frac{\left(\sum_i c_i M_i + \varepsilon_i\right) R_{G,z\ uncorrected} - \sum_i \varepsilon_i r_i^2}{\sum_i c_i M_i} = \frac{\sum_i c_i M_i r_i^2}{\sum_i c_i M_i} \quad (107)$$

As per equation (101), the right hand side of equation (107) is the corrected value of $R_{G,z}$, i.e., $R_{G,z,corrected}$. Simplifying equation (107) results in

$$R_{G,z\ corrected} = \left(1 + \frac{\sum_i \varepsilon_i}{\sum_i c_i M_i}\right) R_{G,z\ uncorrected} - \frac{\sum_i \varepsilon_i r_i^2}{\sum_i c_i M_i} \quad (108)$$

CHAPTER SIX:

SEQUENCE LENGTH HETEROGENEITY[131]

6.1 Introduction: Definition and importance

Sequence length heterogeneity (SLH) is the change in the average number of continuous and similar (i.e., same chemical repeat unit) monomers in a copolymer as the chain grows. This type of heterogeneity exists in the case of a random copolymer, i.e., a polymer comprising two different types of monomers randomly distributed within the chain. A random copolymer is shown in Figure 1, along with the other types of copolymers used in this study. The arrangement of monomers in the polymeric chain is uniform in the case of alternating and block copolymers, not so in the case of random copolymers where the random arrangement of monomers in the chain results in a distribution of the number of continuous and similar monomers. The change in this distribution as a function of molar mass is given the term "sequence length heterogeneity" and abbreviated as SLH.

The ability to detect SLH is important for understanding both its sources and its effect on structure-property relationships. Examples of the polymeric properties affected by SLH are the ability to reduce interfacial surface tension via copolymeric adsorption at a liquid-liquid interface;[132] the conformation and folding of protein-like copolymers;[11, 12, 74, 133-135] and the thermal stability,[67] melting point,[62] mechanical behavior,[136] and transparency of films.[76, 137] SLH originates from the different probabilities with which monomers arrange in a copolymeric chain, from chemical heterogeneity (i.e., from the change in the relative percentage of a particular monomer among copolymeric chains of different molar mass)[31], and from the change in mutual miscibility of monomers during the copolymerization process. Here, we show a new, semi-quantitative method capable of detecting SLH in random copolymers. This method provides an approach to understanding the "randomness" of a random copolymer, i.e., to determining whether a random copolymer is of blocky, statistical, or alternating nature, and to ascertaining how this randomness changes as a function of molar mass.

Previous approaches to study how copolymeric randomness has focused on SLD or the instantaneous monomer sequence length. Theoretical approaches included some computational and theoretical work to study the probability of distributing the monomers in the copolymeric chain[62, 63] while experimental approaches in this regard included using: 1) light scattering and dynamic light scattering to study distribution of monomers in a copolymeric chain by studying the coil-to-globule chain transition at critical conditions[74], 2) Selective degradation of one monomer in a copolymer chain followed by NMR analysis to study SLD[75], 3) adding metal halide to control the co-monomer sequence distribution during a free radical polymerization followed by NMR analysis[138], 4) detecting the effect of a catalyst on the SLD by NMR analysis[76], 5) Relating the peak

shift in FT-IR of certain monomeric functionalities in to the neighboring groups of that monomer[64, 65].

6.1.1 Previous approach versus our approach

In this study, we relate SLH to the enthalpic intrachain repulsion which manifests itself in the form of entropic change affecting the conformation of the copolymer in solution. This intrachain repulsion occurs at the junction points between dissimilar monomers (as explained by the Flory-Huggins theory in the Appendix).[80-82] Consequently, the change in the dispersion of the monomers in a copolymeric chain, i.e., the SLH, results in a change in intrachain repulsion along the copolymeric chain due to the variation in the percentage of the number of junction points as a function of the degree of polymerization. These intrachain enthalpic interactions force the chain to adopt a conformation that minimizes intrachain repulsion. Therefore, the change in enthalpy is balanced by a change in entropy in the form of conformational change.[81] In this project, we use the ratio of the viscometric radius to the radius of gyration, R_η/R_G, to determine the conformation of the copolymer in solution and to detect the SLH by detecting the change in conformation (as will be explained subsequently). Our conclusions are supported by results from infrared experiments and agree with research from a probability theory model.

6.2 The R_η/R_G ratio

The radius of gyration (R_G) is a statistical radius as well as the only nonequivalent-hard-sphere radius used to define the size of a polymer in solution. This radius can be determined via static multi-angle light scattering and it depends on the difference in the intensity of the scattered light measured at dissimilar angles. The radius of gyration of the polymer is defined as per[22, 28, 91, 101, 139].

$$R_G = \left[\left(\frac{1}{n+1} \right) \sum_i (r_i - R_{cm})^2 \right]^{1/2} \tag{109}$$

where n is the number of monomers in a polymeric chain, r_i is the location of the ith monomer, and R_{cm} is the location of the center of mass.

The viscometric radius (R_η) is defined as the radius of a hard sphere that enhances the viscosity of the solvent by the same amount imparted by the polymer. This radius is calculated using an equation relating the intrinsic viscosity [η] to the molar mass M of a polymer. Because [η] is obtained from viscosity and M form static light scattering, both techniques are needed to obtain R_η. The equation for calculating the viscometric radius was shown previously in equation (81) as:[22, 91, 101]

$$R_\eta \equiv \left(\frac{3\,[\eta]\,M}{10\,\pi\,N_A} \right)^{1/3} \tag{81}$$

R_η/R_G is the ratio of the viscometric radius to the radius of gyration. This dimensionless ratio is indicative of the conformation of the polymer in solution. It is also indicative of the topology of the polymer, i.e., polymers with different topologies have different R_η/R_G values. For example, polystyrene star polymer has an R_η/R_G value larger than 0.87 and approaching the hard sphere limit $(5/3)^{1/2}$ as the number of arms increases, while the R_η/R_G of linear polystyrene is approximately 0.7.[140-142]

6.2.1 R_η/R_G values of the different conformations in solution

The ratio of the viscometric radius to the radius of gyration is a dimensionless parameter that is indicative of the polymer structure in solution. This ratio increases as the compactness of the polymer in solution increases. Thus, a polymer A which is more expanded in solution than polymer B is expected to have a smaller R_η/R_G ratio than that of B. The expected R_η/R_G values of the different polymeric structures in solution are shown in Figure 20. A rigid rod conformation is the most extended structure a polymer can adopt in solution. The expected R_η/R_G value for this conformation is approximately 0.3, which is similar to the value obtained for a highly extended polymer[143]. The hard sphere structure is the most compact structure of a polymer in solution. This structure has an R_η/R_G value of approximately 1.3. The random coil conformation of polymers in solution is a flexible conformation having R_η/R_G values covering the range of approximately 0.70 to 0.90[22, 141, 144, 145].

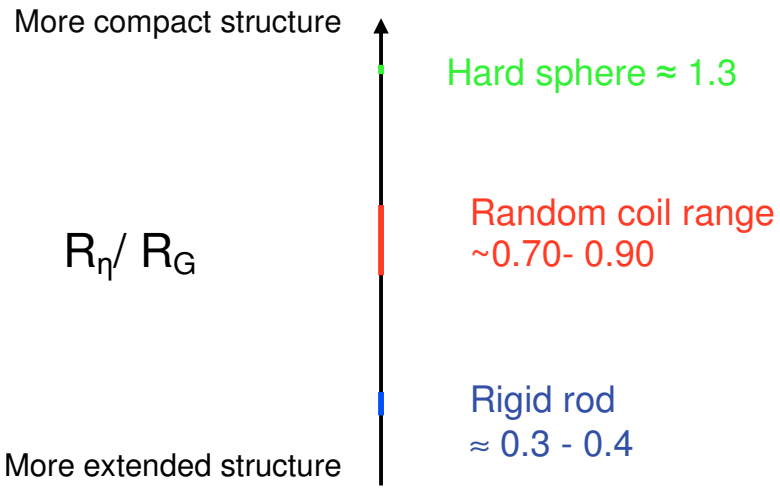

Figure 20. The R_η/R_G value of the different conformations in solution

The dimensionless ratio R_η/R_G is known to depend on polymer architecture. This ratio increases as the compactness of the polymer in solution increases, and vice-versa. Thus, as a polymer adopts a more extended conformation in solution, its R_η/R_G ratio decreases. A rigid rod conformation is the most extended structure a polymer can adopt in solution, and the theoretical R_η/R_G value for this conformation is ~0.3[143]. The hard sphere structure is the most compact structure a polymer can adopt and has an R_η/R_G value of approximately $\sqrt{5/3}$. Random coil polymers adopt a flexible conformation in solution, corresponding to R_η/R_G values in the range of approximately 0.70 to 0.90.[22, 141, 144, 145] Previous work in this area has focused on using either the sequence length distribution which is conceptually different than SLH (similar to the difference between chemical composition distribution and chemical heterogeneity), or the instantaneous monomer sequence length to study how copolymeric randomness changes as a function of *M*. A distinct advantage of the present method is that it relies solely on physical properties (angular dissymmetry and intrinsic viscosity) of the copolymers; i.e., success is not contingent upon chemical properties as preferential UV absorption of one monomer over another in a copolymer. An additional advantage of the method is that it does not rely on specialized equipment. Rather, it utilized a type of separation-detector combination that is nowadays commonplace in most polymer characterization laboratories.

Needed for our approach is a separation technique capable of fractionating polymers according to molar mass, and which can also measure R_η and R_G as a continuous function of *M*. Multi-detector size-exclusion chromatography (SEC) using multi-angle static light scattering (MALS), differential viscometry (VISC), and differential refractometry (DRI) detection fits the bill and is, thus, our method of choice.[89, 90] Thus, this triple-detector SEC technique can be used to obtain the R_η/R_G ratio as a continuous function of *M*, a novel approach which, to our knowledge, is the first experimentally established link between R_η/R_G and SLH.

6.3 Experimental

6.3.1 Materials. Homopolymers of polystyrene (PS) and poly(methyl methacrylate) (PMMA) were obtained from Varian/Polymer Laboratories and Toyo Soda, copolymers of PS-PMMA and PS-PBMA from Polymer Source, unstabilized THF was obtained from EMD, methylene chloride from VWR. All materials were used as received, without further purification.

6.3.2 Multi-Detector Size-Exclusion Chromatography: SEC/MALS/VISC/DRI and SEC/MALS/UV/DRI. For the multi-detector SEC experiments, a concentration of 1 mg/mL of each copolymer in THF was prepared and left on a laboratory wrist-action shaker overnight to ensure dissolution. For increased precision, two different 1 mg/mL solutions of each sample were prepared and, from each dissolution, two injections were performed, for a total of four injections per sample. The SEC system consisted of a

Waters 2695 Separations Module (Waters), three PLgel 10 μm particle size Mixed-B SEC columns, (Varian/Polymer Laboratories), and three detectors connected in series: A DAWN EOS multi-angle static light scattering (MALS) photometer (Wyatt Technology Corp.), followed by either a Model 166 UV detector (Beckman-Coulter) or a ViscoStar differential viscometer (Wyatt), followed by an Optilab rEX differential refractometer (Wyatt). The wavelength of the lamp in the UV detector is set to 260 nm, where styrene (S) absorbs strongly and methyl methacrylate (MMA) does not absorb. A 31,400 g/mol narrow polydispersity (M_w/M_n = 1.02) linear PS standard was used for normalization of the MALS unit photodiodes as well as for calculating interdetector delays and for interdetector band broadening correction. Data acquisition was performed using Wyatt's ASTRA software (V.5.3.2.1), plotting and calculations were performed with OriginPro 7.5 (V.7.5885, Origin Lab Corp.).

Table 4. Polymers used in this study.

Polymer	M_w/M_n [a]	% of styrene	Manufacturer
PS (186k)[b]	1.07	100	Toyo Soda
PS (533k)[b]	1.05	100	Varian/Polymer Laboratories
PS (723k)[b]	1.05	100	Varian/Polymer Laboratories
PMMA (343k)[b]	1.02	0	Varian/Polymer Laboratories
PMMA (467k)[b]	1.06	0	Varian/Polymer Laboratories
PS-*b*-PMMA (46K, 138K)[c]	1.16	25[d]	Polymer Source
PS-*b*-PMMA (131K, 46K)[c]	1.10	75[d]	Polymer Source
PS-*ran*-PMMA (Mn 126K)[b]	1.39	20[a]	Polymer Source
PS-*ran*-PMMA (Mn 186K)[b]	1.43	25[a]	Polymer Source
PS-*alt*-PMMA (Mn 235K)[b]	1.85	50[a]	Polymer Source
PS-*co*-PMMA (Mn 140K)[e]	1.42	24.4[a,f]	Polymer Source
PS-*co-tert*-PBMA (Mn 96K)[b]	1.7	50.0[a]	Polymer Source

[a] Values from the manufacturer
[b] Value in parenthesis represents number-average molar mass, M_n, as reported by manufacturer.
[c] First value in parenthesis represents M_n of PS block, second value represents M_n of the PMMA block, both values as reported by manufacturer.
[d] Percentages are calculated using the molar mass of each block
[e] Gradient random copolymer
[f] Average value. %S in this copolymer extends from ~ 30% at the low end of the MMD to ~ 20% at the high end of the MMD.

6.3.3 Fraction collection. To collect elution fractions of the random copolymers, for subsequent characterization by FT-IR (see below), we employed an SEC system consisting of a Waters 2695 Separations Module, three PLgel 10 μm particle size Mixed-B SEC columns, a DAWN EOS MALS photometer, and an F203B fraction collector (Gilson). A concentration of 6 mg/mL of each the 126k and the 186k random copolymers

in uninhibited THF was prepared and left on a laboratory wrist-action shaker overnight to ensure dissolution. For each copolymer, twenty injections were performed and, from each injection, three fractions were collected: Fraction 1 was collected between the range of 35.6 and 39.6 mL elution volumes, fraction 2 between 40.1 and 42.1 mL, and fraction 3 between 42.6 and 46.6 mL.

6.3.4 FT-IR. The solvent collected from the previous experiment was vaporized using a rotary evaporator and the remaining dried polymer was dissolved in ~3 mL of methylene chloride. The solution was then added dropwise to the surface of a KBr crystal dropwise and left until the solution dried out completely. FT-IR spectra of the copolymer deposited on the surface of the crystal were obtained using a Thermo Nicolet Avatar 360 FTIR (Termo Nicolet Corp.). Data acquisition was performed using OMNIC (V.6.0, Thermo Nicolet Corp.), peak fitting and calculation of area under the peaks at 1074 and 1730 cm^{-1} were performed with the peakfit module of OriginPro 7.5 (V.7.5885, Origin Lab Corp.). Peak fitting was performed to calculate the area under the peak at 1074 cm^{-1}, because of the partial overlap of two peaks at 1074 and 1064 cm^{-1} in the spectra of the random copolymers.

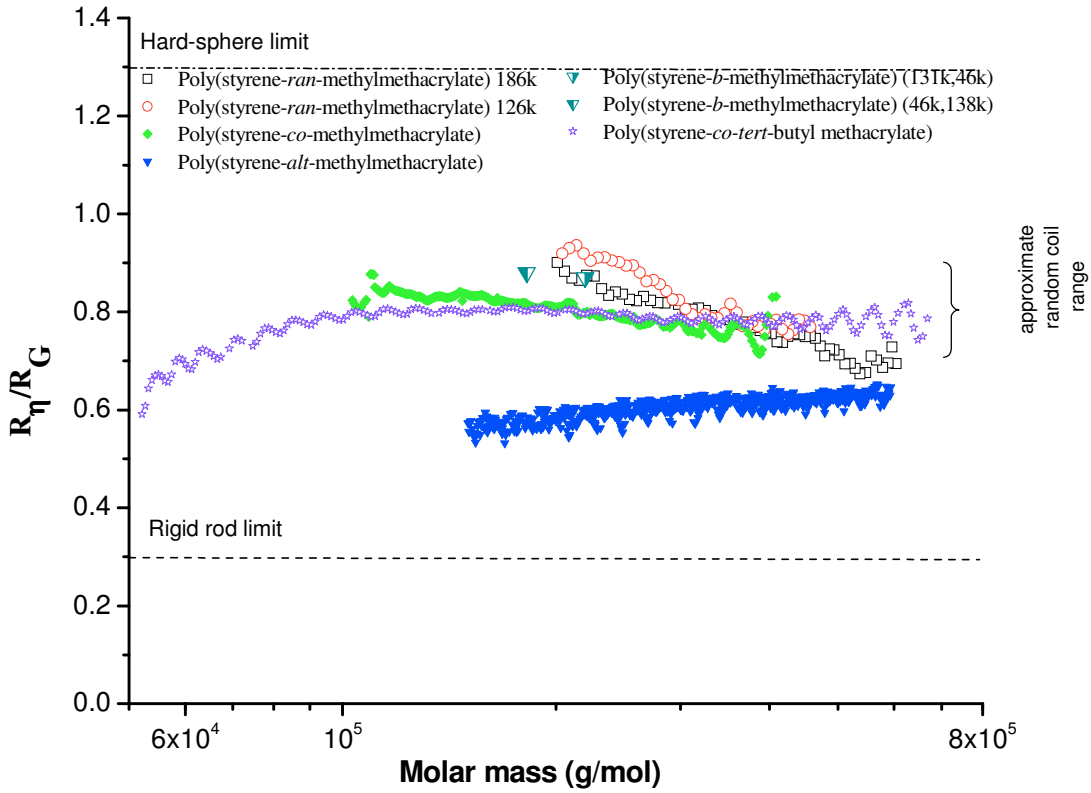

Figure 21. R_η/R_G ratio of homopolymers and block, alternating, random, and gradient random copolymers of styrene and methyl methacrylate.

6.4 Results and discussion

Polystyrene, poly(methyl methacrylate), and their respective random, block, alternating, and gradient random copolymers were used in this study. Polystyrene is denoted as PS, poly(methyl methacrylate) as PMMA, random copolymers as PS-*ran*-PMMA, block copolymers as PS-*b*-PMMA, alternating copolymer as PS-*alt*-PMMA, and gradient random copolymer as PS-*co*-PMMA. We shall also denote the copolymer of styrene and *tert*-butyl methacrylate as PS-co-*tert*-BMA. Table 4 gives relevant properties of the copolymers used in this study, while Figure 1 shows generic versions of the different types of copolymers

In Figure 21, we observe a variation in the R_η/R_G ratio as a function of molar mass for the two random copolymers studied. The R_η/R_G ratio varies from a maximum value in which the random copolymers appear to behave like either a homo- or block copolymer, to a minimum value where the random copolymers adopt a structure resembling that of the alternating copolymer studied. Here, we show that this decrease in the R_η/R_G ratio, and thus the increase in chain extension of the copolymer, is due to SLH. In what follows, we define a quantity termed the junction point ratio (*JPR*), which will be used to interpret the R_η/R_G and supporting FT-IR results. *JPR* is explained subsequently.

6.4.1 Junction point ratio (JPR)

The junction point ratio is defined as the ratio of the total number of junction points between dissimilar monomers to the total number of junction points between any two monomers. The latter is equivalent to the degree of polymerization minus one (i.e., to *n-1*). For large degrees of polymerization ($n >> 1$), the total number of junction points between dissimilar monomers is essentially equal to the degree of polymerization. The junction point ratio is defined as per:

$$\text{Junction point ratio} = JPR = \frac{\text{total number of junction points between dissimilar monomers}}{\text{total numbers of junction points}} = \frac{\text{total number of junction points between dissimilar monomers}}{\text{degree of polymerization - 1}} \quad (110a)$$

and for large degree of polymerization as:

$$\text{Junction point ratio} = JPR = \frac{\text{total number of junction points between dissimilar monomers}}{\text{degree of polymerization}} \quad (110b)$$

The value of the *JPR* shown in equation (110b) varies between two limiting cases which are provided by alternating copolymers, for which the *JPR* =1, and by block copolymers or homopolymers, for which the *JPR* is ~0. For both types of copolymers, alternating and block, as well as for homopolymers, at large *n* the *JPR* is expected to be molar-mass-independent, i.e., to remain constant as a function of *M*. In the case of

random copolymers, the *JPR* changes depending on the distribution of monomers in the chain. As a random copolymer becomes more alternating than blocky, the *JPR* approaches 1; as the copolymer becomes more blocky than alternating, the *JPR* approaches 0. The change in the *JPR* value is indicative of the presence of sequence length heterogeneity, as seen in Figure 22. In this figure, the SLH is manifested as a change in the *JPR* value, as shown in the change from 3a to 3c and from 3a to 3d. The change from 3a to 3c results in an increase in the *JPR* value, i.e., $\Delta JPR = JPR_{final} - JPR_{initial} \approx 0.83\text{-}0.64 = 0.19 > 0$, which indicates that the distribution of monomers in copolymer 3c is more alternating than it is in copolymer 3a. The change from 3a to 3d results in a decrease in the *JPR* value, i.e., $\Delta JPR = JPR_{final} - JPR_{initial} \approx 0.39\text{-}0.64 = -0.25 < 0$, indicating that the distribution of monomers in copolymer 3c is more blocky than that in 3a. The change in the monomeric distribution from 3a to 3b is negligible, i.e., $\Delta JPR = JPR_{final} - JPR_{initial} \approx 0.65\text{-}0.64 \approx 0.01$, which indicates a virtual absence of SLH. From the preceding discussion, it should be evident that a change in *JPR* with increasing *M* of a copolymer is indicative of SLH in a copolymer.

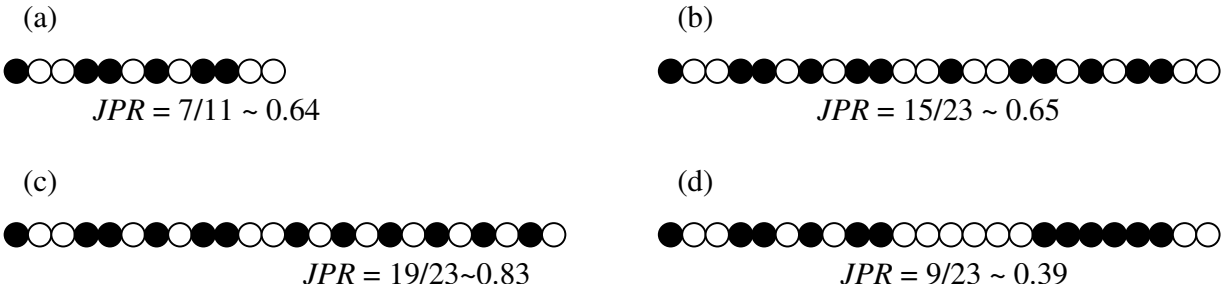

Figure 22. Sequence length heterogeneity (SLH) and its relation to change in the junction point ratio (*JPR*). (a) Random copolymer of molar mass *M*; (b), (c), and (d) random copolymers of molar mass 2*M*. There is absence of SLH in the change from (a) to (b), where $\Delta JPR \approx 0$, whereas SLH occurs in the change from (a) to (c) and from (a) to (d). In the change from (a) to (c), the copolymer becomes more alternating ($\Delta JPR > 0$), while it becomes more blocky when changing from (a) to (d) ($\Delta JPR < 0$).

6.4.2 Quantitative analysis of junction point ratio through FT-IR.

As seen in Figure 23(a), the FT-IR spectra of the alternating copolymer of styrene and methyl methacrylate show a significant peak at ~1074 cm^{-1}, which is absent in the case of both block copolymers and homopolymers. As shown by Mori,[48] the area under this peak at is affected by the presence of a styrene monomer next to a methyl methacrylate monomer. The peak at 1074 cm^{-1} is due to C-C stretching where a phenyl is attached to one of the carbons and a polar group is attached to the other carbon (alternating and random copolymer in Figure 23(b)). In the case where a phenyl groups is substituted into each of the carbons, the C-C shift occurs at a lower wavenumber (1063cm^{-1}) (as in the case of block copolymer and PS in Figure 23(b)). In the case of a random copolymer, the two peaks at 1074 cm^{-1} and 1065 cm^{-1} overlap (see section 6.3.4 for explaining how to calculate the area under peak at 1074 cm^{-1}).

As a result, the area under the peak at ~1074 cm^{-1} in a random copolymer of styrene and methyl methacrylate is proportional to the *JPR* of the copolymer. For both random copolymers used in this study, the area under the peak at 1074 cm^{-1} is expected to increase as a function of molar mass due to the expected increase in *JPR* with increasing *M*. In order to verify this hypothesis, three fractions of different *M* were collected for each of the two random copolymers; the fractions are numbered according to their elution from the SEC column; i.e., fraction 1 elutes first and has the highest *M*, while fraction 3 elutes last and has the lowest molar mass. Fraction 2 is intermediate in both elution volume and molar mass relative to fractions 1 and 3.

Table 5 compares normalized peak areas of the 1074 cm^{-1} FT-IR peaks for the alternating copolymer and both random copolymers studied. Normalization, performed to account for differences in the concentration of the different fractions, was done with respect to the peak at ~ 1730 cm^{-1}, which corresponds to the carbonyl stretch in MMA, while also accounting for the percent MMA in the sample, according to

$$\text{Normalized } 1074\,\text{cm}^{-1} \text{ peak area} = \frac{\text{area under peak at } 1074\,\text{cm}^{-1}}{\text{area under peak at } 1730\,\text{cm}^{-1}} \times \frac{100}{\%\ methyl\ methacrylate} \quad (111)$$

Table 5. Area under FT-IR peak at 1074 cm^{-1}, indicative of *JPR* in copolymer

Fraction number	Normalized 1074 cm^{-1} peak area[a]		
	186k random copolymer	**126k random copolymer**	**Alternating copolymer**
Fraction 1[b]	0.148 ± 0.003	0.080 ± 0.001	0.216 ± 0.014
Fraction 2[c]	0.137 ± 0.003	0.057 ± 0.001	
Fraction 3[d]	0.057± 0.002	0.032 ± 0.001	

[a] As per equation (111)
[b] For SEC slices eluting between 35.6 mL and 39.6 mL.
[c] For SEC slices eluting between 40.1 mL and 42.1 mL.
[d] For SEC slices eluting between 42.6 mL and 46.6 mL.

As seen in Table 5, for both random copolymers the normalized peak area shows a gradual decrease from fraction 1 (highest *M*) to fraction 3 (lowest *M*), indicating that the percent of styrene-methyl methacrylate interaction sites in a random copolymer increases as the molar mass increases with increasing *M*. In Table 5 we also observe the normalized area of the 1074 cm^{-1} peak of the alternating copolymer in substantially longer than the areas for any of the fractions of either random copolymers. This is in agreement with the alternating copolymer possessing the maximal junction point ratio of any copolymeric arrangement of dissimilar monomers. All the above results confirm our conclusions regarding the presence of *SLH* in random copolymers, as discerned from the M-dependence of the R_η/R_G ratio.

Also noted in Table 5 are the larger peak areas of fractions 1-3 of the 186k random copolymer, as compared to the same fraction of the 126k random copolymer. Because each fraction was collected over the same elution volume of each copolymer, some explanation of these differences warranted. Two main factors contribute to these differences in normalized peak areas: First, the percentage of styrene monomer is higher in the 186k random copolymer than its 126k random counterpart. As seen in Figure 24, this corresponds to a higher percentage of "2 interaction" sites (see Figure 24, inset) for a particular degree of polymerization in the 186 random copolymer, i.e., sites in which a styrene monomer bonded to a methyl methacrylate monomers at both ends (see section 6.6 for explanation of model). It is these "2 interaction" sites that contribute maximally to intrachain repulsion in dilute solution. Hence, for particular degree of polymerization, larger normalized FT-IR 1074 cm^{-1} peak areas is expected for the fraction of the 186 random copolymer, due to higher styrene content.

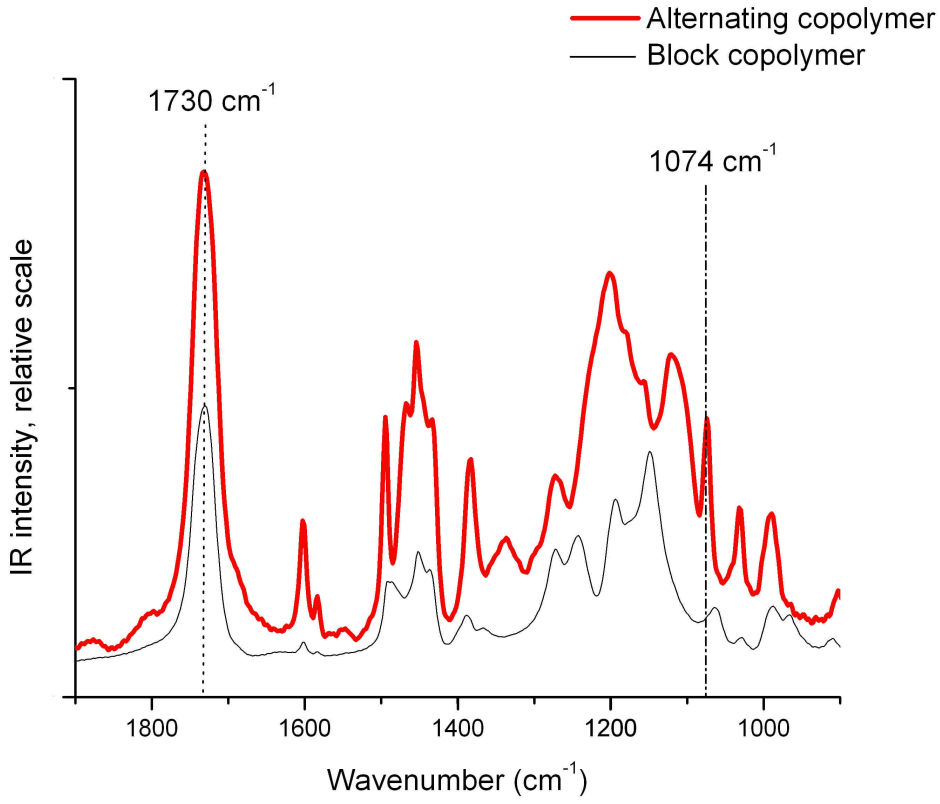

Figure 23(a). FT-IR spectra of alternating and block copolymers of styrene and methyl methacrylate. See text for experimental details

6.4.3 Modeling SLH using the probability theory

The first support to the existence of SLH is based on a probability theory, the details of which are given in Section 6.6. Results of our experiments with the random copolymers are supported by a model based on the change in the percentage of the junction points between the different monomers, i.e., junction points, as the degree of polymerization of a random copolymer increases. Monomers with different interaction sites in a copolymeric chain are shown in Figure 24. A monomer with "0 interactions" either corresponds to a monomer located between two monomers of the same type of repeat unit (for example, monomer 4 in Figure 24), or to a monomer located at the end chain next to a monomer of the same chemistry (for example, monomer 10 in Figure 24). A monomer with "1 interaction" is a monomer located between two monomers of different chemistries (for example, monomers 3, 5, 7, 8, and 9 in Figure 24), or at the end chain next to a monomer of a different chemistry (for example, monomer 1 in Figure 24). A monomer with "2 interactions" corresponds to a monomer located between two monomers of different chemistry than the monomer itself (for example, monomers 2 and 6 in Figure 24). Our model is based on studying the change in the relative percentages of 0, 1, and 2 interactions as a function of molar mass, which is expressed in the form of a statistical repeat unit "n_{rep}" representing several sequential monomeric units in the copolymeric chain. As observed in Figure 24 which shows two generic random AB copolymers with 1:3 and 1:4 ratios of A:B, the percentage of 0 and 1 interactions decreases as the molar mass increases, while the percentage of "2 interactions" increases with molar mass. The decrease in the percentage of 0 and 1 interactions, along with the increase in the "2 interaction" sites, as the degree of polymerization increases indicates that the monomers are becoming more dispersed as the chain grows. The results from the probabilistic model support the conclusion that the change in R_η/R_G of random copolymers is related to the increase in the ratio of junction points.

A second, more prosaic reason for the differences in normalized FT-IR peak areas among fractions of the random copolymers is quite simply that, due to the differences in chemical composition as well as MMD of the copolymers, the same fraction (*e.g.*, fraction 1) will encompass a different region of the MMD of each copolymer. As seen in Figures 15 and 19, all other factors being equal, more intramolecular repulsion (resulting in larger normalized peak areas) is experiences by copolymers of higher M relative to those of lower M.

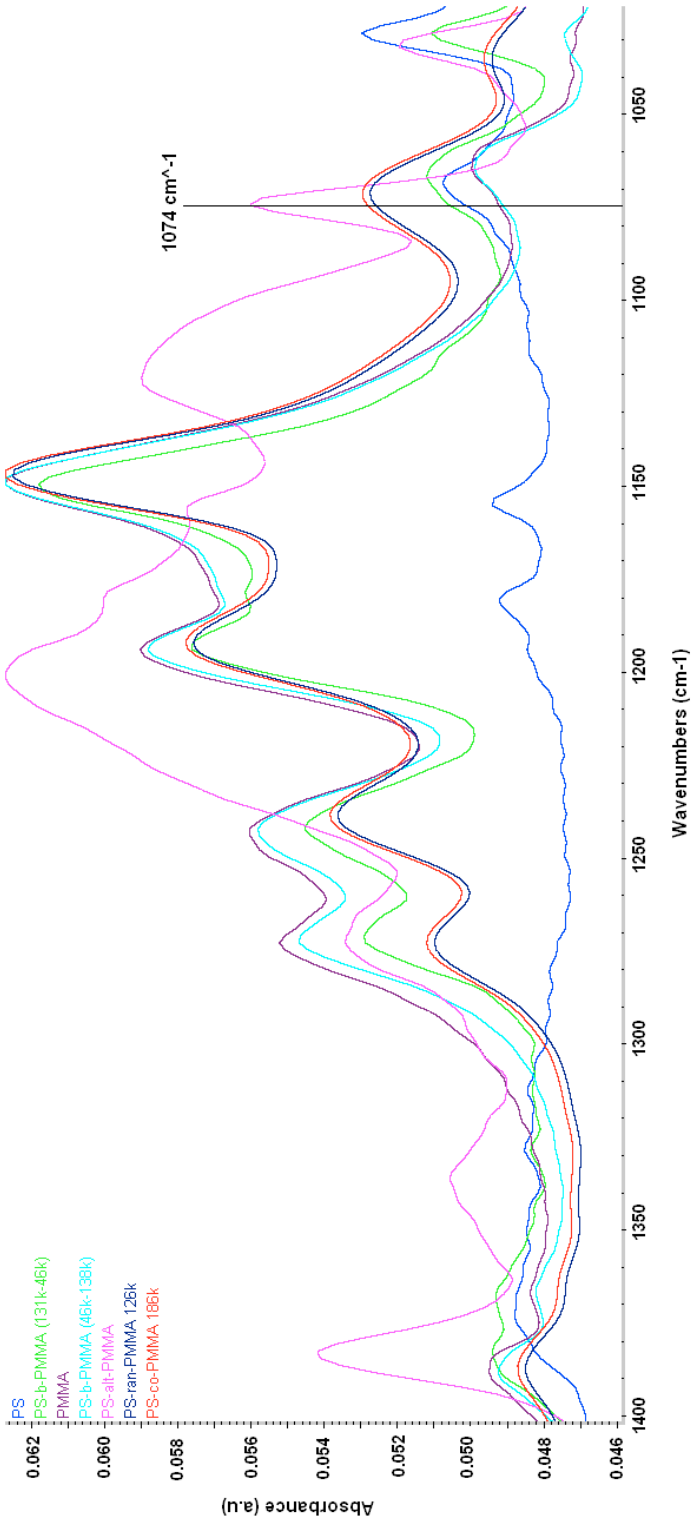

Figure 23(b). FT-IR spectra of polystyrene and methyl methacrylate as well as their corresponding alternating, random, and block copolymers.

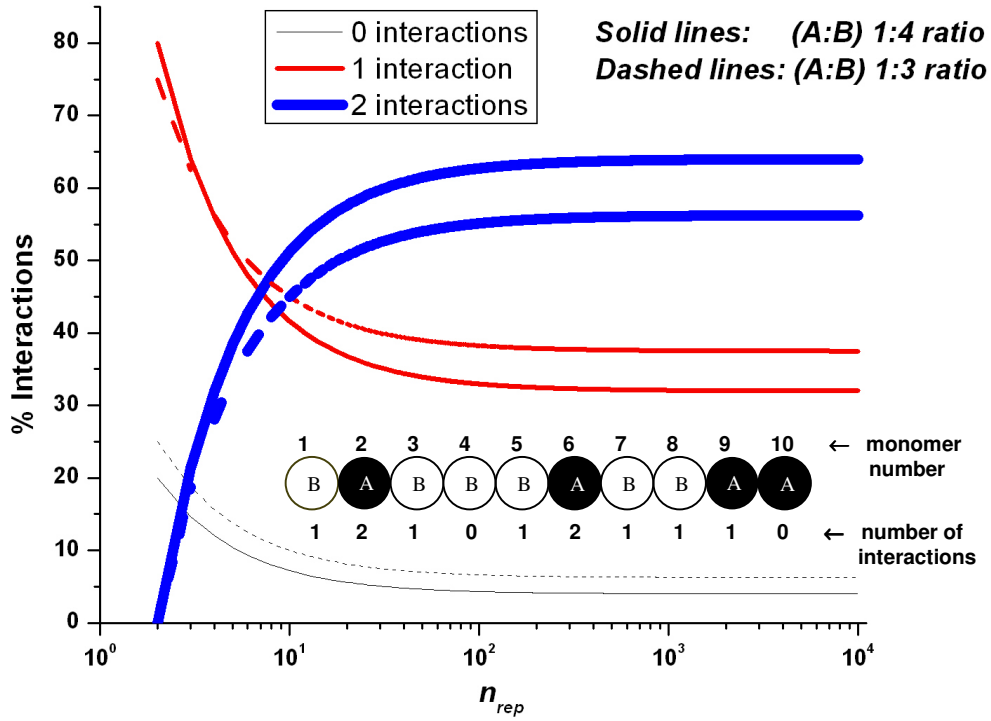

Figure 24. Changes in the percentage of interaction sites as a function of molar mass in a random copolymer. n_{rep} represents the number of statistical repeat units. See Section 6.6. Inset: Dependence of the number of interaction sites of a monomer on the nature of the neighbor monomers.

6.4.4 Examining the possibility of chemical heterogeneity.

Sequence length heterogeneity may originate from the progressive enhancement in the miscibility of the two monomeric solutions during a copolymerization reaction due to the compatibilizing ability of the synthesized copolymer.[4, 146-150] The gradual improvement in the miscibility of the monomers into each other impact the distribution of the monomers in solution and the propagation of the copolymeric chain, thus creating SLH. Another source affecting SLH is chemical heterogeneity, defined as the change in the relative percentages of styrene and methyl methacrylate in the random copolymer as a function of molar mass.

To determine whether chemical heterogeneity affects the structure (and, consequently, the R_η/R_G ratio) of the random copolymers, we measured the chemical heterogeneity of the P(S-*ran*-MMA) copolymer using SEC coupled to MALS, UV, and DRI detectors. The detailed procedure for obtaining the percentage composition at each slice eluting from the SEC columns is described in reference [31]. Figure 25 shows the chemical heterogeneity (or lack thereof) of the random and alternating copolymers, as

measured by the SEC/MALS/UV/DRI method. Both random copolymers show a virtual constancy in % styrene as a function of molar mass, indicating an absence of chemical heterogeneity. Therefore, chemical heterogeneity is not the reason for the expected SLH.

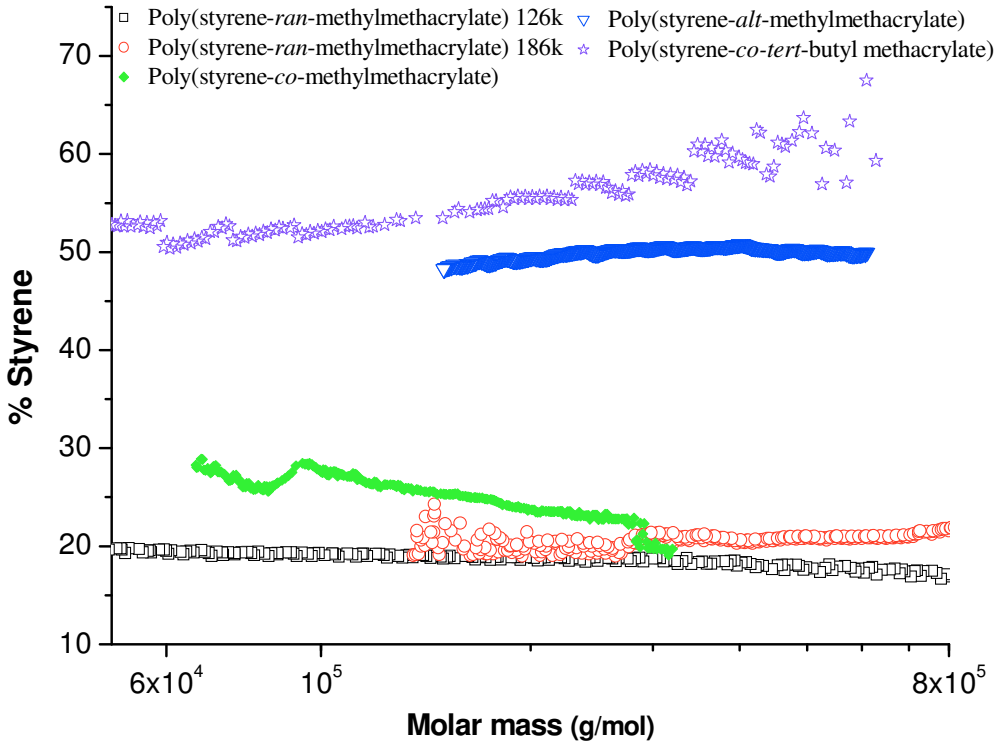

Figure 25. Chemical heterogeneity (given as % styrene) of alternating, gradient, and random copolymers of styrene and methyl methacrylate.

6.4.5 R_η/R_G results of the homopolymers, and block, alternating, and gradient random copolymers.

6.4.5.1 Styrene and methyl methacrylate homopolymers

In the case of the homopolymers, the *JPR* is equal to zero due to the absence of the junction points between S and MMA. As shown in Table 6, in spite of the differences in the chemistry as well as the molar mass of the analyzed homopolymer standards, the R_η/R_G values of both homopolymers are close to each other, fit in the range of random coil structure in solution, and close to the R_η/R_G values of the random copolymer at low molar mass. This is in agreement with our hypothesis that the structures of the homopolymers and random copolymers resemble each other in the case where *JPR* is minimal.

Table 6. R_η/R_G value of the homopolymers and block copolymers

Polymer	R_η/R_G
PS (186k)	0.86 ± 0.02
PMMA (343k)	0.82 ± 0.01
PMMA (467k)	0.81 ± 0.01
PS (533k)	0.82 ± 0.01
PS (723k)	0.82 ± 0.01
PS-b-PMMA (46K, 138K)	0.87 ± 0.01
PS-b-PMMA (131K, 46K)	0.88 ± 0.01

6.4.5.2 Block copolymers of styrene and methyl methacrylate

The R_η/R_G values of the block copolymers PS-*b*-PMMA (46K, 138K) and PS-*b*-PMMA (131K, 46K), as indicated in Table 6, are quite similar to each other, in spite of the large differences in percentage composition of the copolymer: The first block copolymer is composed of 25 %S and 75 %MMA, while second copolymer is composed of 75 %S and 25 %MMA. The R_η/R_G values of the two block copolymers are in the range of values for random coil structures in solution, ~0.7-0.9. This indicates that the PS-*b*-PMMA block copolymers adopt a random coil structure in THF and that, furthermore, this conformation is independent of the percentage composition of the block copolymers.

The R_η/R_G values of the two block copolymers with highly dissimilar compositions are similar to each other because of the single junction point these copolymers possess, as indicated by the arrow in Figure 1. Because of the only junction point in block copolymers, the intrachain repulsion between the different types of monomers has a negligible effect on the overall structure of these copolymers in solution: The solution conformation of block copolymers depends only on the conformation of the constituent homopolymers both of which, PS and PMMA, are shown to adopt random coil structures in THF at room temperature. Hence, the block copolymers of PS and PMMA are also expected to be random coils in solution, as observed.

6.4.5.3 Alternating copolymer of styrene and methyl methacrylate

The R_η/R_G versus molar mass relationship for the alternating copolymer examined in this study is shown in Figure 21. As predicted above, the R_η/R_G value is virtually constant as a function of molar mass. The low R_η/R_G value for the alternating copolymer (~0.65) value, as compared to the R_η/R_G values of the homopolymers and other copolymers (see Figure 21), is an indication of the relatively extended structure which these copolymers can adopt in solution. This extended structure is a direct result of the maximal value of the *JPR* in alternating copolymers, which results in maximum repulsion energy between the dissimilar monomers. The constancy in R_η/R_G with molar mass is due to the independence of the *JPR* on degree of polymerization for alternating copolymers. For the

different types of copolymers, block, alternating, and gradient, the *JPR* is expected to be highest, and the R_η/R_G lowest, for alternating copolymers, in accordance with the results shown in Figure 21.

6.4.5.4 Gradient random copolymer of styrene and methyl methacrylate

The R_η/R_G ratio of the gradient random copolymer decreases as a function of *M*, from a value resembling that of a block copolymer at the low end of its molar mass distribution, to a value close to that of an alternating copolymer at the high molar mass end of the distribution. This decrease in the R_η/R_G ratio as a function of molar mass does not occur as quickly for the gradient as for the random copolymers, due to the presence of chemical heterogeneity. In this gradient random copolymer, the percentage of styrene at the low molar mass end of the molar mass distribution is ~30% and decreases gradually as the molar mass of the copolymer increases, to a value of ~20% S at the high end of the molar mass distribution (as shown in Figure 25). Due to this specific type of chemical heterogeneity, the *JPR* decreases gradually as a function of *M* due to the decrease in the probability of a Styrene monomer to be next to a methyl methacrylate monomer. Therefore, the trend in the R_η/R_G ratio of the gradient random copolymer is expected to change less rapidly than for the random copolymer, as seen in Figure 21.

6.4.5.4 Random copolymer of styrene and tert-butyl methacrylate

The R_η/R_G ratio of poly(styrene-*co-tert*-butyl methacrylate increases as a function of *M* from a value resembling that of an alternating copolymer at low *M* to a value close to that of a block copolymer at high *M*, as shown in Figure 21. This increase in the R_η/R_G ratio as a function of molar mass is due to the chemical heterogeneity in this copolymer. As seen in Figure 25, the % styrene drafts away from the 50% composition as *M* grows. This change in % styrene results in decreasing *JPR* because the highest *JPR* correspond to a percentage composition of 50% of both monomers in a copolymer. As a result of this change in percentage composition, the intrachain repulsion decreases as *M* grows resulting in the increase in the R_η/R_G observed in Figure 25.

6.5 Conclusions

Sequence length heterogeneity (SLH) is the change in the average number of continuous and similar (i.e., same chemistry) monomers in a copolymer as the chain grows. The SLH is proportional to the dispersion of the monomers in the copolymer. Contrary to the case of block and alternating copolymers, the SLH is not constant for random copolymers. Knowledge of the SLH in a random copolymer is important to understanding polymeric properties that are dependent on the distribution of the monomers in the copolymer, such as adsorption of copolymer at a liquid-liquid interfaces,[132] conformation and folding of protein-like copolymers,[11, 12, 74, 133-135] transparency of films,[76, 137] and the ability of copolymers to compatibilize blends.[146, 147, 149, 151, 152] Other Conclusions for this project are explained in Section 7.3.

6.6 Probability Theory Model of Sequence Length Heterogeneity

Let A and B be two species comprising a linear copolymer. Let n be the total number of monomers in the chain and x_i, where $i \in [1, n]$, be the i^{th} position. Assuming there is a fixed percentage p of A, and 1- p of B found in the copolymer, the probability of the number of interactions I can be determined.

Without loss of generality, the probability of an individual A monomer A_0 having zero, one, or two interactions with a B monomer will be found. There are three cases to explore: A_0 has no adjoining B monomer ($I = 0$), A_0 has one adjoining B monomer ($I = 1$), and A_0 has two adjoining B monomers ($I = 2$).

Case 1: $I = 0$

Zero interactions occur when A_0 is located at an end position and the adjoining monomer is an A monomer, or when A_0 is located at an interior position and both adjoining monomers are also A. Hence,

$$P(I = 0) = P(x_1 = A_0 \cap x_2 = A) \cup P(x_n = A_0 \cap x_{n-1} = A) \cup P(x_i = A_0, \text{ where } i \in [2, n - 1] \cap x_{i-1} = A \cap x_{i+1} = A)$$

This simplifies to

$$P(I = 0) = \frac{1}{n} p + \frac{1}{n} p + \frac{n-2}{n} p^2 = \frac{p(2 + np - 2p)}{n} \tag{112}$$

Case 2: $I = 1$

One interaction occurs when A_0 is located at an end position and the adjoining monomer is a B monomer, or when A_0 is located at an interior position and one adjoining monomer is a B monomer and the other adjoining monomer is an A monomer. Thus,

$$P(I = 1) = P(x_1 = A_0 \cap x_2 = B) \cup P(x_n = A_0 \cap x_{n-1} = B) \cup P(x_i = A_0, \text{ where } i \in [2, n - 1] \cap x_{i-1} = B \cap x_{i+1} = A) \cup P(x_i = A_0, \text{ where } i \in [2, n - 1] \cap x_{i-1} = A \cap x_{i+1} = B)$$

This simplifies to

$$P(I = 1) = \frac{1}{n}(1 - p) + \frac{1}{n}(1 - p) + \frac{n-2}{n}(1 - p) p + \frac{n-2}{n} p(1 - p)$$

$$= \frac{2(1 - p)(1 + np - 2p)}{n}. \tag{113}$$

Case 3: $I = 2$

Two interactions occur when A_0 is located at an interior position and the adjoining monomers are both B monomers. Accordingly,

$$P(I = 2) = P(x_i = A_0, \text{ where } i \in [2, n - 1] \cap x_{i-1} = B \cap x_{i+1} = B)$$

This simplifies to

$$\mathrm{P}(I=2)=\frac{(n-2)}{n}(1-p)^2 \tag{114}$$

As the number of monomers in the chain increases (i.e., as $n \to \infty$), the probability of interactions approaches a steady state. This can be found by taking the limits of equations (112-114) as n approaches ∞, resulting in

for zero interactions ($I = 0$), $$\lim_{n\to\infty}\frac{p(2+np-2p)}{n}=p^2 \tag{115}$$

for one interaction ($I = 1$), $$\lim_{n\to\infty}\frac{2(1-p)(1+np-2p)}{n}=2p(1-p) \tag{116}$$

for two interactions ($I = 2$), $$\lim_{n\to\infty}\frac{(n-2)(1-p)^2}{n}=(1-p)^2 \tag{117}$$

Note that the model is based on the population of *A*. It describes the number of interactions that *A* has. It does not describe the total number of interactions, though this can also be calculated using a similar approach.

Examples

For example, let $n = 10$ and assume there is a 1:4 ratio of monomer *A* to monomer *B* (hence, $p = 0.2$). Using equations (112-114), 7.2% of *A* monomers will have no interactions with monomer *B*, 41.6% of *A* monomers will have one interaction with monomer *B*, and 51.2% of *A* monomers will have two interactions with monomer *B*.

When n is large (using equations (115-116)), 4% of monomer *A* will have no interactions with monomer *B*, 32% of monomer *A* will have one interaction with monomer *B*, and 64% of monomer *A* will have 2 interactions with monomer *B*.

Letting "n_{rep}" denote the total number of statistical repeat units (directly proportional, though not necessarily equal, to degree of polymerization), and "% interaction" the relative percentages of 0, 1, and 2 contact point interactions, equations (115-117) are used to plot the change in the % interactions in a copolymer as a continuous function of n_{rep}, as shown in Figure 23. In this figure, the change in the % interactions for two generic 1:3 and 1:4 A:B random copolymers is shown as a function of n_{rep}. As shown in Figure 23, for both copolymer the percent of 0 and 1 interactions decreases as n_{rep} increases, whereas the percentage of 2 interactions which increases with increasing n_{rep}.

APPENDIX

7.1 Flory-Huggins Theory

7.1.1 Introduction

Flory-Huggins theory is the basis of polymer thermodynamics in solution. This theory originates from the field lattice theory used to study the miscibility of two solvents. Flory and Huggins extended the application of this theory to include polymers in solution by taking into consideration the chain nature of the polymer.

The basis of Flory-Huggins theory relies on the representation of the solvent and the polymer in the form of lattice models, as shown in Figure 26. The strength and distribution of the bond energies between solvent molecules in the solvent lattice and the monomers in the polymer lattice is homogenous. This homogenous bond distribution in the two lattices changes when the polymer is dissolved in solution due to the formation of new bonds at the contact sites between the solvent molecules and monomers. In this theory, the effect of the interactions between the solvent molecules and the monomers is studied by making two main assumptions: 1) The monomer and the solvent molecules have the same size. 2) The polymer is monodisperse[153].

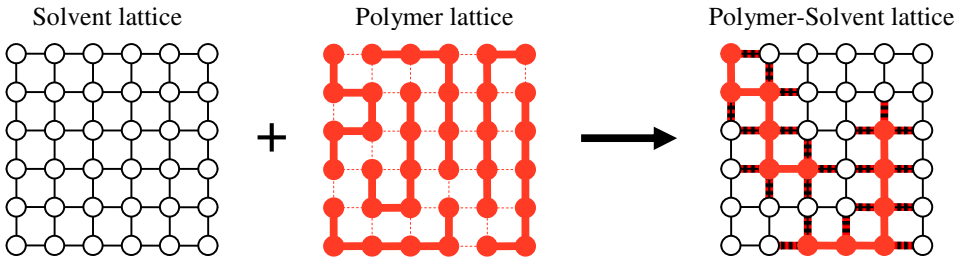

Figure 26. Flory-Huggins theory: Lattice chain models for solvation of polymers

In Figure 26, the hollow circles correspond to the solvent molecules and the straight lines correspond to the bonds between these molecules. The red solid circles represent the monomers, red lines represent the bonds between these monomers, and the red dotted lines correspond to the interchain interaction between polymeric chains. The polymeric lattice represents the melt state where the solvent is absent. In the polymer-solvent lattice, the dotted lines in red and black correspond to the newly formed bonds between the solvent molecules and the monomers.

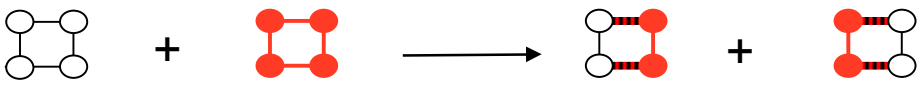

Figure 27. Change in interaction between neighbors due to solvation

The change of the internal energy at each polymer-solvent contact site (as shown in the dotted bonds in Figure 27) is determined using equations (118) through (121).

$$\Delta E = \sum bond\ E_{products} - \sum bond\ E_{reac\tan ts} \tag{118}$$

$$\Delta E = (2\varepsilon_{ss} + 2\varepsilon_{pp} + 4\varepsilon_{ps}) - (4\varepsilon_{ss} + 4\varepsilon_{pp}) \tag{119}$$

$$\Delta E = \varepsilon_{ps} - \frac{\varepsilon_{pp}}{2} + \frac{2\varepsilon_{ss}}{2} \tag{120}$$

$$\frac{\Delta E}{ps_{contact}} = \varepsilon_{ps} - \frac{\varepsilon_{pp}}{2} + \frac{2\varepsilon_{ss}}{2} \tag{121}$$

The energy of the red bonds between monomers is denoted as $\varepsilon_{p\text{-}p}$, the energy of the black bonds between solvent molecules as $\varepsilon_{s\text{-}s}$, and the red-black dotted bonds between monomers and solvent molecules is denoted as $\varepsilon_{p\text{-}s}$.[153]

7.1.2 The Flory-Huggins parameter (χ)

The Flory-Huggins parameter is a unitless parameter proportional to the interaction energy at the contact sites between two particles (determined in equation (121)). The Flory-Huggins parameter at a solvent-monomer interaction site can be calculated according to equation (122). A positive value of this parameter indicates that the initial state is more favored than the final state, i.e, that solvent-solvent and polymer-polymer interactions are more favored than polymer-solvent interaction. A negative value of this parameter indicates that solvation of the polymer is favored.

$$\chi = z\left(\frac{\varepsilon_{ps} - \frac{\varepsilon_{pp}}{2} + \frac{2\varepsilon_{ss}}{2}}{K_B T}\right) \tag{122}$$

z is the coordination number of the lattice, K_B is Boltzman's constant, and T is the absolute temperature.

Table 7. Junction points as a function of monomer distribution in a 6-mer (S:M) copolymer with 1:1 ratio of (S:M)

Probable combination	Number of junction points between S and M	Ratio of junction points	Copolymer type
SSSMMM /\/\	One	1/5	Block
MSSSMM /\/\	Two	2/5	Random (1)
SSMMMS /\/\	Two	2/5	Random (2)
SSMSMM /\/\	Three	3/5	Random (3)
SSMMSM /\/\	Three	3/5	Random (4)
SMSSMM /\/\	Three	3/5	Random (5)
SMMSSM /\/\	Three	3/5	Random (6)
MSSMSM /\/\	Four	4/5	Random (7)
SMSMMS /\/\	Four	4/5	Random (8)
SMSMSM /\/\	Five	5/5	Alternating

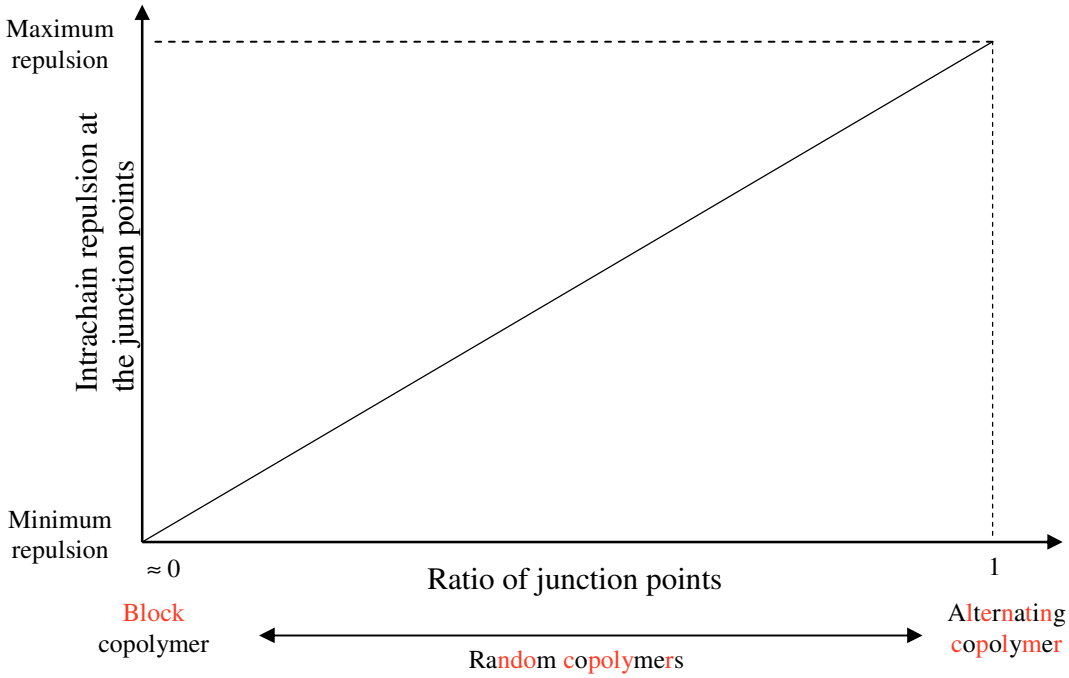

Figure 28. Relation between intrachain repulsion and the ratio of junction points in a copolymer

7.1.3 The Flory-Huggins parameter for monomer-monomer interaction

The Flory-Huggins parameter is used to study the solvent-polymer interaction, but this parameter can also be used to study the interaction between two different monomers. The monomer-monomer interactions are not frequently studied in dilute solutions due to two main reasons: 1) The monomer-monomer interactions are usually weaker than solvent-monomer interactions. Consequently, the monomer-monomer interactions are masked by the solvent-monomer interaction in dilute solution. 2) The monomer-monomer interaction appears within the same chain as intrachain interactions or between two different chains interchain interactions. The intrachain repulsion is constant over the polymeric chain and thus its effect is masked by the solvent effect. The interchain repulsion is usually ignored in dilute solution because the contact between different polymeric chains is virtually non-existent.

7.1.4 The Flory-Huggins parameter for copolymers

Intrachain interactions distort the enthalpic energy of the chain and thus compel the chain to adopt a different conformation to decrease the potential of these interactions. The change in enthalpy is balanced by a change in entropy in the form of conformational change. This change in energy is constant all-over the polymeric chain in the case of the homopolymer and thus the change in energy is masked by the polymer-solvent interactions.

In the case of copolymers, two different types of monomers are incorporated into one polymeric chain. At the junction point between the two different monomers, the Flory-Huggins coefficient is usually positive, which means that the interaction between the two monomers is of a repulsive nature. The repulsion between the different monomers increases the enthalpic interactions within a copolymeric chain. This enthalpic increase is balanced by a decrease in the entropy, expressed as a conformational change. The conformational change is toward a more extended state than that of a homopolymer, due to the unfavorable interactions between the different monomers at the junction points.[81]

In a block copolymer, the intrachain repulsion is minimized because there is only one junction point between the different monomers, as shown in Figure 26. Therefore, the block copolymer is expected to have a conformation similar to that of the constituent homopolymers in the case where the two homopolymers composing the block copolymer have the same structure in solution (*e.g.*, both homopolymers are random coils), or an average conformation of the two homopolymers in the case where the two homopolymers have different conformations (*e.g.*, rod coil copolymers).

The alternating distribution of monomers in the case of an alternating copolymer results in a maximum number of junction points. This maximal number of junction points corresponds to maximum repulsion energy between the different monomers.

Accordingly, the alternating copolymer is expected to have the most extended conformation among the type of copolymers shown in Figure 26.

In a random copolymer, as shown in Table 7 and Figure 28, the junction point ration (and thus the intrachain repulsion) varies from a minimum value in which the random copolymer looks like a block copolymer to a maximum value where the random copolymer resembles the alternating copolymer. Therefore, the structure of the random copolymer varies between the structure of the block copolymer and the structure of the alternating copolymer, depending on the ratio of the junction points and thus to distribution of the monomers in the copolymeric chain.

7.2 Influence of Second Virial Coefficient and Persistence Length on Dilute Solution Conformation[31]

7.2.1 Aim

The persistence length (L_P) in a polymer is a configurational parameter defined as the average projection of the end-to-end distance of a polymer in the direction of the first segment along the backbone of the chain. The persistence length is indicative of the stiffness of the polymer in solution, i.e., as L_p increases the rigidity of the polymer increases, and vice versa. L_p is affected by two types of interactions the short-range interactions between consecutive monomers and long-range interactions such as the excluded volume effect. Here, we study the effect of the different types of intrachain interactions along the polymeric backbone on the persistence length of a polymer as well as on other properties such as solubility, conformation, refractive index, and intrinsic viscosity. The polymers chosen for this study are polystyrene PS, poly(vinyl chloride), PVC, and poly(p-vinylbenzyl chloride), and PpVBC, and the dilute solution properties are obtained using size exclusion chromatography coupled to a multi angle light scattering detector, differential viscometry, and differential refractometer detector. These particular polymers were chosen based on the intrachain interactions specific to each them: Intrachain repulsion between chlorine atoms in PVC, π-π stacking attraction forces between the aromatic groups in PS, and hindered π-π stacking due to the addition of a methyl chloride substituent group to an aromatic ring in the case of PpVBC. In this study, we were able to show the effect of intrachain repulsion between consecutive monomers and second virial coeffiecent (A_2) on polymer solubility and stiffness. The increase in the second virial coefficient increased the solubility and rigidity of the polymer while the increase in the intrachain repulsion between consecutive monomers increases polymer solubility and decreases its rigidity.

7.2.2 Introduction

In polymer analysis, dilute solution conditions refer to the state where a dissolved, fully solvated polymer is in solution at very low concentrations, with the distance separating the polymeric chains from each other much larger than the size of the polymer in solution. With this condition fulfilled, interchain interaction between macromolecules is assumed to be negligible.

Generally, molecular polymeric properties are obtained in dilute solution, rather than in the melt or in concentrated solutions where the structure of a polymer is affected by interchain interactions [22-26]. While important for a variety of reasons, Nondilute studies of polymer solutions can be complicated by a number of factors, including interchain repulsion resulting in a colloidal polymeric phase in solution [154]; interparticle attraction, resulting in aggregation of polymeric solutions [155, 156]; functional group heterogeneity; compositional heterogeneity; and architectural complexities (*e.g.*, branching) [22, 157]. Nondilute solution studies are further complicated by both experimental

and fundamental limitations of techniques such as size-exclusion chromatography, scattering, and viscometric methods.[90, 158]

Interest in dilute solution studies arises from the importance of the polymeric properties obtained and from the relative ease with which the studies can usually be performed. Properties obtained from dilute solution studies include molar mass averages and distributions [84, 89], chemical heterogeneity[32], long- and short-chain branching [157, 159], chain stiffness [143], thermodynamic properties of a polymer under specific solvent/temperature conditions [91], and monomer-monomer and solvent-monomer interactions [93]. Many of the properties obtained are absolute molecular properties related to the nature of the polymer and are independent of the dilute solution conditions. Examples of such properties are molar mass, chemical heterogeneity, and branching.

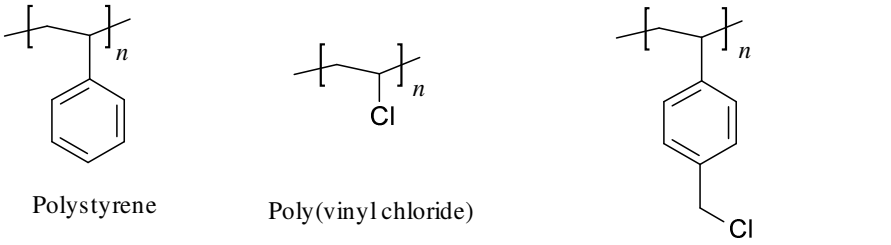

Figure 29. Chemical structures of polystyrene, poly(vinyl chloride), and poly(*p*-vinylbenzyl chloride)

Here we examine, resultant from differences in the nature of chain backbone substituent groups, the differences in the dilute solution properties of three polymers. The polymers studied are polystyrene PS, poly(vinyl chloride) PVC, and poly(*p*-vinylbenzyl chloride) PpVBC, shown in Figure 29, and the analytical technique we have employed is size-exclusion chromatography (SEC) coupled to multi-angle static light scattering (MALS), differential viscometry (VISC), and differential refractive index (DRI) detection.

A specific aim of this project is to elucidate how different types of intrachain interactions along the polymeric backbone affect properties such as chain stiffness and solubility. The three polymers specifically chosen for this study differ from each other with respect to the type of intrachain interaction present in each: Intrachain repulsion between chlorine atoms in PVC, π-π stacking attraction forces between the aromatic groups in PS, and hindered π-π stacking due to the addition of a methyl chloride substituent group to an aromatic ring in the case of PpVBC.

The similarity in molar mass averages and distributions among PS, PpVBC, and PVC helps isolate parameters which affect dilute solution properties, through our ability to compare to each other molecular properties of the three polymers at a given molar

mass. The pronounced difference between properties such as intrinsic viscosity, chain stiffness, refractive index, and second virial coefficient is explained based on both short- and long-range intrachain interactions among monomers in the polymeric backbone. As such, this study should provide a deeper understanding of the effects of solvent-monomer and monomer-monomer interactions on chain conformation and stiffness in dilute polymer solution.

Table 8. Properties of PS, PVC, and PpVBC obtained from off-line MALS and DRI, and on-line SEC/MALS/VISC/DRI.

	PVC	**PS**	**PpVBC**
$\partial n/\partial c$ (mL/g)[a]	0.112 ± 0.001	0.195 ± 0.003	0.182 ± 0.001
A_2 (mol mL/g²)[b]	$(1.01 \pm 0.01) \times 10^{-3}$	$(4.89 \pm 0.08) \times 10^{-4}$	$(3.67 \pm 0.03) \times 10^{-4}$
M_w/M_n[c]	1.73 ± 0.03	1.53 ± 0.02	1.62 ± 0.05
M_n (g/mol)[c]	$(7.05 \pm 0.05) \times 10^4$	$(9.8 \pm 0.2) \times 10^4$	$(7.99 \pm 0.32) \times 10^4$
M_w (g/mol)[c]	$(1.22 \pm 0.01) \times 10^5$	$(1.51 \pm 0.03) \times 10^5$	$(1.30 \pm 0.01) \times 10^5$
M_z (g/mol)[c]	$(2.08 \pm 0.07) \times 10^5$	$(2.31 \pm 0.08) \times 10^5$	$(2.22 \pm 0.08) \times 10^5$
$R_{G,z}$ (nm)[c]	23 ± 1	20 ± 1	15 ± 1
$[\eta]_w$ (mL/g)[c]	119 ± 1	61 ± 1	39 ± 1
L_p (nm)[c]	13 ± 1	15 ± 1	10 ± 1
Mark-Houwink plot slope a[c]	0.68 ± 0.01	0.70 ± 0.02	0.62 ± 0.02
Conformation plot slope α[c]	0.50 ± 0.01	0.56 ± 0.01	0.52 ± 0.01

[a]Determined from off-line DRI analysis.
[b]Determined from off-line MALS analysis.
[c]Determined from SEC/MALS/VISC/DRI using equation (123). See text for details.

7.2.3 Experimental

Materials

Polystyrene was obtained from PSS Polymer Standards Service (Mainz, Germany), PpVBC from Scientific Polymer Products (Ontario, NY, USA), and PVC from Pressure Chemical Company (Pittsburgh, PA, USA); tetrahydrofuran (THF) was from EMD (Gibbstown, NJ, USA). All materials were used as received, without further purification.

Multi-Detector Size-Exclusion Chromatography (SEC/MALS/VISC/DRI)

For the multi-detector SEC experiments, a concentration of 3 mg/mL of each polymer in THF was prepared and left on a laboratory wrist-action shaker overnight to ensure full dissolution and solvation. For increased precision, two different 3 mg/mL solutions of each sample were prepared and, from each dissolution, two injections were performed for a total of four injections per polymer studied. The SEC system consisted of a Waters

2695 Separations Module (Waters, Milford, MA, USA), three PLgel 10 μm particle size Mixed-B columns, (Agilent/Polymer Laboratories), and three detectors connected in series: A DAWN EOS multi-angle static light scattering photometer (Wyatt Technology Corp., Santa Barbara, CA, USA), followed by a Viscostar differential viscometer (Wyatt), followed by an Optilab rEX differential refractometer (Wyatt). A 31,400 g/mol narrow polydispersity (M_w/M_n = 1.02) linear PS standard was used for normalization of the MALS unit photodiodes, as well as for calculating interdetector delays and for interdetector band broadening correction. Data acquisition was performed using Wyatt's ASTRA software (V.5.3.2.13), plotting and calculations were performed with OriginPro 7.5 (V.7.5885, OriginLab Corp., Northampton, MA, USA).

Specific Refractive Index Increment (∂n/∂c) Determination

The specific refractive index increments ($\partial n/\partial c$) of the polymers in THF at 25 °C are 0.195 ± 0.003 mL/g for PS, 0.182 ± 0.001 mL/g for PpVBC, and 0.112 ± 0.002 mL/g for PVC. To obtain these values, the samples were dissolved in THF and left overnight on a wrist-action shaker. For offline $\partial n/\partial c$ determination, six dilutions of each sample, ranging from 1.0-6.0 mg/mL, were injected directly into the Optilab rEX differential refractometer (Wyatt) using a Razel model A-99EJ syringe pump. Flow rate was 0.32 mL/min. Sample solutions were filtered gently through 0.45 μm Teflon syringe filters, neat THF for baseline determination through a 0.02 μm Teflon syringe filter. The wavelength of the lamp in the DRI detector is filtered to match the vacuum wavelength of the laser in the MALS detector (λ_0 = 685 nm). Data acquisition and processing were done with Wyatt's ASTRA V software (V. 5.3.2.13).

Off-line, batch-mode MALS: Zimm plot construction

For the purpose of constructing Zimm plots, from which the second virial coefficient A_2 of the polymer solutions were obtained, a series of at least five sample dissolutions of PS, PVC, and PpVBC each in THF at 25 ^{o}C, ranging from 1.0-6.0 mg/mL, were injected directly into the light scattering photometer, a Wyatt DAWN EOS, using a Razel model A-99EJ syringe pump. Flow rate was 0.32 mL/min. Sample solutions were gently filtered through 0.45 μm Teflon syringe filters, neat solvent for baseline determination through a 0.02 μm Teflon syringe filter. Data acquisition and processing were done with Wyatt's ASTRA V software (V. 5.3.2.13).

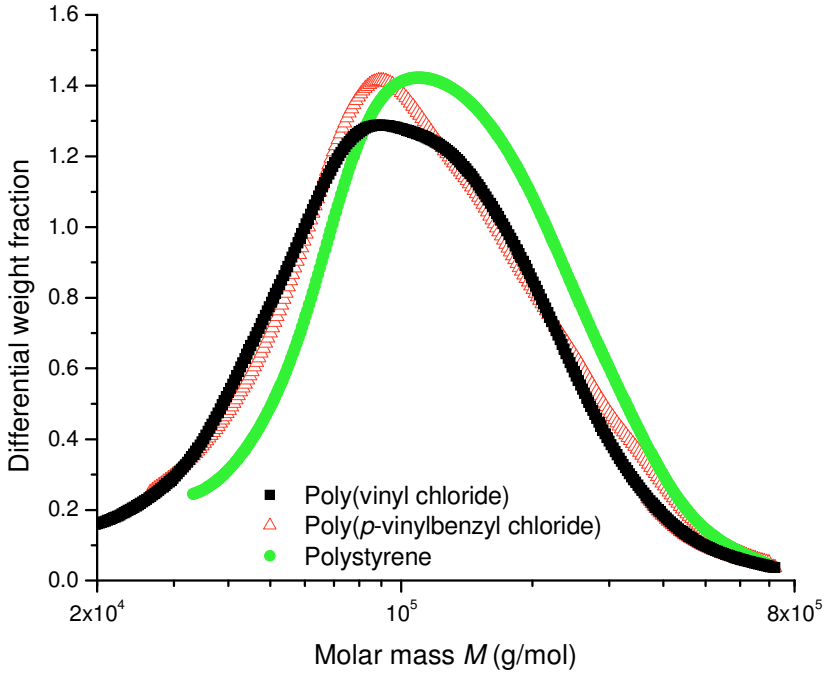

Figure 30. Differential molar mass distributions of polystyrene, poly(*p*-vinylbenzyl chloride), and poly(vinyl chloride)

7.2.4 Results and discussion

As shown in Figure 30, the molar mass distributions of the polymers chosen in this study, PS, PVC, and PpVBC, cover approximately the same molar mass range extending from ~30 to ~700 Kg/mol. The same coincidence occurs for the molar mass averages M_n, M_w, and M_z, of the three polymers, as seen in Table 8. Because of these similarities, we are able to compare to each other polymeric properties of PS, PVC, and PpVBC at any given molar mass M. The absolute, i.e., calibrant-independent, molar mass averages and distributions of the polymers were obtained using static light scattering detection and applying the Rayleigh-Gans-Debye approximation, shown previously in equations (76-78). [90]

The specific refractive index increments of PS, PpVBC, and PVC, needed for calculating absolute molar mass via static light scattering, are obtained form offline-DRI experiments as outlined in the Experimental section. As seen in Table 8, PS and PpVBC have significantly higher $\partial n/\partial c$ values than does PVC. This difference is due to the aromatic group attached to the carbon-carbon backbone in PS and PpVBC, which increases the refractive index of the polymer [160]. This same group is absent in PVC.

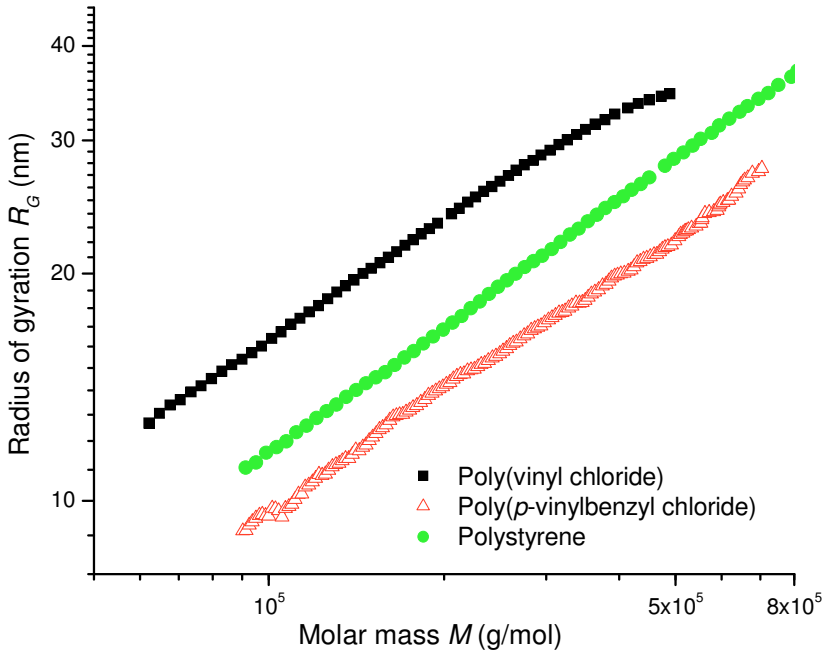

(a)

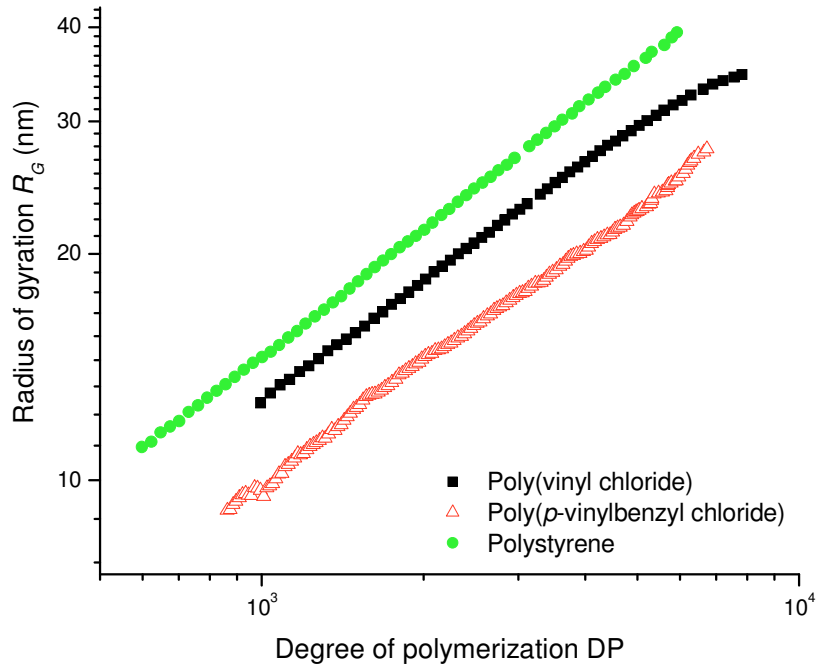

(b)

Figure 31. (a) Conformation plot of polystyrene, poly(*p*-vinylbenzyl chloride), and poly(vinyl chloride). (b) Plot of the radius of gyration versus degree of polymerization of polystyrene, poly(*p*-vinylbenzyl chloride), and poly(vinyl chloride)

The second virial coefficients A_2 of PS, PpVBC, and PVC, also given in Table 8, indicate that PVC is better solvated in THF at room temperature than are either PS or PpVBC. The unfavorable interaction between the *p*-electron clouds on the chlorine atoms along the PVC backbone increases the separation between these groups and thus enhances the solubility of this polymer in THF. In the case of PS and PpVBC, π-π stacking between aromatic rings along the polymeric chain results in intramolecular attraction, thus decreasing the excluded volume of the polymer as compared to PVC, with the result being that the second virial coefficients of PS and PpVBC are both lower than that of PVC [161]. While the A_2 of PS and PpVBC are similar to each other, we cannot at present explain why the A_2 value of PpVBC is slightly smaller than that of PS.

The dilute solution conformations of PS, PpVBC, and PVC are obtained from the slopes of the conformation and Mark-Houwink plots. The slope of the Mark-Houwink plot a and of the conformation plot α are indicative of the structure of a polymer in solution. The value of a ranges from 0 for a hard homogenous sphere to 2 for a rigid rod, with a value in the range of 0.7–0.8 for a linear random coil at good solvent/temperature conditions. The slope α varies between 0.33 for a hard sphere of uniform density to a value of 1 in the case of a rigid rod, with a value of ~0.5–0.6 for a linear random coil structure at good solvent/temperature conditions [90].

From Table 8, it is observed that the slopes of the conformation and Mark-Houwink plots of PS, PVC, and PpVBC are very close to each other, indicating that the polymers all adopt essentially the same conformation as each other in solution. These slopes are also very close to the slope of a linear random coil structure at good solvent/temperature conditions. From Figures 31a and 32a, it is evident that the radius of gyration (in the case of the conformation plot) or the intrinsic viscosity (in the case of the Mark-Houwink plot) at any specific molar mass is highest for PVC and lowest for PpVBC. This difference in the R_G and $[\eta]$ values of PS, PVC, and PpVBC at any specific molar mass may be due to the difference in the degrees of polymerization DP of these polymers. The molar masses of the vinyl chloride, styrene, and *p*-vinylbenzyl chloride monomers are 62.5, 104.5, and 152.6 g/mol, respectively. Therefore, at any given molar mass, the degrees of polymerization of PVC, PS, and PpVBC are considerably different from one another, being highest for PVC and lowest for PpVBC (for example, a molar mass of 15260 g/mol corresponds to a 100-mer of PpVBC, but to a 146-mer of PS and to a 244-mer of PVC). To determine whether this difference in degree of polymerization is the only parameter responsible for the observed differences in R_G and $[\eta]$ at a given M, the conformation and the Mark-Houwink plots have been replotted, with DP as the abscissa, in Figures 31b and 32b, respectively.

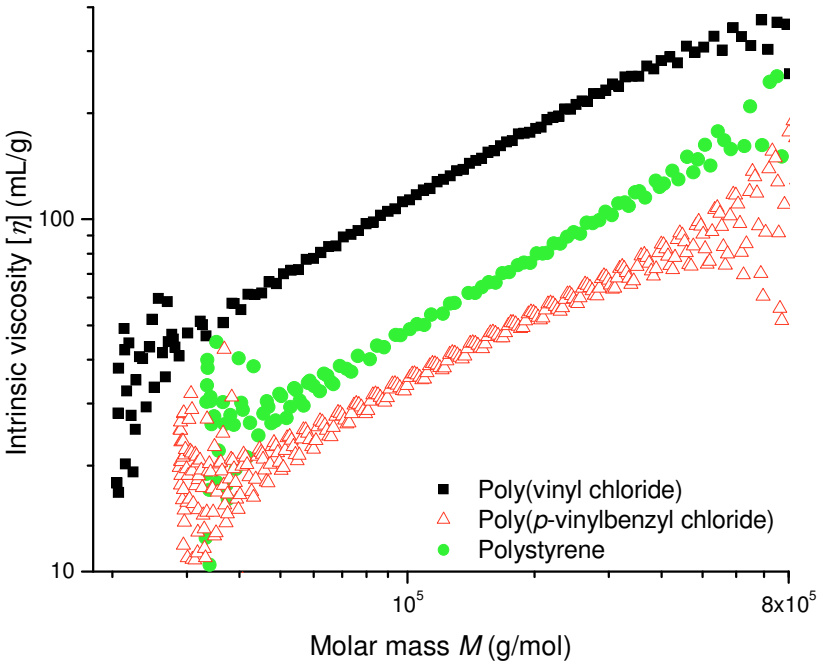

(a)

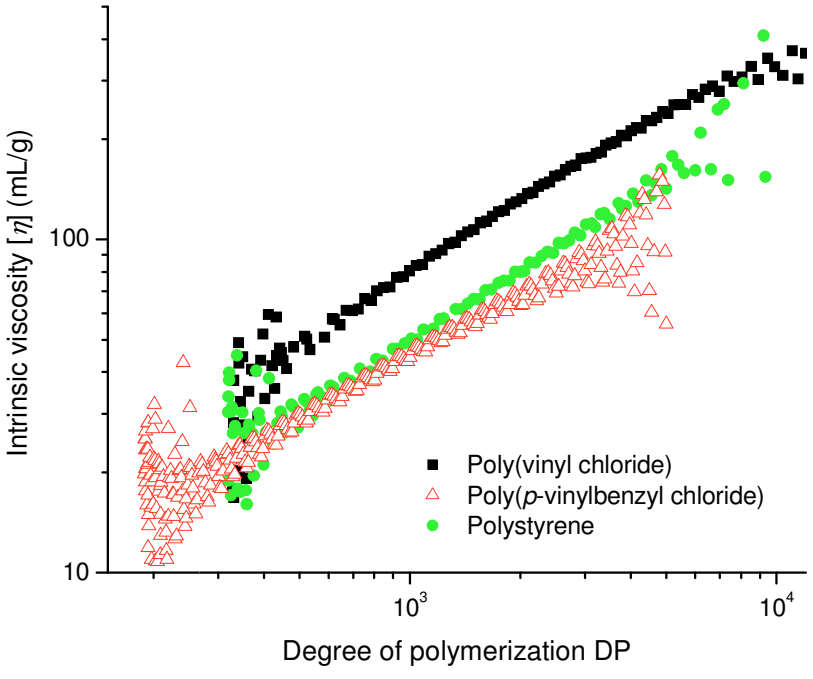

(b)

Figure 32. (a) Mark-Houwink plot of polystyrene, poly(*p*-vinylbenzyl chloride), and poly(vinyl chloride). (b) Plot of the intrinsic viscosity versus degree of polymerization of polystyrene, poly(*p*-vinylbenzyl chloride), and poly(vinyl chloride)

The plot of R_G as a function of the degree of polymerization for PS, PVC, and PpVBC (Figure 31b) shows that, for a given DP, the relative ranking of the three polymers examined is different than when the radii are compared at a given M: For any given DP, R_G rank as $R_{G,PS} > R_{G,PVC} > R_{G,PpVBC}$ while, for any given M, R_G rank as $R_{G,PVC} > R_{G,PS} > R_{G,PpVBC}$. We relate this difference in R_G, when compared at a given M versus when compared at a given DP, to a difference in the stiffness of the polymers examined. As will be shown subsequently when discussing persistence length, PS is the stiffest and PpVBC the most flexible polymer examined, with PVC possessing a degree of stiffness intermediate to those of PS and PpVBC. Because a stiff polymer occupies a larger hydrodynamic volume, it is expected to have a larger radius of gyration than a flexible polymer of the same M.

Somewhat different behavior than that just described for R_G is manifested by the intrinsic viscosity $[\eta]$ of the dilute polymer solutions (Figures 29a,b). When comparing $[\eta]$ at a given M, the order displayed by the polymers is the same as when comparing R_G at a given M, i.e., $[\eta]_{PVC} > [\eta]_{PS} > [\eta]_{PpVBC}$. However, when comparing $[\eta]$ at a given DP, the polymers rank differently than they do when R_G are compared at a given DP: $[\eta]_{PVC} > [\eta]_{PS} \geq [\eta]_{PpVBC}$. The differences in the intrinsic viscosities of the three polymers at a given DP are the result of preferential solvation: PVC is the most solvated and PpVBC is the least solvated polymer, with PS being solvated to an extent less than PVC and more than PpVBC. This ranking agrees with the ranking of the A_2 values from Table 8, i.e., $A_{2,PVC} > A_{2,PS} \geq A_{2,PpVBC}$ [162]. This coincidence between $[\eta]$ and A_2 ranking is expected, as A_2 is a measure of the excess chemical potential, or excess Gibbs free energy of solution, between polymers and solvent molecules in dilute solution [90]. At any given M, the most solvated polymer will occupy the largest hydrodynamic volume as compared to less well solvated polymers, resulting in the largest intrinsic viscosity for the most solvated polymer and vice-versa [163]. Therefore, the intrinsic viscosities of the three polymers at a given DP rank as $[\eta]_{PVC} > [\eta]_{PS} \geq [\eta]_{PpVBC}$.

Another parameter that informs our knowledge of macromolecular rigidity is the persistence length L_p, defined as the average projection of the end-to-end distance of a polymer in the direction of the first segment along the backbone of the chain. The persistence length is indicative of the stiffness of the polymer; as the rigidity of the polymer increases L_p becomes larger and, conversely, as polymer flexibility increases L_p decreases [90, 164]. For neutral polymers (i.e., for non-polyelectrolytes), L_p depends less on short-range interactions between monomeric repeat units and more on long-range interactions such as the excluded volume effect [164-168]. The persistence length can be determined from a plot of $\left(\frac{M^2}{12R_G^2}\right)$ versus M, according to [90]

$$\left(\frac{M^2}{12R_G^2}\right) = M_L^{4/3} + \frac{2M_L^{1/3}M}{15L_p} \qquad (123)$$

where L_p is the persistence length of the polymeric chain and M_L is the molar mass per unit contour length. Both L_p and M_L are obtained from the slope $\left(\frac{2M_L^{1/3}}{15L_p}\right)$ and the y-intercept $M_L^{4/3}$ of the aforementioned plot. Using SEC with on-line MALS detection allows us to construct this plot, through our ability to measure M and R_G at each elution slice.

Persistence length is a configurational parameter that quantifies the stiffness of a polymeric chain. The L_p of PS, PVC, and PpVBC in THF at room temperature are 15, 13, and 10 nm, respectively (Table 8). The differences in the persistence lengths of the three polymers are based on a combination of intrachain interactions and excluded volume effects, with excluded volume defined as the volume of solution not available to a given monomer in the polymer.

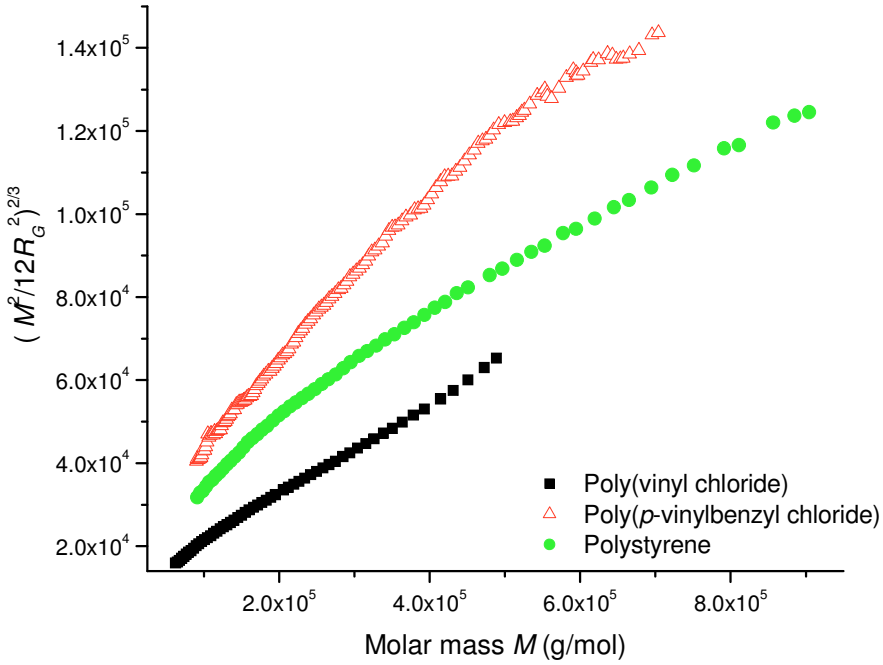

Figure 33. Determination of persistence length of polystyrene, poly(*p*-vinylbenzyl chloride), and poly(vinyl chloride)

The persistence length values in Table 8 indicate that PS is the stiffest, and PpVBC the most flexible, among the three polymers examined. The relative stiffnesses of PS and PVC are the result of two counteracting effects: 1) Intrachain interactions: In the case of PS, the presence of aromatic rings along the polymeric chain induces attractive π-π stacking between monomers, thereby increasing the stiffness of the polymer. In the

case of PVC, intrachain repulsion between the *p*-electron clouds of the chlorine atoms decreases macromolecular stiffness. 2) Excluded volume effects: The second virial coefficient of PVC solutions in THF is significantly higher than that of PS solutions in the same solvent indicating that, at the given conditions, PVC is better solvated than is PS. Therefore, the long-range interactions arising from the excluded volume is lowest for PVC and highest for PS. Excluded-volume effects, thus plays a larger role in solution of PVC than they do in those of PS. These two counteracting effects, intrachain repulsion (short-term interactions) and excluded volume effect (long-term interactions), result in a slightly stiffer PS chain as compared to PVC. In the case of PpVBC, the chloromethyl substituent on the phenyl group hinders π-π stacking of the monomers across the polymeric chain and the contribution of the excluded volume effect is lower (lower second virial coefficient) for PpVBC than for either PS or PVC resulting in PpVBC having the lowest L_p of the three polymers studied. Note that all the aforementioned interactions are relatively minor effects as compared to *e.g.*, intramolecular H-bonding or to the presence of ring structures in main chain, both of which can result in much greater L_p values (*e.g.* in the case of cellulose or PBLG) (16).

Previous work has shown that polymer flexibility is chain length dependent [169-172]. At good solvent/temperature conditions, polymer stiffness can change from rigid at low molar mass to semiflexible and flexible as chain length tends to infinity. This gradual change in polymer flexibility with chain growth manifests itself in the form of a gradual change in the slope of the plot of $\left(\frac{M^2}{12R_G^2}\right)$ versus M of PS and PpVBC, shown in Figure 33, from which the persistence length L_p is derived. The slight decrease in the slope as a function of M results in a significant increase in the y-intercept ($M_L^{4/3}$), as indicated by equation (123). Consequently, the persistence length (L_p), calculated from the slope $\left(\frac{2M_L^{1/3}}{15L_p}\right)$, is expected to decrease as a function of M, resulting in an increase in the flexibility of the PS and PpVBC as molar mass increases. This same increase in flexibility did not manifest itself for PVC over the M range examined.

7.3 Conclusions

7.3.1 Chemical heterogeneity project

we have presented a method by which to obtain the absolute, chemical-heterogeneity-corrected molar mass averages and distributions of copolymers and have applied the method to a gradient random copolymer of styrene and methyl methacrylate in which the styrene percentage decreases from approximately 30% to approximately 19% as a function of increasing molar mass. The method consists of separation by SEC with detection using multi-angle static light scattering, differential viscometry, differential refractometry, and ultraviolet absorption spectroscopy, and relies on the preferential absorption of styrene over methyl methacrylate at 260 nm. Using this quadruple-detector approach, the percentage of styrene (*%St*) in each elution slice is determined using equation (88). This *%St* is then used to determine the specific refractive index increment, corrected for chemical composition, at each elution slice using equation (93). From here, the molar mass at each slice, corrected for chemical composition, is obtained using equation (92). From this corrected molar mass and from the chemical-composition-corrected refractometer response, the absolute chemical-heterogeneity-corrected molar mass averages and distribution of the copolymer are calculated. The corrected molar mass and intrinsic viscosity at each SEC elution slice (the latter from equation (98)) are used to construct a chemical-heterogeneity-corrected Mark-Houwink plot. The slice-wise corrected *M* data are used, in conjunction with the MALS-determined $R_{G,z}$ of each slice, to construct a conformation plot corrected for chemical heterogeneity.

The method also has the advantage of providing the chemical heterogeneity of the copolymer as a function of the absolute, chemical-heterogeneity-corrected *M*, and should be applicable to any copolymer soluble in a solvent with a low UV cutoff and in which one monomer absorbs preferentially in the UV region over the other monomer.

7.3.2 Sequence length heterogeneity project

In this project, we have related the decrease in the dimensionless size parameter R_η/R_G, as a function of *M*, to the presence of SLH in random copolymers. In the case of copolymers, the R_η/R_G ratio is dependent on the *JPR* between dissimilar monomers. As *JPR* increases, the monomers become more dispersed in the chain and the average sequence length decreases, and vice-versa. The *JPR* can depend on either chemical heterogeneity, SLH, or both. It was shown, using SEC/MALS/DRI/UV, that chemical heterogeneity was not responsible for the observed change in the R_η/R_G ratio of the random copolymers examined. Accordingly, the R_η/R_G change with *M* can be used as a semi-quantitative metric of the SLH in random copolymers. The existence of SLH in the random copolymers was assured by quantitating the area under the peak at ~ 1074 cm^{-1} in the IR spectrum which corresponds to the amount of styrene-methyl methacrylate junctions in the copolymer using IR experiments. A decrease in the area under the peak at

~ 1074 cm^{-1} as a function of molar mass for both random copolymers is observed indicating the decrease in the percentage of styrene-methyl methacrylate junctions as the molar mass grows.

To our knowledge, the dimensionless ratio R_η/R_G has never been related to the sequence length heterogeneity of a copolymer. This project adds to our understanding of the conformation-dependent properties of random copolymers, of sequence length heterogeneity, and of intrachain repulsion by showing the first experimental method to detect sequence length heterogeneity in random copolymers.

7.3.3 Influence of second virial coefficient and persistence length on dilte solution conformation project

We have examined the dilute solution behavior of PS, PpVBC, and PVC using multi-detector size-exclusion chromatography in combination with off-line MALS and DRI analysis. These particular polymers were chosen based on the intrachain interactions specific to each them, to study the general effects of interactions on the dilute solution behavior of macromolecules.

We have shown that intrachain repulsion between monomers can enhance polymer solubility while decreasing chain stiffness. Conversely, interchain attraction was seen to decrease solubility and increase stiffness. Using the conformation and Mark-Houwink plots we were also able to determine the effect of the second virial coefficient A_2 on stiffness and intrinsic viscosity. The higher the A_2 value, the better a polymer is solvated and thus the more flexible it is in solution. This increased solvation results in an enhancing of the intrinsic viscosity and to a decrease in polymer stiffness.

The present study should provide for a better understanding of how intrachain interactions along the polymeric backbone influence the dilute solution conformation and behavior of macromolecules. The effects of intrachain repulsion, intrachain attraction, and hindered intrachain attraction on the absolute and relative properties of the polymers examined were demonstrated. We hope our results allow for more acute *a priori* insight into the behavior of polymers in the dilute solution state and of the factors which influence this behavior.

REFERENCES

1. Balsara, N. P.; Tirrell, M.; Lodge, T. P., *Macromolecules* **1991,** *24*, 1975-86.

2. Ding, J.; Tao, Y.; Day, M.; Roovers, J.; D'Iorio, M., *J. Opt. A: Pure Appl. Opt.* **2002,** *4*, S267-S272.

3. Huang, H.; He, Q.; Lin, H.; Bai, F.; Cao, Y., *Thin Solid Films* **2005,** *477*, 7-13.

4. Lee, M. S.; Lodge, T. P.; Macosko, C. W., *J. Polym. Sci., Part B: Polym. Phys.* **1997,** *35*, 2835-2842.

5. Aliyar, H. A.; Hamilton, P. D.; Ravi, N., *Biomacromolecules* **2005,** *6*, 204-211.

6. De Groot, J. H.; van Beijma, F. J.; Haitjema, H. J.; Dillingham, K. A.; Hodd, K. A.; Koopmans, S. A.; Norrby, S., *Biomacromolecules* **2001,** *2*, 628-634.

7. Lai, Y.-C.; Valint, P. L., Jr., *J. Appl. Polym. Sci.* **1996,** *61*, 2051-2058.

8. Robertson, J. R.; Su, K. C. U.S. Patent 4740533, 1988.

9. Hiratani, H.; Baba, M.; Yasui, T.; Ito, E.; Yung, L.-Y. L., *J. Appl. Polym. Sci.* **2003,** *89*, 3786-3789.

10. Ketelson, H. A.; Meadows, D. L.; Stone, R. P., *Colloids Surf., B* **2005,** *40*, 1-9.

11. Khokhlov, A. R.; Khalatur, P. G., *Physica A* **1998,** *249,* 253-261.

12. Khokhlov, A. R.; Khalatur, P. G., *Phys. Rev. Lett.* **1999,** *82,* 3456-3459.

13. Lozinskii, V. I.; Simenel, I. A.; Khokhlov, A. R., *Dokl. Chem.* **2006,** 410, 170-173.

14. Lozinsky, V. I.; Simenel, I. A.; Kulakova, V. K.; Kurskaya, E. A.; Babushkina, T. A.; Klimova, T. P.; Burova, T. V.; Dubovik, A. S.; Grinberg, V. Y.; Galaev, I. Y.; Mattiasson, B.; Khokhlov, A. R., *Macromolecules* **2003,** *36*, 7308-7323.

15. Ermoshkin, A. V.; Chen, J. Z. Y.; Lai, P. Y., *Physical Review E* **2002,** *66*, 1-6.

16. Chen, H.; Wang, C.-G.; Ying, L.; Cai, H.-S., *J. Appl. Polym. Sci.* **2004,** *91*, 4105-4108.

17. Nassar, A. M.; Ahmed, N. S., *Int. J. Polym. Mater.* **2006,** *55*, 947-955.

18. Qureshi, G. J.; Padha, N.; Gupta, V. K.; Kamalasanan, M. N.; Singh, A. P.; Kapoor, A.; Tripathi, K. N., *Opt. Laser Technol.* **2003,** *35*, 401-407.

19. Ghawana, K.; Singh, S.; Tripathi, K. N., *Nouv. Rev. Opt.* **1998,** *29*, 265-267.

20. Kim, H. J.; Kim, K.; Chin, I.-J., *Mol. Cryst. Liq. Cryst.* **2007,** *463*, 383-388.

21. Kim, D. H.; Lau, K. H. A.; Robertson, J. W. F.; Lee, O. J.; Jeong, U.; Lee, J. I.; Hawker, C. J.; Russell, T. P.; Kim, J. K.; Knoll, W., *Adv. Mater.* **2005,** *17*, 2442-2446.

22. Burchard, W., *Adv. Polym. Sci.* **1999,** *143*, 113-194.

23. Stockmayer, W. H.; Moore, L. D., Jr.; Fixman, M.; Epstein, B. N., *J. Polym. Sci.* **1955,** *16*, 517-30.

24. Clarke, C. J.; Eisenberg, A.; LaScala, J.; Rafailovich, M. H.; Sokolov, J.; Li, Z.; Qu, S.; Nguyen, D.; Schwarz, S. A.; Strzhemechny, Y.; Sauer, B. B., *Macromolecules* **1997,** *30*, 4184-4188.

25. Angerman, H.; Hadziioannou, G.; Tenbrinke, G., *Physical Review E* **1994,** *50*, 3808-3813.

26. Russell, T. P.; Hjelm, R. P.; Seeger, P. A., *Macromolecules* **1990,** *23*, 890-893.

27. Mayo, F. R.; Lewis, F. M., *J. Am. Chem. Soc.* **1944,** *66*, 1594-1601.

28. Elias, H. G.; Editor, Ed.; An Introduction to Polymers, VCH: Weinheim, Germany, 1996.

29. Young, R. J., Ed.; Introduction to Polymers, Methuen, Inc., New York, N. Y: USA., 1981.

30. Kramer, I.; Pasch, H.; Handel, H.; Albert, K., *Macromol. Chem. Phys.* **1999,** *200*, 1734-1744.

31. Haidar Ahmad, I. A.; Striegel, A. M., *Anal. Bioanal. Chem.* **2010,** 396, 1589-1598.

32. Albert, K., *J. Chromatogr. A* **1995,** *703*, 123-47.

33. Hiller, W.; Pasch, H., *Polym. Prepr.* **2001,** *42*, 66.

34. Handel, H.; Albert, K., Albert, K. Ed.; Application of on-line LC-NMR and related techniques, John Wiley & Sons Ltd.: Chichester, West Sussex, 2002.

35. Philipsen Harry, J. A., *J Chromatogr A* **2004,** *1037*, 329-50.

36. Hiller, W.; Pasch, H., In; Cheng, H. N.; English, A. D. Ed.; NMR Spectroscopy of Polymers in Solution and in the Solid State., ACS: Washington, DC, 2003.

37. Maurizio, S. M., In; Cheng, H. N.; English, A. D. Ed.; NMR Spectroscopy of Polymers in Solution and in the Solid State., ACS: Washington, DC, 2003.

38. Hiller, W.; Hehn, M.; Hofe, T.; Oleschko, K., *Analytical Chemistry* **2010,** *82*, 8244-8250.

39. Schimpf, M. E., *J. Liq. Chromatogr. Related Technol.* **2002,** *25*, 2101-2134.

40. Lee, S.; Kwon, O.-S. In *Chromatographic Characterization of Polymers. Hyphenated and Multidimensional Techniques;* Advances in Chemistry Series 247; American Chemical Society: Washington, DC, 1995; pp 93.

41. Messaud, F. A.; Sanderson, R. D.; Runyon, J. R.; Otte, T.; Pasch, H.; Williams, S. K. R., *Prog. Polym. Sci.* **2009,** *34*, 351-368.

42. Gunderson, J. J.; Giddings, J. C., *Macromolecules* **1986,** *19*, 2618-2621.

43. Schimpf, M. E.; Giddings, J. C., *J. Polym. Sci., Part B: Polym. Phys.* **1989,** *27*, 1317-32.

44. Medrano, R.; Laguna, M. T. R.; Saiz, E.; Tarazona, M. P., *Phys. Chem. Chem. Phys.* **2003,** *5*, 151-157.

45. Hunt, B. J.; Holding, S. R.; Eds., *Size Exclusion Chromatography*. Blackie: Glasgow, U.K., 1989.

46. Kok, S. J.; Arentsen, N. C.; Cools, P. J. C. H.; Hankemeier, T.; Schoenmakers, P. J., *J. Chromatogr., A* **2002,** *948*, 257-265.

47. Karami, A.; Balke, S. T.; Schunk, T. C., *J. Chromatogr., A* **2001,** *911*, 27-37.

48. Mori, S., *J. Appl. Polym. Sci.* **1989,** *38*, 547-55.

49. Macko, T.; Schulze, U.; Bruell, R.; Albrecht, A.; Pasch, H.; Fonagy, T.; Haeussler, L.; Ivan, B., *Macromol. Chem. Phys.* **2008,** *209*, 404-409.

50. Kok, S. J.; Wold, C. A.; Hankemeier, T.; Schoenmakers, P. J., *Journal Of Chromatography A* **2003,** *1017*, 83-96.

51. Fitzpatrick, F.; Ramaker, H.-J.; Schoenmakers, P.; Beerends, R.; Verheggen, M.; Phillipsen, H., *J. Chromatogr.* **2004,** *1043*, 239-248.

52. Nielen, M. W. F., *Mass Spectrom. Rev.* **1999,** *18*, 309-344.

53. Raeder, H. J.; Schrepp, W., *Acta Polym.* **1998,** *49*, 272-293.

54. Servaty, S.; Koehler, W.; Meyer, W. H.; Rosenauer, C.; Spickermann, J.; Raeder, H. J.; Wegner, G.; Weier, A., *Macromolecules* **1998,** *31*, 2468-2474.

55. Sroka-Bartnicka, A.; Ciesielski, W.; Libiszowski, J.; Duda, A.; Sochacki, M.; Potrzebowski Marek, J., *Anal Chem* **2010,** *82*, 323-8.

56. Maurizio, S. M., English, H. C. a. A. Ed.; NMR spectroscopy of Polymers in Solution and in the Solid State, Society of Chemical Industry: London, U. K., 2003.

57. Pasch, H.; Schrepp, W., ed.; MALDI-TOF mass spectrometry of synthetic polymers, Springer: Berlin, Heidelberg, **2003.**

58. Netopilík, M.; Bohdanecký, M.; Kratochvíl, P., *Macromolecules* **1996,** *29*, 6023-6030.

59. Stoyanov, C.; Shirazi, Z. H.; Audu, T. O. K., *Chromatographia* **1978,** *11*, 63-69.

60. Mori, S.; Uno, Y., *J. Appl. Polym. Sci.* **1987,** *34*, 2689-99.

61. Braun, D.; Kramer, I.; Pasch, H.; Mori, S., *Macromol. Chem. Phys.* **1999,** *200*, 949-954.

62. Dadmun, M. D., *Macromol. Theory Simul.* **2001,** *10*, 795-801.

63. Kamide, K.; Hisatani, K., *Polym. J.* **1992,** *24*, 1377-95.

64. Oi, N.; Moriguchi, K.; Shimada, H.; Hashimoto, F., *Bull. Chem. Soc. Jap.* **1973,** *46*, 634-5.

65. Kandil, S. H.; El-Gamal, M. A., *J. Polym. Sci., Part A: Polym. Chem.* **1986,** *24*, 2765-71.

66. Kim, Y.; Harwood, H. J., *Polymer* **2002,** *43*, 3229-3237.

67. Brar, A. S.; Kapur, G. S., *Polym. J.* **1988,** *20,* 371-376.

68. Katritzky, A. R.; Smith, A.; Weiss, D. E., *J. Chem. Soc., Perkin Trans. 2* **1974**, 1547-54.

69. Van der Velden, G. P. M., *Macromolecules* **1983,** 16, 1336-1640.

70. Kakugo, M.; Naito, Y.; Mizunuma, K.; Miyatake, T., *Macromolecules* **1982,** *15*, 1150-2.

71. Kolbert, A. C.; Didier, J. G., *J. Appl. Polym. Sci.* **1999,** *71*, 523-530.

72. Koinuma, H.; Tanabe, T.; Hirai, H., *Macromolecules* **1981,** *14*, 883-5.

73. Witt, U.; Mueller, R.-J.; Deckwer, W.-D., *Macromol. Chem. Phys.* **1996,** *197*, 1525-35.

74. Siu, M.; Zhang, G.; Wu, C., *Macromolecules* **2002,** *35,* 2723-2727.

75. Denchev, Z.; Duchesne, A.; Stamm, M.; Fakirov, S., *J. Appl. Polym. Sci.* **1998,** *68*, 429-440.

76. Shi, Y.; Wu, M., *J. Appl. Polym. Sci.* **1995,** *57,* 1311-14.

77. Catalgil-Giz, H.; Giz, A.; Alb, A. M.; Koc, A. O.; Reed, W. F., *Macromolecules* **2002,** *35*, 6557-6571.

78. Alb, A. M.; Enohnyaket, P.; Drenski, M. F.; Head, A.; Reed, A. W.; Reed, W. F., *Macromolecules* **2006,** *39*, 5705-5713.

79. Florenzano, F. H.; Strelitzki, R.; Reed, W. F., *Macromolecules* **1998,** *31*, 7226-7238.

80. Tonelli, A. E., *Macromolecules* **1977,** *10*, 633-5.

81. Kent, M. S.; Tirrell, M.; Lodge, T. P., *J. Polym. Sci., Part B: Polym. Phys.* **1994,** *32*, 1927-1941.

82. Kent, M. S.; Tirrell, M.; Lodge, T. P., *Macromolecules* **1992,** *25*, 5383-5397.

83. Yau, W. W.; Kirkland, J. J.; Bly, D. D., Ed.; Modern size-exclusion liquid chromatography, John Wiley and Sons, Inc.: New York, N. Y., **1979**.

84. Wyatt, P. J., *Anal. Chim. Acta* **1993,** *272*, 1-40.

85. Pethrick, R. A.; Dawkins, J. V., ed.; Modern Techniques for Polymer Characterization, Wiley: New York, **1999.**

86. Striegel, A. M., ed. *Multiple Detection in Size-Exclusion Chromatography*; ACS Symposium. Series 893; American Chemical Society: Washington, DC, **2005**.

87. Kalvoda, R., Ed.; Operational Amplifiers in Chemical Instrumentation, **1975**.

88. Haidar Ahmad, I. A.; Striegel, A. M., *Instrum. Sci. Technol.* **2009,** *37*, 574-583.

89. Striegel, A. M., *Analytical Chemistry* **2005,** 77, 104A-113A.

90. Striegel, A. M.; Yau, W. W.; Kirkland, J. J.; Bly, D. D; *Modern Size-Exclusion Liquid Chromatography, 2nd ed.* Wiley: New York, 2009.

91. Smith, M. J.; Haidar, I. A.; Striegel, A. M., *Analyst* **2007,** *132*, 455-460.

92. Striegel, A. M., *Polym. Int.* **2004,** *53*, 1806-1812.

93. Haidar Ahmad, I. A. Master's Thesis, Florida State University, Tallahassee, FL, 2008.

94. Strelitzki, R.; Reed, W. F., *J. Appl. Polym. Sci.* **1999,** *73*, 2359-2368.

95. O'Leary, K.; Paul, D. R., *Polymer* **2004,** *45*, 6575-6585.

96. Stejskal, J., *Polym. Int.* **2005,** *54*, 108-113.

97. Stejskal, J.; Kratochvil, P., *Macromolecules* **1978,** *11*, 1097-1103.

98. Nielsen, L. E., *J. Am. Chem. Soc.* **1953,** *75*, 1436-1439.

99. Benkoski, J. J.; Fredrickson, G. H.; Kramer, E. J., *J. Polym. Sci., Part B: Polym. Phys.* **2001,** *39*, 2363-2377.

100. Pasch, H.; Trathnigg, B. ed.; HPLC of Polymers, Springer: Berlin, **1999**.

101. Mourey, T., *Int. J. Polym. Anal. Charact.* **2004,** *9*, 97-135.

102. Brandrup, J.; Immergut, E. H.; ed.; Polymer Handbook, Fourth Edition, Wiley: New York, N. Y., **1998**.

103. Ahuja, S. K., *Rheol. Acta* **1980,** *19*, 299-306.

104. Kennedy, M. A.; Peacock, A. J.; Failla, M. D.; Lucas, J. C.; Mandelkern, L., *Macromolecules* **1995,** *28*, 1407-21.

105. Alamo, R. G.; Viers, B. D.; Mandelkern, L., *Macromolecules* **1993,** *26*, 5740-7.

106. Alamo, R. G.; Mandelkern, L., *Macromolecules* **1991,** *24*, 6480-93.

107. Alamo, R. G.; Chan, E. K. M.; Mandelkern, L.; Voigt-Martin, I. G., *Macromolecules* **1992,** *25*, 6381-94.

108. Huser, T.; Yan, M., *J. Photochem. Photobiol.* **2001,** *144*, 43-51.

109. Nguyen, T.-Q.; Doan, V.; Schwartz, B. J., *J. Chem. Phys.* **1999,** *110*, 4068-4078.

110. Kohjiya, S.; Iwata, K.; Yamashita, S.; Miyamoto, T.; Inagaki, H., *Polym. J.* **1983,** *15*, 869-874.

111. Kotaka, T.; White, J. L., *Macromolecules* **1974,** *7*, 106-16.

112. Inagaki, H.; Tanaka, T., *Pure Appl. Chem.* **1982,** *54*, 309-322.

113. Dekmezian, A. H.; Morioka, T.; Camp, C. E., *J. Polym. Sci., Part B: Polym. Phys.***1990,** *28*, 1903-15.

114. Mirabella, F. M.; Barrall, E. M.; Johnson, J. F., *J. Appl. Polym. Sci.* **1975,** *19*, 2131-2141.

115. Mori, S.; Suzuki, T., *J. Liq. Chromatogr.* **1981,** *4*, 1685-96.

116. Meselson, M.; Stahl, F. W.; Vinograd, J., *Proc. Nat. Acad. Sci. U.S.A.* **1957,** 43, 581-8.

117. Stacy, C. J., *J. Appl. Polym. Sci.* **1977,** *21*, 2231-40.

118. Poddubnyi, I. Y.; Podalinskii, A. V.; Grechanovskii, V. A., *Vysokomol. Soyed* **1972,** *14*, 714-721.

119. Staggemeier, B.; Huang, Q. R.; Dubin, P. L.; Morishima, Y.; Sato, T., *Anal. Chem.* **2000,** *72*, 255-258.

120. Provder, T., ed.; Chromatography of Polymers: Hyphenated and Multidimensional Techniques., ACS Symposium Series 731; American Chemical Society: Washington, DC, **1999**.

121. Montaudo MS, In: Striegel, AM (ed) Multiple Detection in Size-Exclusion Chromatography. ACS symposium series, vol 893. American Chemical Society, Washington, DC, **2005,** pp 152-167

122. Stuting, H. H.; Krull, I. S., *Anal. Chem.* **1990,** *62*, 2107-14.

123. Lee, D. C.; Speckhard, T. A.; Sorensen, A. D.; Cooper, S. L., *Macromolecules* **1986,** *19*, 2383-90.

124. Trainoff, S. P. U.S. Patent 20050075851, **2005**.

125. Balke, S. T.; Mourey, T. H., *J. Appl. Polym. Sci.* **2001,** *81*, 370-383.

126. Gillespie, D.; Yau, W. W.; Gibson, T. 1998 *Int GPC Symp Proc*, Waters, Milford, MA, **1999**; pp 32-47.

127. Blythe, A. R., *Electrical Properties of Polymers*. Cambridge University Press: Cambridge, England, **1979**.

128. Schmack, G.; Tandler, B.; Vogel, R.; Beyreuther, R.; Jacobsen, S.; Fritz, H. G., *J. Appl. Polym. Sci.* **1999,** *73*, 2785-2797.

129. Koningsveld, R., *Chem. Zvesti* **1972,** *26*, 263-87.

130. Krause, S., *Pure Appl. Chem.* **1986,** *58*, 1553-60.

131. Haidar Ahmad, I. A.; Striegel, D. A.; Striegel, A. M., *Polymer* **2011***, 52,* 1268-1277.

132. Yeung, C.; Balazs, A. C.; Jasnow, D., *Macromolecules* **1992,** *25,* 1357-1360.

133. Zheligovskaya, E. A.; Khalatur, P. G.; Khokhlov, A. R., *Phys. Rev. E: Stat. Phys., Plasmas, Fluids,* **1999,** *59,* 3071-3078.

134. Balazs, A. C.; Sanchez, I. C.; Epstein, I. R.; Karasz, F. E.; MacKnight, W. J., *Macromolecules* **1985,** *18,* 2188-2191.

135. Balazs, A. C.; Karasz, F. E.; MacKnight, W. J.; Ueda, H.; Sanchez, I. C., *Macromolecules* **1985,** *18,* 2784-2786.

136. Rana, D.; Mounach, H.; Halary, J. L.; Monnerie, L., *J. Mater. Sci.* **2005,** *40,* 943-953.

137. Galvin, M. E., *Macromolecules* **1991,** *24,* 6354-6356.

138. Hirai, H., *Polym. Adv. Technol.* **2003,** 14, 266-272.

139. P. J. Flory, Ed.; Principles of Polymer Chemistry, Cornell Univ. Press: Ithaca, N.Y., **1953**.

140. Striegel, A. M., *J. Biochem. Bioph. Methods* **2003,** *56*, 117-139.

141. Roovers, J.; Martin, J. E., *J. Polym. Sci., Part B: Polym. Phys.* **1989,** *27*, 2513-2524.

142. Roovers, J., *Plast. Eng.* **1999,** *53*, 285-341.

143. Ostlund, S. G.; Striegel, A. M., *Polym. Degrad. Stab.* **2008,** *93*, 1510-1514.

144. Graessley, W. W.; *Polymeric Liquids and Networks: Structure and Properties,* Garland Science: New York, **2003**.

145. Striegel, A. M., *Biomacromolecules* **2007,** *8*, 3944-3949.

146. Jo, W. H.; Kim, H. C.; Baik, D. H., *Macromolecules* **1991,** *24*, 2231-5.

147. Kim, J.; Gray, M. K.; Zhou, H.; Nguyen, S. T.; Torkelson, J. M., *Macromolecules* **2005,** *38*, 1037-1040.

148. Dadmun, M., *Macromolecules* **1996,** *29*, 3868-74.

149. Hellmann, G. P.; Dietz, M., *Macromol. Symp.* **2001,** *170*, 1-8.

150. Zaremski, M. Y.; Kalugin, D. I.; Golubev, V. B., *Polymer Science Series A* **2009,** *51*, 103-122.

151. Kim, J.; Zhou, H.; Nguyen, S. T.; Torkelson, J. M., *Polymer* **2006,** *47*, 5799-5809.

152. Arlen, M. J.; Dadmun, M. D., *Polymer* **2003,** *44*, 6883-6889.

153. Teraoka, I., Ed.; Polymer Solutions: An Introduction to Physical Properties, John Wiley & Sons Ltd: Hoboken, N. J., 2002.

154. Dozier, W. D.; Huang, J. S.; Fetters, L. J., *Macromolecules* **1991,** *24*, 2810-14.

155. Nguyen, T.-Q.; Doan, V.; Schwartz, B. J., *J. Chem. Phys.* **1999,** *110*, 4068-4078.

156. Sun, T.; King, H. E., Jr., *Macromolecules* **1996,** *29*, 3175-81.

157. Orofino, T. A.; Wenger, F., *J. Phys. Chem.* **1963,** *67*, 566-75.

158. Brown, W.; Nicolai, T., *Colloid Polym. Sci.* **1990,** *268*, 977-90.

159. Striegel, A. M., In *Encycl. Chromatogr.,* 3rd ed., Cazes, J.; ed.; Florida; **2010;** pp1417-1420.

160. Biron, M., *Pop. Plast. Packag.* **2010,** *55*, 49-53.

161. Ye, X.; Li, Z.-H.; Wang, W.; Fan, K.; Xu, W.; Hua, Z., *Chem. Phys. Lett.* **2004,** *397*, 56-61.

162. Zimm, B. H.; Stockmayer, W. H.; Fixman, M., *J. Chem. Phys.* **1953,** *21*, 1716-23.

163. Kok, C. M.; Rudin, A., *J. Appl. Polym. Sci.* **1981,** *26*, 3583-97.

164. Cantor, C. R.; Schimmel, P. R., W. H. Freeman. Ed.; Biophysical Chemistry of Macromolecules, Part III: The Behavior of Biological Macromolecules, San Francisco, CA, **1980**.

165. Skolnick, J.; Fixman, M., *Macromolecules* **1977,** *10*, 944-8.

166. Odijk, T.; Houwaart, A. C., *J. Polym. Sci., Polym. Phys.* **1978,** *16*, 627-39.

167. Kroemer, H.; Kuhn, R.; Pielartzik, H.; Siebke, W.; Eckhardt, V.; Schmidt, M., *Macromolecules* **1991,** *24*, 1950-4.

168. Schellman, J. A.; Harvey, S. C., *Biophys. Chem.* **1995,** *55*, 95-114.

169. Drube, F.; Alim, K.; Witz, G.; Dietler, G.; Frey, E., *Nano Lett.* **2010,** *10*, 1445-1449.

170. Gutjahr, P.; Lipowsky, R.; Kierfeld, J., *Europhys. Lett.* **2006,** *76*, 994-1000.

171. Yanagisawa, M.; Isogai, A., *Biomacromolecules* **2005,** *6*, 1258-1265.

172. Hsu, H.-P.; Paul, W.; Binder, K., *Macromolecules* **2010,** *43*, 3094-3102.

BIOGRAPHICAL SKETCH

Imad Haidar Ahmad was born in Beirut/Lebanon in 1981. He lived his childhood in his Village Ras Oasta and in Beirut. From 2000 till 2004, Imad went to the Lebanese University at Al-Hadath where he got his maîtrise degree in Chemistry. Imad Joined FSU in Fall 2005 as a graduate student and worked in the area of Analytical Chemistry under the supervision of Dr. André Striegel. In 2008, he got his Master's degree from FSU. After Graduating, he will be joining Professor Peter Carr's group as a postdoctoral researcher.